In Vivo Time-Lapse Imaging of the Retina in the Developing Zebrafish (*Danio Rerio*)

Tilak Das

Trinity College, University of Cambridge

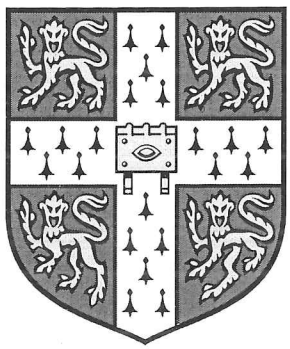

A dissertation submitted for the degree of Doctor of Philosophy

August 2002

Femtosecond or Picosecond? 50
Non-descanned Detectors 50

The Use of Software in Processing 4D Data 52
Sampling for 3D Visualisation 52
Methods of Exploring 3D Data 53

Conclusion 57

Chapter 3: Cell Division in the Zebrafish Retina 63

Introduction 63

Methods and Materials 68
Fish 68
Bodipy-Ceramide Labelling 68
Plasmids 68
In vivo Imaging 69
Visualisation 70
Definition of Retinal Axes 70
Analysis of Orientation of Cell Division (Zebrafish) 70
Analysis of Orientation of Cell Division (Rat) 71
Analysis of the Basal Process 72

Results 73
I. There are no apico-basal divisions in the zebrafish retina 73
II. The orientation of cell division shifts from a central-peripheral to a circumferential axis over time 74
III. The distribution of orientation of cell divisions also shifts over time in the developing rat retina 75
IV. Orientation of division in syu mutants 75
V. Retinal ganglion cells followed from division 77
VI. Partner of Numb, a potential molecular marker for asymmetric division 78
VII. The basal process persists during mitosis 80
VIII. Inheritance of the basal process after cell division 81

Discussion 83
I. Orientation of Cell Division 83
II. The Basal Process 88

Chapter 4: The Development Of Retinal Cell Mosaics 104

Introduction 104

Methods and Materials 114
Fish 114
Imaging 114
Visualisation and Analysis 115

Results 116
I. Pax6GFP zebrafish express GFP in neuroepithelial cells and amacrine cells 116
II. Amacrine cell mosaics in the retina 117
III. Amacrine cell death in the retina 118
IV. Cell death and intercell distance 119
V. Cellular processes and cell death 121
VI. Cell movement within mosaics 122

Discussion 124
I. Amacrine cells undergo apoptosis in the zebrafish retina 124
II. The role of cell-cell interactions in amacrine cell apoptosis 125

III. Tangential cell movement 128

Chapter 5: General Summary 135

References 138

List of Figures

Fig 1.1 Cartoon of major retinal cell types in the zebrafish retina 7

Fig. 2.1 Jablonski diagram schematising the different electronic energy levels of a molecule 10

Fig 2.2 Normalised excitation (or absorption) and emission spectra for fluorescein 11

Fig 2.3 Mechanisms of photodamage 12

Fig 2.4 The numerical aperture (NA) of an objective lens 14

Fig. 2.5 The resolution of an optical system is determined by the Airy disc radius 15

Fig. 2.6 Oblique illumination provided by a higher NA condenser will improve resolution 16

Fig. 2.7 Principles of confocal microscopy 58

Fig. 2.8 Diagram of the scanning typically used in many confocal microscopes 23

Fig. 2.9 A Jablonski diagram representation of multi-photon events 28

Fig. 2.10 a) External detectors enhance the detection of emission when using TPELSM b) A comparison of CLSM and TPELSM in depth 59

Fig. 2.11 Photobleaching and photodamage in CLSM and TPELSM 60

Fig. 2.12 Melanin pigmentation hinders TPELSM imaging of the zebrafish retina 61

Fig 2.13 The power output of the TPELSM laser depends on the wavelength chosen 48

Fig. 2.14 3D reconstructions of optical sections. 62

Fig. 3.1 Time-lapse analysis of cell division in the zebrafish embryonic retina 92

Fig. 3.2 Retinal neuroepithelial cells divide parallel to the retinal apical surface 93

Fig. 3.3 Orientation of cell division with respect to the apico-basal axis and retinal surface. 94

Fig. 3.4 Analysis of cell divisions orientated parallel to the apical surface 95

Fig. 3.5 Cumulative distributions of orientations of cell divisions parallel to the retinal surface over time 96

Fig. 3.6 Brn3c-GFP transgenic zebrafish 97

Fig. 3.7 Tracing RGCs back to their final division 98

Fig. 3.8 Tracing cell divisions forward in time in 1dpf Brn3c-GFP embryos injected with H2B-GFP 99

Fig. 3.9 Pon-GFP labelling in the retina 100
Fig. 3.10 Persistence of the basal process during cell division in vivo 101
Fig. 3.11 Asymmetric inheritance of the basal process 102
Fig. 3.12 Sequence of events for some cell divisions in the developing zebrafish retina 103
Fig. 4.1 Diagram of the cone mosaic found in the adult zebrafish retina 110
Fig. 4.2 Pax6-GFP transgenic embryos express GFP in amacrine cells 130
Fig. 4.3 The distribution of intercell distances at 48hpf and 60hpf 117
Fig. 4.4 Apoptosis of amacrine cells in the developing zebrafish retina 131
Fig. 4.5 Comparison of dying cells and survivors with respect to distance from the nearest neighbour (NN) to each cell 119
Fig. 4.6 Cumulative frequency curves for dying cells and survivors with respect to distance from the nearest neighbour (NN) to each cell 120
Fig. 4.7 Established amacrine cells can undergo apoptosis 132
Fig. 4.8 Amacrine cell death coincides spatially and temporally with the approach of dendrites from neighbouring cells 133
Fig. 4.9 A scatter plot showing the time-averaged distance between five 'new' cells in the time-lapse series and their nearest neighbours 123
Fig. 4.10 Relatively rapid moving cells (highlighted in green) tend to undergo apoptosis or may be macrophages 134

Acknowledgements

I am grateful for the encouragement and patience of the many people who have shared the best times with me and helped me through the toughest times of this phase of my life. Mum, dad and Tanya must be the first to thank. I can never thank them enough for all that they have done for me at home and away.

Imaging as a project was introduced to me by Charles Kimmel, to whom I shall always be grateful. I am also indebted to Jeremy Skepper for the enthusiasm with which he spent time helping me on the imaging systems as well as advising me on experiments and for very useful discussions on all things imaging. Thanks to Richard Adams for help and providing software, and to Steve Wilson for use of his facilities and fish. Ulrike Tauer was very helpful with technical advice and for providing encouragement. Thanks to Tobias Roeser and Herwig Baier for training me in fishy stuff, and for providing their materials. The Harris/Holt lab has been a source of great inspiration, but mainly laughter (in a good way). I had a wonderful time working and enjoying life with Karl, Kiersten, Mike, Andrea, Muriel, Shinichi, Fanny, Richard, Del, Asha, Susie, and all those who have passed through over the years. I'm very grateful to Berni for his help and hard work above and beyond the call of duty, and to Ilina for her timely help in a crisis. Of course, I have to mention Ruben and Gio, if only because I said I would. I am forever indebted to Nilima for all the support, encouragement and dictatorial finesse with which she got me to this final stage and for allowing me to exploit her editorial skills. Finally, Bill receives a special award for his patience and encouragement. His advice is always valuable and I am extremely grateful for having had this wonderful opportunity that will, without a doubt, serve me well in the future.

Declaration

This dissertation is the result of my own work and includes nothing which is the outcome of work done in collaboration except where specifically indicated in the text.

Summary

In vivo time-lapse imaging of the retina in the developing zebrafish (*Danio rerio*).

The zebrafish is used as a model organism to explore issues pertaining to the development and organisation of the vertebrate retina *in vivo*. The transparency of zebrafish embryos, their rapid development and amenability to experimental as well as genetic manipulation are features that are readily taken advantage of for *in vivo* imaging. Four-dimensional imaging of large structures is currently relatively underused as a tool to study developmental processes due to difficulties in imaging specimens in depth and for a significant length of time. Two-photon laser scanning microscopy (TPLSM) is a relatively new optical sectioning technique that has been important for the implementation of four-dimensional imaging of fluorescent biological specimens as specimens can be scanned for long lengths of time while causing less phototoxic damage to the fluorophore and the specimen itself compared to other fluorescence microscopy techniques. The feasibility of using TPLSM for long-term imaging of the zebrafish embryo is assessed qualitatively.

TPLSM is the approach used to address how asymmetric cell divisions might take place in the retina. Asymmetric cell division is a mechanism thought to be involved in generating neuronal diversity from a homogeneous progenitor population, and may be mediated by the orientation of progenitor cell divisions. 3D reconstructions of the developing zebrafish retina were analysed for orientation of cell division. Contrary to currently proposed models for vertebrate asymmetric divisions, apico-basally oriented cell divisions, perpendicular to the ventricular surface, are not found to occur in the zebrafish retina during the formation of postmitotic neurons. However, a shift in the orientation of cell division from central-peripheral to circumferential orientations occurs within the plane of the ventricular surface at a time when neuronal cells are differentiating. The shift from central-peripheral to circumferential divisions is absent or delayed in the *sonic you* (*syu*) mutant, in which retinal ganglion cell production is grossly affected. This delay correlates with a delay in neuronal differentiation, suggesting that the circumferential orientations of division may represent asymmetric, neuron-generating cell divisions.

In vivo imaging also shows that mitotic cells, found in the apical side of the neuroepithelium, retain a process connected to the opposite basal surface, and that this process can be inherited asymmetrically by one daughter cell. Although this may also a play a role in asymmetric cell division, it does not correlate with a specific orientation of division. It may be important for the radial migration of newborn neurons to the appropriate layer of the retina.

After neuronal differentiation, tangential migration of cells and cell death may be required to maintain regularity in newly-formed neuronal cell mosaics. The *in vivo* behaviour of amacrine cells in early development was studied using TPLSM. Amacrine cell death, correlated with short distances between cells, is shown to occur in early retinal development, although evidence for tangential cell migration is not found. It is plausible that apoptosis, thought to be a rare event in the zebrafish retina, is in fact required for the formation of regular cell mosaics by the removal of incompatible cells from a mosaic by short-range interactions with other cells in the mosaic.

Chapter 1: General Introduction

The 'neuron theory' states that "the nervous system is made up of innumerable nerve units which are anatomically and genetically independent of each other." Put forward by Wilhelm Waldeyer in 1891 and established by the classical work of Santiago Ramón y Cajal (Ramâon y Cajal, 1995), this discovery was a great advancement in the study of the nervous system. The realisation of the nervous system's complexity has not diminished but augmented our desire to understand how it functions. The vertebrate retina is but one specialised part of the central nervous system, although it is perceived, perhaps deceptively, as a simpler structure than many other parts of the central nervous system. The major cell types that make up the vertebrate retina and the ordered organisation of these cell types into retinal laminae is well defined (Dowling, 1987). Coupled with the accessibility of the tissue to various forms experimentation, from excision of the entire structure for *in vitro* study to the stimulation of retinal cells and the ability to detect the effects *in situ*, the retina is a model system studied both as an essential component of the visual process and as a model for broader questions in neurobiology and cell biology. General principles learnt from the study of the retina and its development are applicable to the development and function of the nervous system as a whole. This thesis is an attempt at addressing specific issues pertaining to the development of the vertebrate retina using the zebrafish as a model organism and *in vivo* imaging as the main experimental modality.

Retinas in vertebrates derive from the neural tube, the embryological precursor of the central nervous system as antero-lateral evaginations known as the optic vesicles. The lateral surface of the optic vesicle is adjacent to the overlying surface ectoderm, where the lens placode is induced. Although general mechanisms in retinal development are preserved across vertebrate species (Fini et al., 1997), the initial stages of optic vesicle development are known to differ in teleosts, such as the zebrafish (Walls, 67, Schmitt, 94). In zebrafish, the neural tube is a solid mass of cells known as the neural keel. Optic lobes form as lateral thickenings of the anterior neural keel approximately 11 hours post-fertilisation (hpf) at the 6-somite stage. The lumen of the optic vesicle forms at about 12hpf by cavitation of the neural keel. Similar to other vertebrates, the optic vesicle invaginates in its centre to form the optic cup at about 15hpf. The lateral surface of the optic cup will form the neural retina, while the closely apposed medial surface will form

the retinal pigment epithelium (RPE). During optic cup formation, the connection between the optic cup and the neural tube narrows to become the optic stalk, and the lens placode, now known as the lens pit, continues to thicken. The lumen of the optic stalk will later be filled by axonal projections from the retinal ganglion cells to become the optic nerve. By the end of somitogenesis in zebrafish at 24hpf, the lens pit detaches from the surface ectoderm to form the rudimentary lens vesicle, while the optic cup consists of the 'inner' or lateral neural retina and the single-cell thick 'outer' or medial RPE. The neural retina thickens due to an increase in the proliferation rate of retinal progenitor cells (Li, 00), and forms a pseudostratified columnar epithelium. The progenitor cells will eventually give rise to all the neuronal and glial cells of the retina.

Although neurogenesis does not begin before 28hpf (Hu and Easter, 1999), the typical laminated organisation of the retina is evident by 60hpf, when neurogenesis in the central retina is thought to be complete (Nawrocki, 1985) and rudimentary visual behaviours such as startle responses start to be expressed (Easter and Nicola, 1996). The peripheral retina continues to proliferate, adding new cells as the retina grows. A marginal area known as the ciliary marginal zone (CMZ) will exist into adulthood, similar to the Xenopus retina, although in contrast to mammals. The retina is ultimately organised into six distinct layers and consists of six neuronal and one glial cell types (Dowling, 1987) (Fig. 1.1). An outermost photoreceptor layer (PRL), followed by the outer nuclear layer (ONL) contain the rod and cone photoreceptors (PRs). A thin outer plexiform layer (OPL) separates the ONL from the inner nuclear layer (INL), which contains the cell bodies of bipolar cells, amacrine cells, horizontal cells and Müller glial cells. The ganglion cell layer (GCL), containing the ganglion cells or output cells of the retina, lies innermost and is separated from the INL by the inner plexiform layer (IPL). The plexiform layers consist of the synapses between different cells from the adjacent layers. The OPL is formed of processes and synapses between PRs, bipolar cells and horizontal cells, which lie in the outermost part of the INL. The IPL consists of synapses between bipolar cells, retinal ganglion cells (RGCs), and amacrine cells, which are mainly found in the inner part of the INL and occasionally in the GCL. Membranes from Müller glial end-feet and a basement membrane form the inner limiting membrane of the retina, while the outer ends of the glial cells form the outer limiting membrane.

Both the neuronal and glial cells come from the same population of progenitor cells in the vertebrate retina. Retinal progenitor cells were found to be multipotent at different stages

in lineage tracing experiments in rat and Xenopus. Infection of rat retinal progenitors using retroviral vectors expressing β-galactosidase or direct injection of tracers such as horse radish peroxidase (HRP) or fluorescent dextran into Xenopus cells, revealed cell clones consisting of multiple cell types, including neuronal and glial cells (Holt et al., 1988; Turner and Cepko, 1987; Wetts and Fraser, 1988). Clone sizes varied with smaller clones being produced on average later in development. Nonetheless no correlation could be found between the size of the clone or the time it was labelled and the cell types generated, suggesting that retinal progenitor cells are multipotent throughout retinal development. Yet, a stereotypical order of histogenesis is also characteristic of vertebrate retinal development. Different cell types are born in a particular chronological sequence, although the period during which a particular cell type is born can overlap with that of another cell type (Cepko et al., 1996; Marquardt and Gruss, 2002). In most vertebrates, ganglion cells are born first and rod photoreceptors are born last (Hu and Easter, 1999; McCabe et al., 1999; Stiemke and Hollyfield, 1995; Young, 1985), although the exact sequence varies between species. In zebrafish, the identification of post-mitotic cells by the exclusion of BrDU injected at different times elegantly shows an inner to outer sequence of cells becoming post-mitotic (Hu, 99). Cells in the innermost layers are born before cells in the outer layers. A combination of extrinsic factors from other cells of the same or different types as well as factors intrinsic to the cells themselves, are likely to be responsible for the relative order in the timing of neurogenesis (Livesey and Cepko, 2001; Marquardt and Gruss, 2002). The multipotency of progenitor cells, whether restricted to some extent by intrinsic factors, and the temporal overlap in histogenesis for different cell types, raises the question of whether retinal progenitor cells can divide asymmetrically to produce two different daughter cells, perhaps one that will continue to proliferate while the other differentiates. The work described in Chapter 3 on 'cell division in the zebrafish retina' sets out to address this issue. The orientation in which a cell divides may play an important role in imparting asymmetry to division by allowing cell fate determinants or other intrinsic factors already asymmetrically localised within the dividing cell to segregate asymmetrically to one daughter cell. Thus, the preliminary questions concerning retinal cell division include whether dividing cells show any pattern in their orientation at mitosis, and whether this pattern might correlate with periods of neurogenesis where one would expect to see asymmetric divisions, if they existed. In addition, attempts are made to follow daughter cells *in vivo* during retinal development in

order to define their fates, and thus definitively identify the divisions that gave rise to them in terms of their symmetry.

Another interesting finding from the cell lineage studies was that clones of cells tended to remain restricted to radial columns within the retina. Cell division in the retina always occurs at the ventricular, or apical, surface (Hinds and Hinds, 1974) and post-mitotic cells migrate basally to the lamina appropriate to their fate. In the developing diencephalon, where clones also remain in radially organised groups, neuronal cells are known to migrate to their appropriate layers by using glial cell processes that span the cortex radially (Hatten and Mason, 1990). The equivalent cell in the retina may be the Müller glial cell although Müller glia are thought to differentiate later than many of the other retinal cell types (Linser et al., 1997; Peterson et al., 2001). Retinal progenitor cells also span the entire thickness of the retina, and their processes could function as a scaffold for migrating retinal cells. Observations on cell division made by *in vivo* imaging and described in chapter 3, show that this process remains attached basally throughout mitosis and is often inherited by one of the two resulting daughter cells. The hypothesis that the asymmetric inheritance of the basal process may be a sign of asymmetric cell division is considered.

As neuronal cells migrate to their appropriate layers, some neuronal cell types form regular arrays or mosaics with other cells of the same type. Functionally, this allows cells with a particular role in visual processing to cover the entire retina with little overlap or redundancy, and without leaving any gaps in the visual field. Although the existence of such arrays has been established, very little is known about how they develop (Cook and Chalupa, 2000). Chapter four represents the first attempts to study the formation of cell mosaics in zebrafish *in vivo* by the direct observation of newly-born amacrine cells, a cell type known to form retinal mosaics in the adult vertebrate retina. In particular, *in vivo* evidence for amacrine cell death and the role it may play in the formation of retinal mosaics is presented in this chapter.

The zebrafish has proven to be an extremely useful model for the study of dynamic developmental processes. Zebrafish are mostly transparent during development and develop rapidly as exemplified by the formation of a functional retina within three days of fertilisation (Easter and Nicola, 1996; Nawrocki, 1985). Apart from being valuable features for *in vivo* imaging, the transparency and rapid development of zebrafish embryos have also enabled rapid screening for morphological defects to be carried out

feasibly after large-scale random mutagenesis experiments (Haffter et al., 1996; Mullins et al., 1994). This has resulted in a large number of mutant zebrafish becoming available for the study of different systems in vertebrate biology. Zebrafish embryos are also amenable to both classical embryological manipulation and current techniques in genetic manipulation. The ability to transiently express particular proteins in the embryo and to create transgenic fish that permanently express proteins of interest has been, along with the introduction of fluorescent proteins, propitious for *in vivo* imaging, as very specific targets can be visualised.

Almost all of the work described here is based on *in vivo* imaging experiments. *In vivo* imaging can help define dynamic processes without the interference of artefacts often introduced by studies of cells and tissues outside of their native context or by the biochemical effects of fixation processes. The description of dynamic processes can then become the basis for biological assays for experimental testing. To image the entire thickness of the zebrafish retina over time, optical sectioning techniques were used to generate three-dimensional representations of the retina at regular time intervals. In particular, two-photon excitation laser scanning microscopy (TPELSM) was used extensively for this purpose. Although similar to confocal laser scanning microscopy (CLSM) in terms of generating optical sections of a fluorescent specimen without the need to physically cut it, TPELSM holds additional advantages. The main advantage, particularly in imaging animals *in vivo,* is that overall exposure to excitation energy is reduced, thus enabling imaging to be carried out over a longer term while causing less damage to the specimen itself. Light-induced damage is an important limiting factor for *in vivo* imaging. Chapter 2 introduces the physical principles behind fluorescence imaging and TPELSM in particular, with reference to my experience using this technique. Subtle differences between TPELSM and CLSM, explored in this chapter on the basis of the physics of the two modalities, can mean that TPELSM will not provide an advantage over CLSM in every experimental case. This chapter is intended to be of use to those who wish to use TPELSM for their experiments, but have little experience in doing so. Four-dimensional (three-dimensional plus time) imaging presents particular challenges in terms of processing and analysing data. Although this process is changing rapidly and benefits from continuous progress in computer hardware and software development, the basic methods used to process the data presented in this thesis are outlined in this chapter.

The ability to visualise biological processes as they happen *in vivo* is exciting in itself, and can yield surprising new insights into well-known phenomena. Questions that previously could not be answered with any certainty are within reach, as the behaviour or fate of individual components of living tissue can be studied *in situ* and compared to the population to which they belong. *In vivo* imaging is not a new field. However, the co-incidence of available tools, such as TPELSM and fluorescent protein-based transgenic organisms, has played a very large part in setting the questions that are addressed in this work. I hope that this work will provide a basis for others considering the use of *in vivo* imaging, particularly using two-photon excitation laser scanning microscopy, by illustrating the type of questions that can be posed, the answers that can be found, and some of the advantages and disadvantages of using such methods. I also hope that the questions raised about established concepts in retinal development will pique the curiosity and interest of others, providing some stimulus to the next questions being posed.

Fig 1.1 ***Cartoon of major retinal cell types in the zebrafish retina.*** A retinal section from a 7dpf zebrafish, stained with methylene blue, showing the different layers of the differentiated retina: Retinal Pigment Epithelium (RPE), Photoreceptor layer (PRL), Outer Nuclear Layer (ONL), Outer Plexiform Layer (OPL), Inner Nuclear Layer (INL), Inner Plexiform Layer (IPL), Ganglion Cell Layer (GCL). Cartoon cells overlaid on the section represent the 7 major cell types found in the different layers of the vertebrate retina.

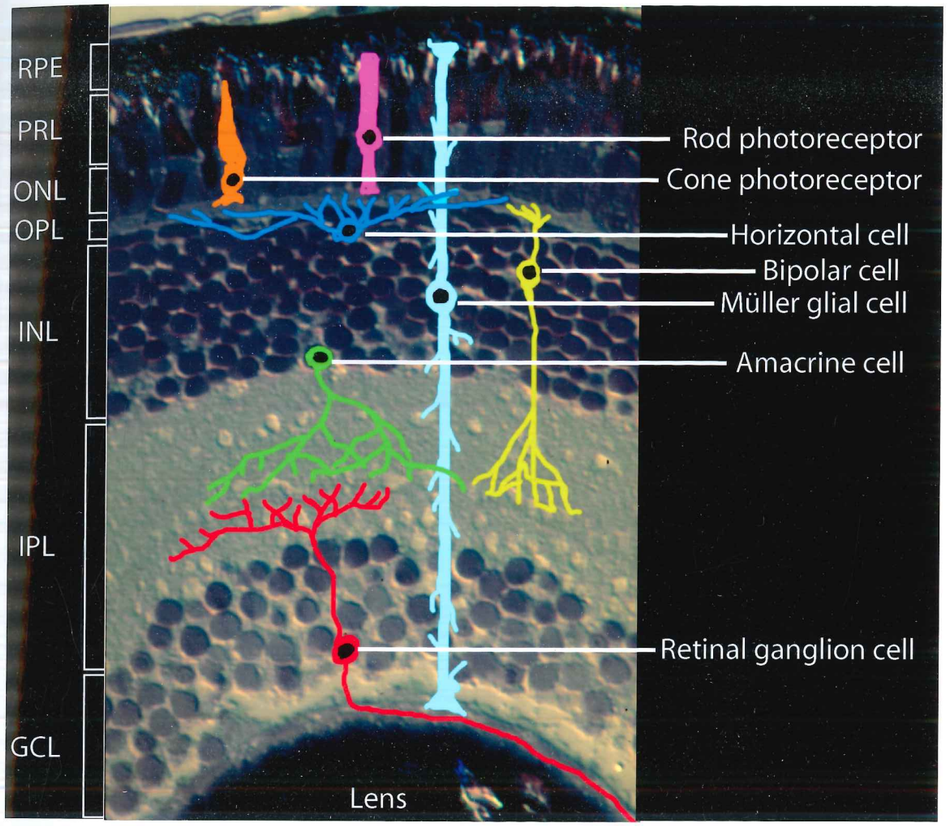

Fig. 1.1

Chapter 2: *In vivo* imaging by two-photon excitation laser scanning microscopy

Introduction

The nature of in vivo imaging in three dimensions requires that the optical system being used to image a live specimen be as efficient as possible. Ideally, the specimen should be exposed to a minimum amount of light energy while a maximum of the emitted light returning from it is detected. Exposure to intense light will always be detrimental to a live specimen and any probes being used to visualise its parts, however the more light incident on the specimen, the more returning light can be detected. As in most physical systems, 100% efficiency is an ideal, and the real efficiency of an optical system will depend on a number of factors such as loss of light scattered by a specimen, a limit to the amount of light collected by an objective lens, losses along the light path to the detector, the efficiency of specific probes being visualised and the efficiency of detectors to convert photons into electrical signals. This section describes the principles behind fluorescence microscopy in general, the major factors that affect the efficiency of a fluorescent microscope and how some problems with wide-field microscopy* are overcome with the use of confocal and two-photon excitation laser scanning microscopes. Two-photon excitation microscopy is compared to confocal microscopy from a theoretical as well as a practical perspective and the suitability of two-photon microscopy to *in vivo* imaging applications is explored.

* Wide-field microscopy refers to the 'conventional' method of epifluorescence microscopy in which incoherent light sources such as mercury vapour lamps are used as opposed to coherent sources such as lasers.

Fluorescence

The widespread use of fluorescent probes in microscopy stems from the huge range of fluorescent probes available to label cells, sub-cellular components or proteins, and the high specificity of these probes. The range includes stains, labelled antibodies, physiological indicators and fluorescent proteins that can be expressed in specific contexts. These are available with various physical properties and different excitation and emission characteristics (i.e. colours). Fluorescence microscopy can also be a very sensitive method, in which low levels of background noise, and therefore high levels of contrast, are achieved, yielding a high 'signal-to-noise ratio'. An explanation of fluorescence in the context of microscopy is warranted as this will help explain the high specificity and sensitivity of fluorescence microscopy, as well as how confocal and two-photon laser scanning microscopy can improve on the more conventional wide-field microscopy.

Mechanism of Fluorescence

Fluorescence is a photophysical process by which a molecule absorbs energy from incident light and emits light of a longer wavelength. This longer wavelength is equivalent to a lower energy, as the energy of a photon is inversely proportional to its wavelength. The relationship between energy and wavelength is described as:

$$e = h c / \lambda \qquad (1)$$

where 'e' is the energy of the photon and 'λ' is the wavelength. 'h' is Planck's constant and 'c' is the velocity of light.

In fluorescence, the emission lasts as long as the incident light is present, unlike phosphorescence, in which emission can persist a few seconds after removal of the incident light. The dependence of fluorescence on incident light is a useful property in microscopy since the observed emission can always be directly correlated to the incident light. Fig. 2.1 shows a Jablonski diagram, a method of describing the energy changes that occur in the electrons of molecules during absorption and emission of light. On absorption of a photon, an electron is raised from its stable ground state to a higher energy state (S0 to S1). The excitation energy required corresponds to the wavelength of the incident light. Each energy state consists of multiple substates and within the higher energy state, the electron loses some vibrational energy and descends to the lowest excited substate. The electron then descends to the ground state by emitting energy as a photon. The energy emitted corresponds to the emission wavelength of the molecule. Since the electron loses some vibrational energy, the energy of the emitted photon is less than the energy of the excitation photon, and therefore has a longer wavelength. The fact

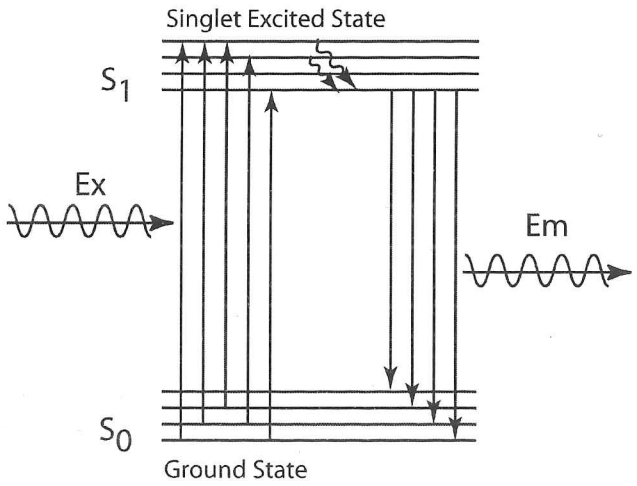

Fig. 2.1 ***Jablonski diagram schematising the different electronic energy levels of a molecule***. The absorption of a photon of appropriate energy can excite the molecule to a higher energy level (Ex). A molecule can return to its stable ground state by losing energy as an emitted photon (Em) producing fluorescence. Each energy state has multiple substates. Thus, a range of excitation wavelengths can excite a molecule to different excited substates, represented by different length upward arrows. Similarly, a range of emitted wavelengths can return a molecule to a substate in the ground state, represented by the downward arrows. These excitation and emission ranges produce spectra of excitation and emission wavelengths. Most molecules initially return to the lowest of excited states by 'internal conversion' or the loss of vibrational energy (wavy arrows).

that the emission wavelength is longer than the excitation wavelength in fluorescence is known as 'Stoke's Law'. The difference between the excitation and emission wavelengths is known as 'Stoke's Shift'. The efficiency of a fluorophore in converting excitation energy to emission energy is the product of two constants – its extinction coefficient (ε) which is a measure of how many incident photons are required to cause an excitation event to take place and its quantum yield (QY), a measure of the probability of fluorescence taking place compared to other methods of de-excitation of the excited fluorophore. The higher this product, the more useful the fluorophore will be.

Excitation And Emission Spectra

Fluorescent molecules are generally excited by a spectrum of wavelengths with a specific bandwidth and shape and emit a similarly shaped spectrum of longer wavelengths. The excitation and emission spectra for fluorescein, a commonly used fluorochrome, are shown in Fig. 2.2. Spectra are mainly the result of the multiple substates within the ground and higher energy levels of a fluorochrome. For example, descent from a slightly higher substate within the excited state to the ground state would result in a shorter wavelength (greater energy) emission, while descent from the lowest excited state to a higher substate in the ground state would result in a longer wavelength (lower energy) emission. Various excitation and emission wavelengths are represented by the arrows of different lengths in the Jablonski diagram (Fig. 2.1). Excitation and emission spectra often overlap. Since excitation light needs to be blocked from reaching the detector, the

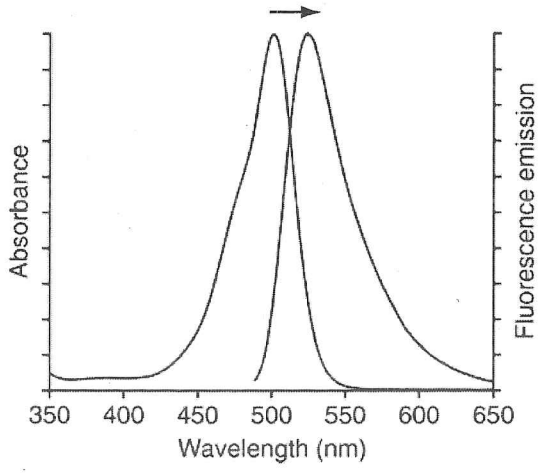

Fig 2.2 ***Normalised excitation (or absorption) and emission spectra for fluorescein.*** The difference between the excitation and emission peaks is the 'Stoke's Shift' (arrow). Excitation and emission spectra often overlap. Upward and downward arrows of the same length in the Jablonski diagram in fig. 2.1 represent this overlap. (fig from www.probes.com)

greater the difference (or Stoke's shift) between the spectra, the easier it is to detect the emission by isolating it from the excitation. Emission light is generally much weaker than excitation light. Thus, the separation of the two is an important consideration to prevent the excitation light from overwhelming the signal produced by the emission and reducing the sensitivity of the system. The spectra are also important factors when conducting experiments with multiple fluorophores. In such experiments, the emission spectra of the multiple fluorophores can be detected separately. For example, fluorescein and propidium iodide (PI) can both be excited by light at 488nm. However, their emission peaks differ: fluorescein emits 530nm light, while PI emits at 630nm. The difference between their Stoke's Shifts enables them to be easily separated by appropriate filters. Alternatively, the fluorophores can be excited by different wavelengths of light. Inadequate separation between the emission spectra or between the excitation spectra would lead to 'crossover' or overlap between the signals from the multiple fluorophores. The overlap between excitation and emission spectra can be made redundant in certain situations when using two-photon laser scanning microscopy, a point that will be revisited later.

Photobleaching and Phototoxicity

An extremely important consideration for *in vivo* imaging is how much photobleaching (loss of fluorescence) and phototoxicity (damage to the specimen) is associated with the

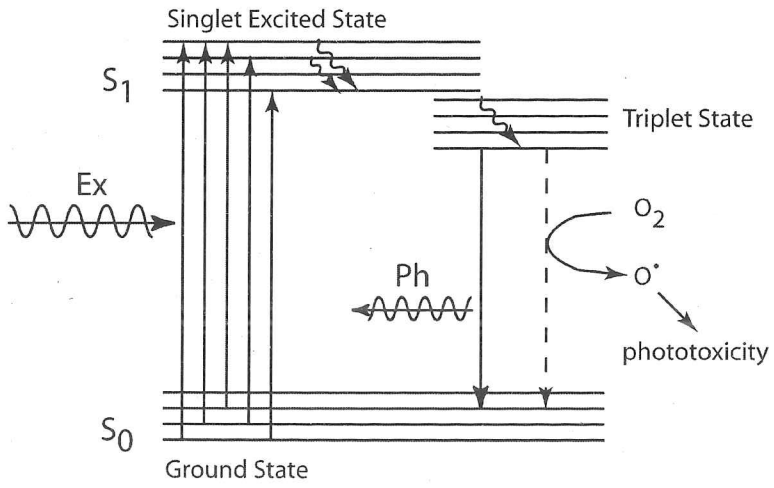

Fig 2.3 *Mechanisms of photodamage.* If a molecule were to undergo 'intersystem crossing' to a triplet state, the probability of returning to a ground state by emitting phosphorescent radiation (Ph) is low. A triplet state will therefore persist until quenched or involved in a chemical reaction. Oxygen readily quenches triplet states and turns into a more reactive singlet state oxygen. This can lead to phototoxicity.

excitation of a fluorophore. Photobleaching is an irreversible loss of fluorescence resulting from the lengthy exposure of a fluorophore to high-intensity light. The mechanism of photobleaching depends on the fluorophore itself as well as interactions with other molecules and fluorophores in its environment. For example, when excited, a fluorophore can move into a different energy state known as a 'triplet state' by 'inter-system crossing' instead of returning to its ground state (Fig. 2.3). Oxygen in the direct environment is converted to singlet state oxygen or oxygen radicals by interaction with the triplet state fluorophore (Yuste et al., 1999). The high oxidative capability of oxygen radicals may be responsible for damage or phototoxicity to the cell containing the fluorophore. Interestingly, green fluorescent protein (GFP), a fluorescent protein isolated from the jellyfish *Aqueorea Victoria,* is more resistant to photobleaching and phototoxicity than many chemical fluorophores (Tsien, 1998). This may be attributed to its structure, as the chromophore (that emits the fluorescence) is shielded from interaction with water or oxygen within a cylindrical protein structure formed by 11 β-sheets. Nonetheless, photobleaching of GFP is still possible with an intense enough light source, particularly if GFP expression levels are low. For *in vivo* imaging, the time and intensity of light that a specimen is exposed to has to be balanced against the amount of photobleaching and phototoxicity that such exposure would cause. Thus, the most efficient optical collecting system possible is required in order to minimise light exposure.

Numerical Aperture

The efficiency of most microscopes, including wide-field, confocal and two-photon excitation laser scanning microscopes, are greatly influenced by the numerical aperture (NA) of the system. The numerical aperture of an objective is a measure of its ability to gather light from a specimen, or in the case of a condenser, the maximum incident angle with which light can be focused onto an area of the specimen. It is defined as

$$NA = n \sin \theta \quad (2)$$

where θ is half the angular aperture subtended by the objective lens (Fig. 2.4) and n is the refractive index of the medium between the objective and the specimen. If we consider imaging a single fluorescent point source in a specimen, the spherical wavefront emitted by the point is diffracted as it passes through the specimen and enters the limited pupil of the objective. The detected image of the point is not a point itself, but rather the diffraction pattern of the point, known as an 'Airy pattern', after work by the astronomer G.B. Airy in 1834. The Airy pattern consists of a central disc (the 0^{th} order maximum) known as the 'Airy disc' surrounded by concentric rings of declining intensity (the 1^{st}, 2^{nd}, 3^{rd} etc. order maxima). The central disc is the most intense part of the diffraction pattern and contains 84% of the light energy emitted from the specimen (Fig. 2.5).

Numerical Aperture and Resolution

The resolution of an objective is the smallest distance that can be distinguished between two points such that they can be said to be separate entities. As the images of the points are Airy discs, two points can only be distinguished if the centres are separated by the

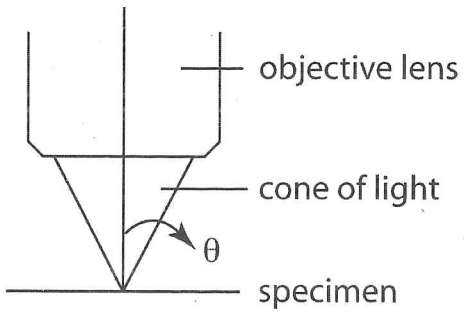

Fig 2.4 ***The numerical aperture (NA) of an objective lens.*** NA is defined as n sin θ, where n is the refractive index of the medium between the objective and the specimen. (Adapted from Yuste et al., 1999)

radius of one disc (Fig. 2.5). This distance is known as the Rayleigh criterion. Thus, the resolution of an objective depends on the radius of the Airy disc produced by that objective. The radius of the Airy disc in turn depends on the NA of the objective. The higher the NA, the smaller the radius of the Airy disc, and the greater the resolving power of the objective. As the image of a specimen is in fact the interference pattern of the diffracted emission from the points that make up the specimen, the higher the orders of diffracted light that can be captured by the objective, the greater the information or detail that can be resolved by the objective. Since higher order diffracted rays are diffracted at greater angles, an objective with a greater NA would be able to capture more higher order rays than a low NA objective, produce a more precise (and smaller) Airy pattern and thus, resolve more detail about the fluorescing points. Mathematically, the Rayleigh criterion (d_0) can be calculated as

$$d_0 = 0.61 * \lambda / NA \quad (3)$$

where λ is the wavelength of the emitted light. The formula also shows that resolution is dependent on wavelength such that lower wavelengths will allow for higher resolutions.

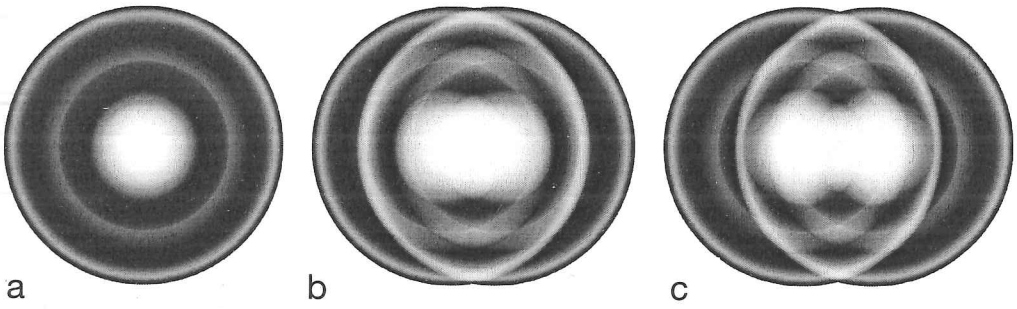

Fig. 2.5 ***The resolution of an optical system is determined by the Airy disc radius.*** **a)** The image of a single point is an Airy disc – a bright central disc surrounded by concentric rings of diminishing intensity. **b)** If two points are too close together (less than the Airy disc radius), they cannot be resolved. **c)** Two points slightly further apart (greater than one Airy disc radius) can still be resolved.

The NA of the condenser that is used to illuminate the specimen is also important for the resolution that can be achieved by the system. If the specimen can be illuminated obliquely, the 0 order rays will be emitted at an oblique angle, but a greater proportion of higher order diffracted rays can be collected by the objective than using only normally angled illumination (Fig. 2.6). This is reflected in the following formula:

$$d_0 = 1.22 * \lambda / (NA_{obj} + NA_{cond}) \quad (4)$$

where NA_{obj} is the objective NA, and NA_{cond} is the condenser NA.

The Rayleigh criterion is a measure of the transverse resolution of the system. For 3-dimensional microscopy, the axial resolution or depth of field of the objective is an important factor. Similar to the Airy patterns in the transverse plane, a point source will have an axial diffraction pattern that will limit the resolution of the objective in the z-axis (δ). This is defined by the refractive index (n), emitted wavelength (λ) and the NA of the objective:

$$\delta = 2n\lambda / NA^2 \quad (5)$$

The greater the NA of the objective, the smaller the axial distance between two points that can be resolved. As the transverse resolution varies inversely with the NA for each transverse dimension and the axial resolution varies inversely with NA^2, the 'volume resolution' of an optical system will vary inversely with NA^4 of the objective. Thus, high NA objectives and condensers will provide better resolutions.

Note that the high axial resolution can be seen as a disadvantage in some situations related to the depth of field. The depth of field is the thickness of the specimen that

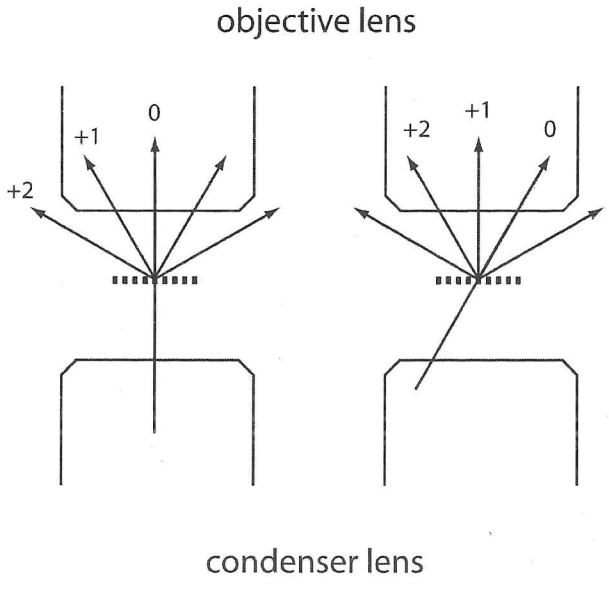

Fig. 2.6 Oblique illumination provided by a higher NA condenser will improve resolution. Higher orders of diffracted light can be captured by the objective if the specimen is illuminated obliquely. Also, smaller diffraction gratings (i.e. objects that are closer together) will cause wider diffractive angles. The use of oblique illumination with high NA condensers allows more widely diffracted light to be captured, so that system resolution is improved (Adapted from Yuste et al., 1999).

appears to be in focus at any one time. A high NA lens will have a shallow depth of field, which can make identification of the area of the specimen to be imaged difficult. It can also produce images with thin sections in focus, while sections above and below are undesirably out of focus. However, this is generally not an issue when using confocal or two-photon excitation laser scanning microscopes, or other optical sectioning methods, where the advantages of using a high NA lens are more significant.

Numerical Aperture and Brightness

Perhaps a more important role played by the numerical aperture of an objective for *in vivo* imaging is its relationship to the efficiency of the objective in collecting light, especially in fluorescence microscopy where the photon flux from the specimen is limited. The larger the aperture of the lens, the more light it will be able to capture coming from a specimen. In fact, it has been shown that the brightness varies approximately with NA^4, and also with $1/M^2$, where M is the magnification of the lens. The variation with magnification can be explained by the fact that higher magnification lenses will collect light from a smaller field of view, containing fewer emitting points that will be spread over the same area of a detector. However, the dependence of optical efficiency on NA means that the highest-NA lens available that is compatible with the application should always be used.

Equation 1 shows the NA also depends on the refractive index of the medium between the objective and the specimen. Air has a refractive index of 1.0, while water is 1.33, glycerol is 1.47 and oil is approximately 1.51 (this varies with manufacturers). Water- or oil-immersion lenses will therefore have higher NAs than non-immersion objectives. Although oil-immersion lenses would provide the highest NA, a specimen in a live imaging application should have a refractive index close to that of water. Refractive index mismatches are a source of optical aberrations in the system (upto 50% in the z-axis), which would produce a misrepresented image of a specimen, so water-immersion lenses are generally used for *in vivo* imaging applications.

One property of lenses that is usually compromised for their high numerical apertures is the working distance. This makes sense, as the closer an objective is to a specimen, the larger the angle of the cone of light emitted that it can capture. However, short working distances make specimens more difficult to work with, particularly when imaging *in vivo*, where specimens can be thicker or the areas to be imaged may be relatively deep. In such

cases, the working distance (as with the choice of immersion media) can be a limiting factor to the choice of available high-NA lenses.

Epifluorescence Microscopy

In epifluorescence microscopy, the objective lens of the microscope is used to illuminate the specimen as well as collect light from the specimen. This design resulted from the difficulty in isolating emission from excitation light in the typical transmitted mode. In the transmitted mode, excitation light originating from a source passes through a condenser in order to illuminate the specimen. Light from the specimen is collected by the objective on the opposite side and sent to the detector. With fluorescence, both emission and excitation light will enter the objective directly after passing through the specimen. Although filters are generally used to block excitation wavelengths, this becomes more difficult the greater the brightness of excitation light compared to emission from the specimen. In epifluorescence microscopy, most of the excitation light passes through the specimen and is lost behind it, while emission from the specimen is collected by the same objective that illuminated it. Any excitation light that is reflected back into the objective will be much attenuated compared to the incident light, and will be blocked by the dichroic filters in the microscope.

Confocal Laser Scanning Microscopy

Although wide-field microscopy is used regularly for *in vivo* imaging, it is not as well suited to 3-dimensional imaging. Emission from a specimen being imaged by wide-field microscopy does not originate purely from the plane of focus of the objective, but also from above and below focus. This extraneous emission comes from excited fluorescent molecules around the focal plane but within the path of the excitation light, and results in blurring of the detected image. Excitation light in a wide-field microscope is made to illuminate the whole field of view evenly, so that the blurring is seen throughout the image. This is not necessarily a problem for the three-dimensional imaging of specimens containing few distinguishable labelled objects with hardly any fluorescence surrounding them, such as individually labelled axons and growth cones. However, it becomes a problem with heavily labelled specimens, perhaps with many objects in which out-of-focus fluorescence prevents them from being distinguishable in three dimensions. To overcome these problems, optical sectioning methods can be used, where thin planes or 'optical sections' can be imaged within the specimen without interference from emission from surrounding tissue. Confocal laser scanning microscopy (CLSM) is possibly the

most commonly used optical sectioning method, and was the starting point for the projects presented in this thesis.

CLSM improves on wide-field microscopy in three areas – contrast, resolution and optical sectioning. Of these, contrast and optical sectioning have been crucial to its use in the live imaging of three-dimensional specimens.

To understand the concept behind laser scanning microscopy, it is useful to understand the concept of the point-spread function (PSF) of an optical system, and its relationship to resolution and contrast. Essentially, the PSF of an objective is the same as the Airy pattern generated by the image of a point source of light, or the pattern generated as light is focused onto a point by that objective. It is the result of diffractive processes on light as it enters or exits the objective. In the focal plane, the PSF looks like the Airy pattern described above, with a bright central disc surrounded by gradually attenuated concentric rings. In 3D, the PSF is hourglass shaped, with the 2D Airy pattern seen at its waist. As with the Airy pattern, the intensity of the PSF is greatest at the centre, and rapidly decreases away from this point. The extent of the PSF is greater in the z-axis than it is in the transverse axis.

The principle underlying CLSM is that at any one time, a single point in the specimen is illuminated, and only emission from that single point is detected. A microscope implementing this principle was originally invented by Marvin Minsky in 1961 (patent no. 3,013,467) and stemmed from his desire to find a way to look at how cells interconnected in dense three-dimensional sections of intact nervous system tissue. By illuminating an array of foci in one plane in series, and detecting the resulting point images, an image of that plane can be built up, exclusive of light scattered from out-of-focus emitting points. The system is confocal because the excitation light path and the emission light path are focused onto the same point and thus focused onto each other (Fig 2.7a). This is a major difference from wide-field microscopy, where the excitation path and the emission path are not confocal. Instead, the excitation light is focused at the back of the objective (the 'back focal plane') such that the specimen is evenly illuminated by it, while the emission light originates from a focal point in the specimen and is ultimately focused onto the detector.

To exclude out-of-focus light, confocal microscopes utilise a pinhole, placed in front of a photomultiplier tube (PMT) detector, in a plane conjugate to the objective focal plane, i.e.

the image of the illuminated point in the specimen is focused onto the pinhole. Emitted rays that make up this image are allowed to pass through the pinhole and reach the detector. The illuminating beam is cone shaped, and although most intense at the focal point, is still intense enough around the focus to excite fluorescent molecules in its path. These molecules would generally contribute to out-of-focus emission, however because they cannot be focused onto the pinhole they are blocked from reaching the detector. The pinhole thus serves to block out-of-focus emission so that only a thin focal plane or optical section is imaged, and also improves contrast by suppressing stray light (including the out-of-focus emission) from reaching the detector.

In theory, the maximum resolution of an optical system is determined by the size of the PSF. As discussed above, two points that generate overlapping PSFs (or Airy discs in two dimensions) will be undistinguishable if the PSFs are closer to each other than the Rayleigh criterion (see equation 3). The image of the focal point that is illuminated is actually the PSF for that point (or diffraction-limited spot) rather than an infinitely small point. Similarly, diffraction effects at the pinhole mean that it acts as a PSF-shaped filter. A PSF in two dimensions can be described by plotting the intensity of light against the distance from the centre (Fig. 2.7b). The central peak corresponds to the bright central disk of the 0^{th} order diffracted rays, while the smaller peaks correspond to the attenuated concentric rings (higher orders). Similarly, the central peak of the pinhole PSF represents the area where all light falling on it is allowed through (the 0th order rays), while the smaller peaks represent the areas where light passing through will be attenuated. When two PSFs are superimposed, the resulting PSF is in fact the product of the two. From the example in Fig. 2.7b, considering the central peaks, 100% of the light from the illuminated point (at 100% intensity) will be allowed through, resulting in a peak of 100%. For the 1^{st} order peaks, only 5% of the light at 5% intensity will be allowed through resulting in a peak of 5% * 5% = 0.25%. For the 2^{nd} order peaks, 1% of light at 1% intensity results in a 2^{nd} order peak of 0.01%. Thus, the shape of the resulting PSF is one where the central peak is at a much higher intensity than the higher order peaks, and is also narrower. Since the resolution of the system depends on the width of this peak (the diameter of the resulting central disc), the use of the pinhole has improved the resolution of the system. Note that this assumes the pinhole size is at the diffraction limit for the emission wavelength. The pinhole size can be varied, and although a small pinhole will enhance resolution and allow less out-of-focus light through, it will also reduce signal

intensity and increase the signal-to-noise ratio of the system. On the other hand, a large pinhole will allow more out-of-focus light to reach the detector and make the resulting image brighter but will also increase depth of field and reduce resolution. In fact, the optimum pinhole size for balancing the signal-to-noise ration with resolution is thought to be 0.75 AU (Wilson, 1989; Yuste et al., 1999).

The illumination of a single plane of focus at a time also plays a role in achieving high contrast and generating thin optical sections from a specimen. By illuminating a single point, fluorescence from the rest of the specimen is prevented from interfering with the image formed by the point being focused on. In wide-field microscopy, this 'flare' is an important limiting factor when imaging very bright and label-dense specimens. One can imagine that if the whole specimen were illuminated, stray light scattered from other points distant from the focus would also pass through the pinhole to the detector, generating erroneous and lower contrast images. Single-point illumination is also the reason intense lasers are used as light sources in confocal microscopy. Very bright excitation light is required to produce enough emission from the single excited point for it to be detected quickly. Speed is important in order to scan all the desired points on a specimen in a reasonable amount of time.

As only one point in the specimen is illuminated at a time, any light reaching the detector is assumed to have originated from that point. Thus a sensitive PMT detector is used rather than the digital CCD or film cameras generally used in epifluorescent microscopes. All the signal detected by the PMT is assigned to the part of the specimen being scanned at the time of detection. This allows low levels of fluorescence and small yet rapid changes in fluorescence to be detected. It also provides some flexibility in the pixel density of the image (or how often the field of view is sampled by the illuminating laser) as the laser can be set to scan the field of view at a desired pixel density.

In order to implement the simultaneous excitation and detection of single points in the specimen and to collect the image data from these points to build up images, a method of scanning the specimen is generally used. One relatively simple method is to scan the specimen under a fixed light path, however this can be relatively slow and impractical depending on the apparatus used to mount or keep the specimen alive. Typically, a pair of mirrors is used to direct the excitation laser beam reflected by a dichroic mirror onto a point on the specimen (Fig. 2.8). Emitted light from that point is returned via the same pair of mirrors (a process called descanning) to a dichroic mirror that allows the light to reach the detector. This maintains the 'confocality' of the system as mentioned above. The mirrors are mounted on galvanometers such that one mirror scans the X-dimension while the other scans the Y-dimension of the field of view. A computer controls the mirrors to scan the laser across the specimen in a line-by-line raster pattern. Emitted light from all the points is put together by a computer to produce an optical section, a 2D image of the scanned focal plane. The objective or the stage are driven by a motor to move the laser beam in the z-axis of the specimen so that images from multiple focal

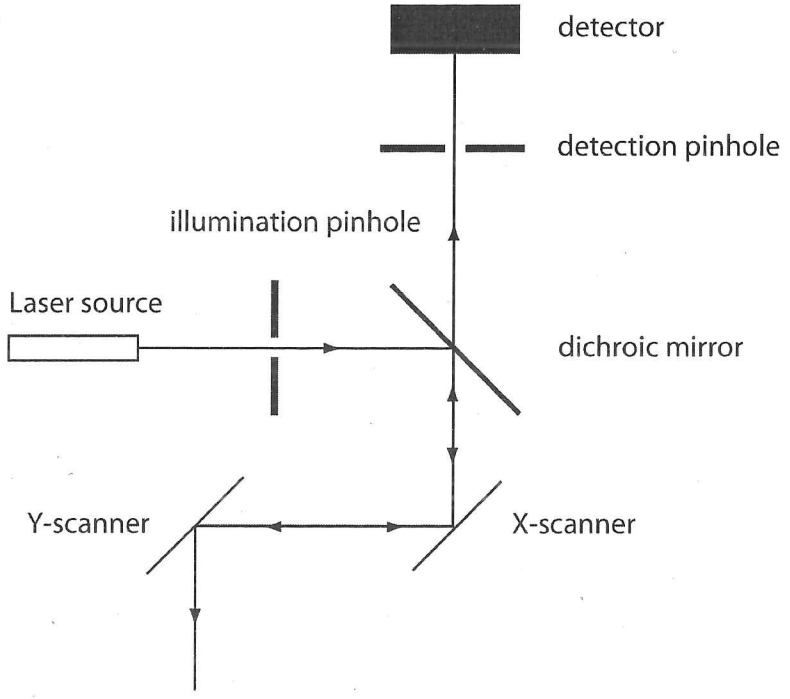

Fig. 2.8 ***Diagram of the scanning typically used in many confocal microscopes.*** Excitation light is directed onto a particular point in the focal plane by the X- and Y- dimension scanning mirrors. Emitted light from the same point returns by the same path to reach the detector. It is said to be 'descanned' (Adapted from Yuste et al., 1999).

planes can be captured at precise intervals. These optical sections can then be put together to produce a 3D representation of the specimen. Thus, the confocal laser scanning microscope is an extremely useful tool to generate 3D representations of samples without necessarily having to fix or physically invade them.

Problems with CLSM

There are still some limitations to the use of confocal laser scanning microscopy. Part of the problems arise from the way the intense laser beam affects the tissue being imaged, while others arise due to the properties of the tissue itself. As the laser is focused onto a point, it also excites fluorescent molecules in its path outside the focal plane. Although the emission and scatter from these points is mostly dealt with by using the detector pinhole, the excitation of these points creates other problems. First, fluorescent molecules have a maximum emission rate and the intensity of emission from a fluorophore will initially increase with excitation intensity but plateau as it saturates. Saturation can easily occur at the laser intensities that are used in confocal microscopes. However, increasing the intensity beyond the saturation point may still seem to brighten the image. This is because fluorescent molecules outside the focal plane, where the laser intensity will be lower than at the focus, are being increasingly excited thus contributing more signal to the image. One should therefore always be wary of using high laser intensities as very little benefit can be realised at the focal plane. More importantly, prolonged or repeated excitation of a fluorophore will lead to it bleaching – indefinitely losing its capacity to fluoresce. The probability of a fluorescent molecule to be excited to a triplet state by inter-system crossing is low (for example, 30-fold lower than normal excitation for fluorescein), however the lifetime of the triplet state lasts longer (μseconds) than the normal excited state (nanoseconds.) This leads to an accumulation of triplet state excited molecules with prolonged excitation and an inability to emit light. Prolonged excitation for one fluorescent molecule is well within the time a single pixel is excited by the confocal laser, thus this accumulation occurs under normal conditions of use. Triplet state molecules do not emit fluorescent light and are wasted as far as imaging is concerned. Furthermore, they cause the formation of free radicals that contribute to photobleaching of the molecules and toxicity to the specimen tissue. Just as the fluorescent molecules outside the plane of focus are excited and contribute more noise to the detected signal, they are also bleached and contribute to phototoxicity by virtue of the same excitation. In the context of three-dimensional *in vivo* imaging, which involves repeated scanning of the

same specimen over time, the photobleaching and phototoxicity around each focal point can severely limit the application of CLSM. Photodamage is an expense for which no benefit is recouped – the emission generated by those surrounding molecules has to be rejected by the pinhole in front of the detector.

To understand the extent of the problem, one can consider a single focal plane being imaged and sections above and below this plane in the specimen. The probability of absorption (Abs.) of a photon (and thus of emission or of a photochemical reaction) is directly proportional to the intensity (I) of the laser.

$$\text{Abs.} \propto I \tag{6}$$

The intensity itself is inversely proportional to the area (A) that the excitation is spread over while the area is proportional to the square of the distance from the focus (z)

$$I \propto 1 / A \text{ and } A \propto z^2 \tag{7) and (8}$$

$$\therefore \text{Abs.} \propto 1 / z^2 \tag{9}$$

Thus, a point on a section away from the focal point is less likely to absorb a photon. However, this same point will be exposed to the scanning laser beam for a time proportional to the area of excitation corresponding to its section. As the laser scans the specimen, this particular point has an equal probability of absorbing a photon to the focal point. On average, it absorbs photons to the same extent as the focal point even though it is not in focus – the drop in intensity in the broader parts of the beam is offset by the area covered by the beam. This means that the entire thickness of the specimen is continuously being affected by photochemical changes, such as bleaching, caused by excitation as the laser scans through it. Although chemicals such as DABCO and other anti-fading reagents are available to reduce the effects of photobleaching and toxicity, these work by reducing oxygen levels in the tissue and are not useful for live specimens.

Finally, confocal laser scanning microscopy runs into difficulties when the specimen under examination is thick and the tissue is highly scattering, such as thick brain slices or lens tissue. Lasers have a limited penetration, dependent on the density of the tissue and the wavelength of the laser. In my experience, the limit for confocal microscopy has been around 100μm with zebrafish retina. A reasonable signal at depth is possible with high intensities but this must again be compromised for photodamage to the specimen and fluorophores. Scattering is part of the problem. Both incident and emitted light are

scattered in practically random directions by any molecules in the tissue. Light is scattered more than it is absorbed. Unfortunately, this is another place where light is wasted. Incident light, when scattered, is likely to excite fluorescent molecules outside the focal point. Emissions from such points is not useful for the signal that will make up the image and will be rejected by the pinhole. Emission light from the focal point, once scattered, can no longer be correctly attributed to the focal point and, for all intents and purposes, is the same as out-of-focus light. It is therefore also rejected by the pinhole. Overall, with out-of-focus light rejection by the pinhole and scattering in the tissue, one estimate suggests that 99% of the fluorescent light generated by a thick specimen is wasted (Yuste et al., 1999).

The potential to visualise and experiment on dynamic processes in intact tissue, and the flexibility provided by the prolific amount of fluorophores now available, have pushed confocal laser scanning microscopy to its limits. A new development from the last decade is helping to push these boundaries further – the two-photon excitation laser scanning microscope.

Two-Photon Excitation Laser Scanning Microscopy

Two-photon excitation laser scanning microscopy (TPELSM) directly tackles the greatest limitation of confocal laser scanning microscopy – the excitation of out-of-focus molecules. As described above, this is the reason the pinhole is required in confocal microscopes. If the focal point could truly be excited in isolation, as occurs in TPELSM, there would be no need for a pinhole to block out-of-focus light and scattered light could also be collected increasing the efficiency of the system. Of course, TPELSM introduces its own problems. The theory behind TPELSM and how it improves on confocal microscopy is described below. This is followed by a description of the confocal/two-photon excitation laser scanning setup used in most of the experiments in this thesis and a discussion of my practical experiences with the instrument. Not all of these matched the theory – possible reasons for this and further changes that could be made to such a setup are also discussed.

The Basis of TPELSM

TPELSM is based on the fact that the energy required to excite an electron orbiting a fluorescent molecule from its ground state to its excited stated can be provided by two photons, each providing half the energy required. Two-photon excitation, as this phenomenon is called, was described theoretically by Maria Goeppert-Mayer (the second woman to win a Nobel prize) in 1931. Her results were proven experimentally in 1961 with the development of the first laser, a ruby laser that emitted long wavelength light. The realisation that two-photon excitation events could be exploited for fluorescence microscopy came in the late 1970s (Diaspro, 1999), while the development of the two-photon laser scanning microscope occurred in 1990 (Denk et al., 1990).

Two-photon excitation has the same effect on the fluorescent molecule as single-photon excitation, the process described earlier as the basis for the emission of light from fluorescent molecules. When the electron returns to the ground state from the excited state, it emits a photon with a wavelength equivalent to the energy lost on its return. Thus, although the excitation process of the fluorescent molecule is different, the emission wavelength will be the same. This is illustrated in the Jablonski diagram in Fig. 2.9. As the energy required per photon is about half that required for single-photon excitation, lasers used for two-photon excitation are generally in the 650 to 1000nm range (near infra-red and infra-red light) – around double the wavelengths used in confocal

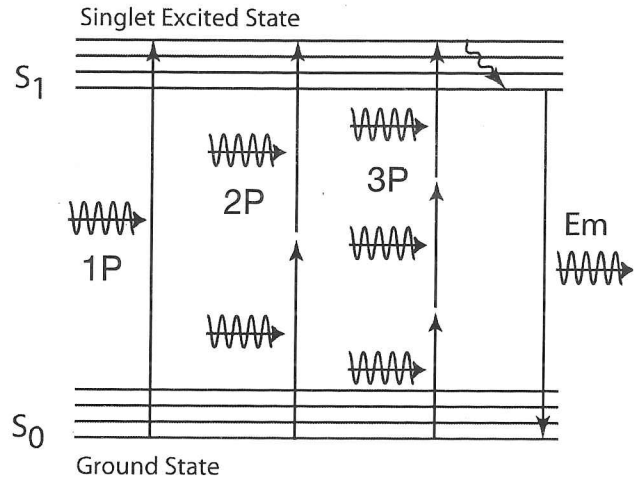

Fig. 2.9 ***A Jablonski diagram representation of multi-photon events.*** Two-photon excitation (2P) events occur when two photons of approximately half the wavelength used to excite a fluorophore by single-photon excitation (1P), excite a fluorophore at almost the same time. Similarly, three-photon excitation (3P) can occur when three photons of one-third that wavelength excite a fluorophore at the same time.

microscopes. The movement of an electron to an excited state is an extremely short event occurring on a femtosecond (10^{-15} s) timescale. For two-photon excitation, two photons are required to excite the same molecule within this short timescale, an event possessing a very low probability. This low probability is the basis for the ability of two-photon excitation lasers to exclusively excite molecules in the volume of the focal point. In terms of distance from the focus (z), equation 9 still applies, such that the intensity of the laser is inversely proportional to the square of the distance z. However, the probability of absorption of two photons is proportional to the square of the intensity:

$$\text{Abs.} \propto I^2 \qquad (10)$$

Thus, the probability of absorption is inversely proportional to the fourth power of the distance from the focus:

$$\text{Abs.} \propto 1 / z^4 \qquad (11)$$

This is a rapid decay in probability of absorption from the focus and even with the wider area covered by the beam, and thus a longer overall exposure to it, the requirement for an extremely short spatial and temporal interval between two photons for the excitation of one molecule makes it an unlikely event in sections above and below the focus. This means that any emission from the specimen after excitation with an infra-red wavelength laser can be assumed to have originated from the focal point, even if it consists of photons

scattered in the tissue of the specimen or endogenous fluorescent molecules. The pinhole becomes unnecessary and more photons can be detected to make up the signal that makes up the image. The system becomes more efficient than the confocal system (Yuste et al., 1999), while the image generated of the scanned focal plane is a reliable representation. One need not worry about emission produced by scattered incident light, as this light would be too 'dilute' of photons to be able to cause two-photon excitation events. In practical terms, many two-photon laser scanning microscopes are added onto or converted from confocal microscopes. As described above, the focal emission in confocal microscopes is descanned via the scanning mirrors to be focused onto the pinhole. Just as the pinhole is unnecessary, so is the descanning process. A more efficient way to collect emitted photons from the specimen is to have 'non-descanned' detectors (similar to transmitted light detectors) as close to the specimen as possible. The shorter the light path to the specimen, the fewer photons are lost on the way. Thus detectors on the condenser side of the specimen can be used for photon detection in addition to those on the objective side. Adding the signal from both of these will improve the signal to noise ratio.

Scattering and Depth Penetration

Another advantage of TPELSM is that the excitation wavelengths used are relatively long. Scattering depends on the size of particles relative to the wavelength of light being scattered such that long wavelengths are scattered less than short wavelengths. For small particles, such as molecules in cells, scattering efficiency (S) is inversely proportional to the fourth power of the wavelength (λ).

$$S \propto 1 / \lambda^4 \qquad (12)$$

With increased scattering within a material, the intensity of light will decrease as it traverses it, a phenomenon known as extinction. The longer wavelength light used in TPELSM is scattered less than CLSM laser light according to equation 12. Thus, there is less extinction of the laser in TPELSM and greater penetration into the tissue.

Photodamage

Avoiding fluorescence emission from being generated by out-of-focus molecules means that any photochemical interaction with those molecules is avoided. This includes those that lead to photobleaching and phototoxicity. In two-photon laser scanning microscopy, the damaging reactions still occur but only at the focal point being scanned (Koester et

al., 1999; Konig, 2000; Maiti et al., 1997). The rest of the specimen is not affected by the infra-red or near infra-red radiation. This translates into the following: the thicker the section of specimen and the longer it is scanned, the less average damage there would be as compared to the same extent of scanning by confocal microscopy. Thin specimens may be damaged by as much, if not more, as using CLSM. Damage to the specimen using TPELSM increases in a non-linear way with excitation intensity (Hopt and Neher, 2001; Koester et al., 1999). Over a certain intensity threshold, within the range expected to be safe for living tissue, cells being imaged can show morphological and biochemical signs of damage. Thus, the intensity of the laser used in TPELSM experiments needs to be carefully regulated to avoid damage. Below this threshold, cells were as viable as control cells.

The benefits of using TPELSM over CLSM for *in vivo* imaging of thick specimens become obvious, as photochemical reactions are the main limiting factors in imaging such specimens over the long term. Given the advantages of TPELSM —increased detection efficiency, usefulness of scattered emission, less overall photodamage and phototoxicity and better depth penetration—t this method of microscopy comes unto its own when used on **thick** and **scattering** specimens. The thicker and more scattering the specimen, the more useful TPELSM will be over CLSM or wide-field microscopy. This is an important point when considering applications suitable for TPELSM. Experiments on thin sections or cell culture systems may not be able to exploit the advantages that come from two-photon excitation, and the disadvantages of TPELSM may become more significant. TPELSM and photodamage is discussed further below.

Resolution

The resolution of two-photon laser scanning microscopes is not higher than ideal confocal microscopes. Theoretically, the resolution is a function of the wavelength being used (see equation 3). Since the wavelengths used are about twice as long as those used in confocal microscopes, one would expect the resolution of TPELSM to be lower. However, the pinhole in CLSM is rarely used at a diffraction-limited size, which would be required to benefit in terms of resolution. Aberrations and other imperfections in the light path that increase the scatter of emitted photons also reduce resolution. These do not affect the collection efficiency of two-photon laser scanning microscopes significantly, so that the real resolution loss is not necessarily significant. Of course, how significant the loss in

resolution might depend on the application. Note that aberrations in the incident light path still affect the performance of the system (Neil et al., 2000).

Fluorophores

One aspect that has helped two-photon laser scanning microscopy gain acceptance among biologists is that the same fluorophores can be used as in confocal laser scanning microscopy. In theory, simply using an excitation wavelength double that normally used should be enough to enable a fluorophore to emit fluorescent light. However, experience has shown that the behaviour of fluorophores in terms of their excitation is not straightforward to predict under TPELSM (Xu et al., 1996). The peak excitation wavelength required for many common fluorophores is actually blue-shifted (or shorter) than double the single-photon excitation wavelength. For example, fluorescein, normally excited at 488nm, is maximally excited by approximately 800nm in TPELSM. This blue-shift in expected excitation wavelengths can be seen as an advantage. Currently, the more commonly used Ti:S infra-red laser can be tuned between about 700nm and 1000nm, with the most power available between 750nm and 850nm, although this depends on the mirror sets and optics installed within the laser cavity. The blue-shift means that more fluorophores will be accessible using the Ti:S laser than if their peak excitations had been greater, as fluorophores with excitation peaks above 500nm would have been difficult to excite. Work on determining the excitation spectra (also known as the absorptional cross-section) of fluorophores under TPELSM has shown that these spectra tend to be very broad. This means that a single wavelength could be used to excite multiple fluorophores. For example, Xu et al. used an excitation wavelength of 705nm to image cells labelled with four different fluorophores in four compartments: pyrene for the plasma membrane, DAPI as a nuclear stain, bodipy sphingomyelin as a golgi stain and rhodamine 123 for mitochondria. In confocal microscopy, it is likely that at least three different laser lines (351nm, 514nm and 568nm) would have been required, making this a more complex and possibly slower process. An additional benefit of using long wavelength excitation is that the excitation and emission spectra are better separated, which simplifies the filtration of emission light to the detector. The whole emission spectrum can be used to detect fluorescent emission without having to worry about excitation light being detected, helping to increase the collection efficiency further.

Autofluorescence is the fluorescence that emanates from endogenous molecules in cells such as flavins and NADH. Yolk cells in xenopus and zebrafish embryos are also heavily autofluorescent. Autofluorescence is generally undesirable if a fluorescent probe is being used to target the cells or specific parts of cells unless the power required to cause specific emission is less than that required to generate autofluorescence. However, it has also been used experimentally with NADPH fluorescence as well as to measure redox reactions in cells of rabbit corneas (Piston et al., 1995). NADPH autofluorescence would require short wavelength UV lasers for excitation, however such lasers are very damaging to living cells. Instead, by using TPELSM, oxidative changes could be monitored in these cells over time. TPELSM has no intrinsic advantage over CLSM in terms of undesirable autofluorescence, other than preventing autofluorescence from being generated from regions out of the plane of focus that would affect the background in resulting images. Autofluorescence that existed in the same optical section as the object being imaged would not be eliminated unless the molecules causing the autofluorescence had not been excited by the IR wavelengths used in TPELSM. In fact, due to the broad excitation characteristics of IR lasers, autofluorescence is more likely to be generated by TPELSM compared to CLSM, which generally has narrower excitation spectra.

Laser Source

In part, TPELSM has only become feasible due to technological advances made in scanning and laser technology. The properties of the laser used in TPELSM are crucial to its operation. Very high laser intensities are required to produce a reasonable and useful probability of two-photon excitation events occurring at the focal point. These are of the order of kW or MW per cm^2. Such intensities would be destructive to the specimen if delivered continuously. To get around this, mode-locked (a technique to produce very short laser pulses) pulsed lasers are used with very short pulse durations, between 100 fs to 10 ps, pulsing at frequencies around 100Mhz, with each pulse with a high peak intensity of, say, 0.1kW. The average power from such lasers is fairly low in the mW range, a more feasible range for live specimens (Konig, 2000):

Pulse peak power * pulse duration * frequency = average power (13)

10^2 W / cm^2 * 10^{-12} sec * 10^8 Hz = 10^{-2} W / cm^2

In reality, the actual power at the specimen will be much lower due to losses in the light path through the microscope. Pulsed lasers with such short pulse durations and

appropriate wavelengths have only become available commercially in the last decade. They are still expensive, perhaps prohibitively so, for many research groups. Further development of cheaper laser sources will be important if TPELSM is to become a widely used tool.

Microscopy and Specimen Preparation

The following section describes the system that was used for the experiments in this thesis. Slight modifications were made to the system by the manufacturers over the course of experimentation to help improve the system's performance, however, being a commercial multi-user system, some desirable modifications could not be made.

Microscopy

A Leica DM-IRBE inverted microscope was used with a Leica TCS-SP scanhead. The scanhead contains the scanning apparatus and 4 PMT detectors. Rather than using regular filters with fixed properties in front of the detectors to filter the emission light, the scanhead contains a prism spectrophotometer detector system. This allows the emission wavelengths to be detected by each PMT to be specifically chosen, permitting more flexibility in detection. For two-photon microscopy, these detectors are not optimal as any light reaching the detectors has to pass through the pinhole designed for confocal emission, and has a long light path through numerous lenses and mirrors resulting in a significant loss of photons. Note that the confocal pinhole can be an advantage if the specimen is very bright, as image resolution can be improved by reducing its diameter. A transmitted light detector for use with two-photon excitation was later added behind the condenser of the microscope. Although the signal to noise was greatly improved, only a longpass filter was available to block the long wavelength excitation light, and only single colour emission could be detected, even if the descanned detectors were used in combination. Another disadvantage with the transmitted light detector was that in this implementation, the light path was not fully enclosed. Thus any background light in the room would affect the sensitivity of the detector. To avoid this, the microscope needs to be covered with a black sheet during scanning, and all sources of light in the room switched off, including mercury vapour lamps and, if possible, computer displays. Four lasers were attached to the microscope: a He/Ne laser providing a 633nm laser line, an Argon laser providing 458, 476, 488 and 514nm lines, a Kr laser providing a 568nm laser line and a Ti:S pulse laser providing an infra-red range from 700nm to 870nm initially and eventually 720nm to 980nm for two-photon microscopy. The objective lens used for all experiments was a Plan Apochromat 63x 1.2NA water immersion lens with a 225μm working distance and a correction collar for use with different thickness cover slips. This particular lens was chosen as having the best combination of desired features, namely a

high NA with a long working distance. The 'Plan' and 'Apochromat' designations signify that the lens corrects for spatial and chromatic aberrations. Because the specimens to be imaged were live zebrafish embryos, a water-immersion lens was chosen over oil immersion lenses, as the refractive index of live specimens are considered to be close to that of water (1.33). In addition, despite their high NAs, oil immersion lenses have very short working distances. In my application, where a zebrafish retina was being imaged in three-dimensions, with the zebrafish lying laterally under a coverslip, the short working distances were impractical. Oil-immersions lenses would touch the coverslip, compressing the specimen before the total desired depth had been imaged in addition to causing a refractive index mismatch. The magnification of the lens (at 63X) was a slight drawback, with the field of view (158μm square) unable to cover the whole of a 1-day-old zebrafish retina. However no lower magnification lenses (40X) could be found with a high NA and a long working distance. The NA of 1.2 is close to the theoretical maximum NA of water-immersion lenses (1.33) and is probably at the practical limit of economically feasible lenses currently available. Initially, a 40x dry lens was used due to its long working distance, however compared to the 63x water-immersion lens, the intensity of the signal was low, thereby requiring higher intensities to image specimens.

Specimen preparation

The preparation of the zebrafish embryos for *in vivo* imaging was based on methods described in the zebrafish book (Westerfield, 1993) but naturally evolved over time to accommodate requirements of the specific microscope setup and to solve problems that revealed themselves during the acquisition or analysis of data. The imaging experiments were intended to run between 10 hours and 48 hours. Long term imaging of embryos requires that a stable environment be provided for the embryo that mimics the environment that it would normally grow in. This includes: a constant temperature, an appropriate pH and ionic concentration of the embryo's environment, oxygenation and space for the embryo to grow. Simultaneously, the mounting method must maintain the position of the embryo stable in three dimensions especially with the high magnifications used.

Labelled and dechorionated zebrafish embryos are placed in a mounting solution containing salts and at a pH of 7.4, based on the embryo growth medium normally used to raise them. The solution also contains a low concentration (0.2%) of low melting point

agarose and MS-222, an anaesthetic. The anaesthetic prevents muscle twitches in the embryo although it does not stop heart muscle from beating. High concentrations of MS-222 are damaging to embryos. The low concentration agarose helps to keep the embryo in one position. Higher concentrations seem to prevent growth, as embryos released after 24 to 48 hours are stunted compared to unmounted siblings. Lower concentrations are unable to prevent embryos from moving once the effect of the anaesthetic has worn off (generally after 24 hours of use). The embryos themselves are mounted in a very small drop of the mounting solution. This allows the agarose to form a gel quickly and also provides sufficient oxygen to the embryo by allowing for air-filled space around it. It also enables three to four embryos to be mounted in one dish. 32mm petri dishes are used with the bottom replaced by a no. 0 coverslip. The thinnest possible coverslip is used to minimise the amount of glass between the specimen and the lens. This is a compromise to increase the available working distance and reduce pulse attenuation of the IR laser at the expense of resolution, as the lens itself is corrected for thicker no. 1 coverslips. Despite the use of agarose, vertical movement of the embryo can still occur as the embryo stabilises within the agarose drop. To prevent this, another coverslip is used above the embryo, such that the thickness of the embryo fills the space between the two, without it being squashed. Finally, the 32mm petri dish is placed in a heated stage on the microscope. A temperature probe measures the temperature of water in the dish, above the top coverslip, and feeds back to the thermostat controlling the temperature of the stage.

Comparing TPELSM with CLSM

Prior to the installation of the two-photon laser scanning microscopy system, the confocal system was used for experiments in imaging zebrafish embryos. A few fluorophores or vital stains had been found that were useful for *in vivo* imaging, however it was not known whether these would be usable under two-photon laser scanning microscopy. Bodipy FL C5-Ceramide and GFP were two fluorophores found to be usable under TPELSM, but with slightly different results. They became a useful way of making basic but practical comparisons between CLSM and TPELSM.

A useful vital stain for *in vivo* imaging has several characteristics. It must be relatively easy to load into the specimen, without causing damage; it must be efficiently visualised by the imaging mode used and under the growth conditions required for the specimen; it must not affect the development of the specimen or produce artefacts during the imaging process and it must reliably label known cellular or tissue compartments. Although a very wide range of fluorescent chemicals exists, many are unsuitable for *in vivo* experiments. Of those that are used *in vivo*, the majority are designed for use in cell culture, where most cells can be exposed to the dye-containing medium directly, either by diffusion, active cellular processes such as endocytosis, or by the use of specialised techniques such as electroporation. For whole embryos, the presence of epithelial tissue can make the penetration of chemicals by diffusion difficult. For example, Hoechst 33342 (Molecular Probes, Oregon) is a cell-permeant stain that emits blue fluorescence when bound to dsDNA, and is used extensively for counterstaining histological slides as well as cells in culture. In an attempt to stain the intact retina of 1dpf zebrafish embryos with Hoechst 33342, only nuclei in the most superficial cell layers could be labelled, even at the limits of solution concentration and time in solution that were compatible with viable embryos. The retinas of wholemount, fixed embryos have been successfully stained however (B. Payer, personal communication). Finding useful vital dyes for *in* vivo, whole embryo experiments is largely a matter of trial and error. Additionally, the use of many fluorescent dyes with confocal laser scanning microscopy is extensively documented while much less experience has been accumulated for the use of dyes with two-photon laser scanning microscopy (Xu et al., 1996).

Fluorophores

Bodipy Ceramide

One dye that held potential for *in vivo* experiments using laser scanning microscopy was Bodipy FL C_5-Ceramide (Molecular Probes, Oregon). Its use in zebrafish embryos was described by Cooper et al. (Cooper et al., 1999). It is applied by simply bathing embryos between 4 and 6 hpf in a relatively high concentration of the dye in DMSO, an organic solvent, for a limited time (about 3 to 6 hours), allowing the dye to diffuse into the embryo. It is often used to label the Golgi apparatus of cells in culture. Indeed, in zebrafish, it initially stains the plasma membrane, Golgi apparatus and cytoplasmic particles of the most superficial cells of the embryo. However, once it diffuses through the superficial cell layer, it is compartmentalised to the interstitial space. Here, the dye diffuses freely between cells throughout the embryo and creates an outline of all embryonic cells (see Fig. 2.11 and 3.1). Interestingly, it does not seem to label blood cells seen in the embryonic circulation. Because of free diffusion of the dye, bleached molecules can be exchanged with unbleached molecules during imaging experiments, making this a robust vital stain for use in laser scanning microscopy. Under confocal laser scanning microscopy, a 488nm laser line is used to excite the dye and emission is detected in the range of 510nm to 550nm. The actual excitation maximum for Bodipy FL C_5-Ceramide is 504nm. One would expect the two-photon excitation wavelength to be about double the single-photon excitation wavelength or half its energy, i.e. approximately 1000nm. Although the IR laser could only be tuned between 720nm and 980nm, we found the best two-photon excitation to actually occur between 730nm and 780nm. The two-photon excitation spectra for many fluorescent dyes have shown a blue-shift (i.e. shorter wavelength) compared to the expected doubled wavelength, however the reasons for this remain unexplained (Xu et al., 1996). The extent of the blue-shift and the actual excitation are so far not predictable simply by looking at the single-photon excitation spectra. We also found that the intensity of emission from the two-photon excitation of Bodipy FL C_5-Ceramide was lower than when using single-photon excitation (Fig. 2.11). The two are relatively difficult to compare directly, as the excitation energy at the sample could not be measured with our setup. The comparison was made by using the highest laser power levels for both single- and two-photon lasers that did not cause any obvious damage to the specimen over 4 to 5 hours, as well as imaging parameters that are normally used for Bodipy FL C_5-Ceramide labelled

Fluorophores

Bodipy Ceramide

One dye that held potential for *in vivo* experiments using laser scanning microscopy was Bodipy FL C_5-Ceramide (Molecular Probes, Oregon). Its use in zebrafish embryos was described by Cooper et al. (Cooper et al., 1999). It is applied by simply bathing embryos between 4 and 6 hpf in a relatively high concentration of the dye in DMSO, an organic solvent, for a limited time (about 3 to 6 hours), allowing the dye to diffuse into the embryo. It is often used to label the Golgi apparatus of cells in culture. Indeed, in zebrafish, it initially stains the plasma membrane, Golgi apparatus and cytoplasmic particles of the most superficial cells of the embryo. However, once it diffuses through the superficial cell layer, it is compartmentalised to the interstitial space. Here, the dye diffuses freely between cells throughout the embryo and creates an outline of all embryonic cells (see Fig. 2.11 and 3.1). Interestingly, it does not seem to label blood cells seen in the embryonic circulation. Because of free diffusion of the dye, bleached molecules can be exchanged with unbleached molecules during imaging experiments, making this a robust vital stain for use in laser scanning microscopy. Under confocal laser scanning microscopy, a 488nm laser line is used to excite the dye and emission is detected in the range of 510nm to 550nm. The actual excitation maximum for Bodipy FL C_5-Ceramide is 504nm. One would expect the two-photon excitation wavelength to be about double the single-photon excitation wavelength or half its energy, i.e. approximately 1000nm. Although the IR laser could only be tuned between 720nm and 980nm, we found the best two-photon excitation to actually occur between 730nm and 780nm. The two-photon excitation spectra for many fluorescent dyes have shown a blue-shift (i.e. shorter wavelength) compared to the expected doubled wavelength, however the reasons for this remain unexplained (Xu et al., 1996). The extent of the blue-shift and the actual excitation are so far not predictable simply by looking at the single-photon excitation spectra. We also found that the intensity of emission from the two-photon excitation of Bodipy FL C_5-Ceramide was lower than when using single-photon excitation (Fig. 2.11). The two are relatively difficult to compare directly, as the excitation energy at the sample could not be measured with our setup. The comparison was made by using the highest laser power levels for both single- and two-photon lasers that did not cause any obvious damage to the specimen over 4 to 5 hours, as well as imaging parameters that are normally used for Bodipy FL C_5-Ceramide labelled

specimens. Along with unexplained behaviour under TPELSM, the lower Bodipy FL C_5-Ceramide emission intensity may be due to the effect of two-photon excitation on eliminating background excitation away from the plane of focus. By accepting a limited amount of the extra-focal emission produced in single-photon excitation, the extra signal can contribute to the image detected by CLSM without causing much blurring if the specimen changes very little in the axial or z-dimension. Since this cannot occur under TPELSM, the confocal image may seem brighter. Interestingly, embryos labelled with both Bodipy FL C_5-Ceramide and Green Fluorescent Protein (GFP) highlight the difference in behaviour between CLSM and TPELSM (Fig. 2.10b). With CLSM, a weak GFP signal could not be detected while the Bodipy signal is very bright. In contrast, under TPELSM, both GFP and Bodipy could be detected simultaneously, although Bodipy is less intense. This could mean that Bodipy is better used with CLSM while GFP is more efficiently excited by TPELSM or simply confirms the broad excitation characteristics of TPELSM. Thus, the behaviour of fluorescent dyes under single-photon excitation cannot be used to reliably predict their behaviours under two-photon excitation.

GFP

Green Fluorescent Protein has, fortunately, been found to be relatively useful with TPELSM. GFP is a fluorescent protein that was discovered in the jellyfish *Aequorea victoria*, and has recently become extremely popular as a versatile fluorescent probe or reporter gene (Tsien, 1998). It fits almost all the criteria that are sought in an *in vivo* probe as described above. As GFP is used as a gene that is allowed to be translated into the protein by the target cell or organism's own transcriptional and translational machinery, it can be delivered by any gene delivery method, such as microinjection or electroporation, without damaging the cell or organism. Its versatility comes from the ability to engineer reporter constructs consisting of specific promoter and enhancer elements driving the expression of GFP in a targeted manner, as well as the creation of fusion proteins without affecting the function of the target protein or GFP itself (Kanda et al., 1998). Integration of the gene or reporter construct into the genome of the target cell or organism can be used to produce inherently fluorescent transgenic cell lines and animals (Higashijima et al., 1997). Although GFP can be sensitive to pH and temperature, it functions well under normal cellular conditions of close to neutral pHs and temperatures ranging from 15 to 37°C. The structure of the protein, with the chromophore on an α-helix contained within a cylinder formed of 11 β-sheets, protects the

chromophore from solvents and O_2 in the environment that would affect its fluorescence. GFPs are, therefore, relatively resistant to photobleaching. A large number of mutations introduced into the wild-type GFP have produced versions that are more suitable for use in eukaryotic cells (Reilander et al., 1996), that are brighter (Cormack et al., 1996) and that have different properties, such as different spectral excitation and emission properties (i.e. different colours) (Heim and Tsien, 1996) or enhanced sensitivity to environmental factors such as pH (Llopis et al., 1998) or Ca2+ levels (Miyawaki et al., 1999; Miyawaki et al., 1997).

The great versatility of GFP and associated fluorescent proteins probably make this family the single most versatile set of fluorescent probes for *in vivo* imaging experiments. Harnessing the advantages of TPELSM, especially for long-term imaging, would be extremely useful for GFP-based experiments. GFP has been shown to work under TPELSM previously (Potter, 96) however different GFP mutants are maximally excited by different IR wavelengths (as is the case for single-photon excitation). In my experience, GFP was found to be maximally excited by wavelengths around 850nm. The reported excitation maximum of GFP under TPELSM is thought to be 930nm (Xu et al., 1996), however this wavelength was unattainable with the available IR laser. The expression of GFP has to be fairly strong in the first place and although this was not quantified, it became obvious only when transgenic zebrafish expressing different levels of GFP became available. The first experiments with GFP expressing transgenic embryos involved transgenics known as 'antje' or Pax6-gfp fish (described in detail in Chapter 4). These embryos express GFP under the control of a Pax6 promoter and retina specific enhancers such that GFP is expressed in retinal neuroepithelial cells initially and amacrine cells ultimately. Initially, signal levels were found to be unacceptable using TPELSM, and CLSM was favoured instead. Unfortunately, these experiments were confounded by the lack of measurability of the laser power, which is directly related to the level of fluorescence detected.

The laser power in a two-photon laser scanning microscope is controlled by the use of neutral density filters of fixed values. Thus this power can only be adjusted in particular incremental steps expressed as percentages (3, 6, 12, 25, 40, 50, 80, 100). With Pax6-GFP embryos, power levels of 80% and post-imaging contrast enhancement were required to get acceptable signal/noise levels. Previously, I found that 100% power levels would easily damage the embryo and as such, I was reluctant to use power levels above 80%. In

these cases, the CLSM had two advantages. First, laser power levels of 15% were required, and these were adequate for relatively long term acquisitions. At 15% power, a confocal laser caused obvious damage only after 10-15 hours, with large volumes of GFP expression in the retina, and time intervals of less than 20 minutes between volume acquisitions. Secondly, the use of Acousto-Optical-Tunable-Filters (AOTF) to control the laser power level allowed finer tuning of the power between 0 and 100%, thereby achieving an acceptable signal/noise ratio while causing minimal damage to the specimen (although this can only really be assessed retrospectively). Note that the comparison of TPELSM and CLSM laser powers as percentages is meaningless, as the actual amount of energy delivered to the specimen could not be measured in either case. The only assay for comparison is the qualitative 'level of damage' caused to the specimen.

One factor that made comparisons difficult was changing conditions in terms of the power delivered to the specimen when using the IR laser for two-photon excitation. This was affected by the pulse frequency of the laser (initially fs pulses, later changed to ps pulses), the coupling of the laser to the microscope (coupled by a flexible fibre optic cable which would cause some loss of power on the way to the specimen) and the alignment of the laser. For unknown reasons, perhaps repeated re-tuning of the laser to different wavelengths, the laser would occasionally be misaligned. This led to gradual reductions in power at the specimen. The laser was regularly re-aligned by engineers from the laser suppliers. Thus, it is difficult to know whether the initial experiments with GFP under TPELSM were unsuccessful due to differences in the laser parameters described above.

External Non-descanned Detectors

Signal/noise ratios and intensities of brighter specimens such as Brn3c-GFP zebrafish and H2B-GFP injected embryos (described in Chapter 3) under TPELSM were generally more acceptable, however the main advance in TPELSM imaging that made it a more feasible solution occurred with the installation of a non-descanned external detector instead of the descanned detector normally used in CLSM. A PMT detector is placed as close as possible to the specimen immediately behind a high NA, oil-immersion condenser lens, with no pinhole in front of it. The high NA of the lens, the short distance between the specimen and the detector and the lack of any obstruction in front of it, allows more reflected and scattered emitted light to be collected from the specimen. As explained above, the two-photon excitation phenomenon implies that any scattered light

originates only from the excited point. In contrast, for detection by a descanned detector, light passes along a longer light path back through the objective, into the confocal scan head, is reflected by a number of mirrors, and, even with an open pinhole, a proportion will be blocked before reaching the detector. The reported improvement in fluorescent signal varies between about 215% and 450% for non-scattering and scattering tissues respectively (Koester et al., 1999), but also depends on the position of the detector. A detector placed at the back of the objective lens would be more efficient than one behind a condenser. The difference between the two types of detectors is dramatic. Signal/noise ratios are increased (Fig. 2.10a), the number of averages (repeated scans of the same section) required is reduced from around 6 to 2, and the scanning speed can be increased. This has the overall effect of reducing the power level and the time required to scan specimens. As photodamage by TPELSM is proportional to increases in two-photon excitation and thus to the power of the laser, any increase in signal by increasing laser power will always be at the expense of a proportional increase in photodamage (Koester et al., 1999). Increasing collection efficiency by the use of non-descanned detectors is therefore an important factor in allowing much longer time-lapse experiments (24 to 48 hours) to be undertaken reliably, with less damage to the GFP-expressing specimen. It also has the advantage of allowing the theoretical increased depth penetration of IR lasers to be exploited. Non-descanned detectors (along with high laser powers) have played an important part in time-lapse experiments where deep cells were imaged in 200μm thick mouse neocortical slice cultures (Nimchinsky et al., 2001) and at depths of 300μm in the rat cortex *in vivo* (Charpak et al., 2001).

Depth Penetration

Increased depth penetration should be possible with TPELSM given the longer excitation wavelengths used, and thus the lower levels of attenuation of the laser by scattering in the tissue. A favourable comparison has been shown in the imaging of pollen grains, Drosophila larvae (Potter et al., 1996) and human skin (Buehler et al., 1999), while deep penetration has been achieved in mouse and rat cortex (Charpak et al., 2001; Nimchinsky et al., 2001; Oheim et al., 2001). Zebrafish embryos stained with Bodipy-FL C_5-Ceramide were used to make initial comparisons of the ability of TPELSM and CLSM to image in depth. Laser power and signal gain were adjusted in both cases to produce reasonable images by eye. Surprisingly, TPELSM did not seem to bring any advantage to depth penetration in the zebrafish retina (Fig. 2.10b). In fact, it seemed that the developing lens

attenuated the laser (or the emitted light) to such an extent that very little was detected below it. Volumes of approximately 110μm thickness could be imaged with either CLSM or TPELSM. Increased depth penetration in either case required increased laser power, but the advantage with TPELSM was that the laser power required to image as deep as in CLSM was less damaging to the embryo in the long term (see next section). The non-descanned detector was not available at this time, however its use later exaggerated this advantage, as even lower IR laser powers were used to image to the same depth.

Photobleaching and Photodamage

Bodipy FL C_5-Ceramide stained zebrafish embryos were also used in an attempt to assess the levels of photobleaching and photodamage caused by CLSM compared to TPELSM. Laser power levels were set to levels slightly lower than that used normally (6% AOTF for the CLSM 488nm laser, with the laser power turned slightly above baseline levels and 40% Neutral Density filters used on the TPELSM IR laser set to 760nm and 5.3W output from the pump laser). Retinas were scanned as 50μm volumes at 1μm intervals, with 6 averages scanned per section. Scanning time was 300 seconds per volume and a 60 second interval was set between volumes. Thus, the laser scans across each volume 300 times every 5 minutes. Scanning was performed for 7hrs under TPELSM and 4 hrs under CLSM on different embryos at the same stage (1.5dpf). The graphs in Fig. 2.11 show the average signal intensity per frame over time. Each spike represents one volume, as the intensity is highest at superficial levels (peaks) and declines with depth (troughs). The average intensity is lower with TPELSM (even though the detector gain was maximal), although a non-descanned detector was not available at the time of the experiment. The deterioration in the average intensity under CLSM is obvious compared to TPELSM. Representative central sections at comparable times in the experiments (t=175 minutes) show the slightly thinner retina and more irregular cellular and retinal outlines in the specimen exposed to CLSM compared to TPELSM. These irregularities and lack of thickness may be indicative of damage to the retina affecting retinal development caused by continuous exposure to CLSM.

The exclusively focal excitation intrinsic to the two-photon excitation phenomenon can be shown by repeatedly scanning a section in a volume of fluorescein solution to force it to bleach, and imaging the cross-section of the volume (Potter et al., 1996). With CLSM, the hourglass-shaped volume exposed to the laser by scanning one section is evident,

especially compared to the single line representing the scanned section bleached by TPELSM. This is shown schematically in Fig. 2.11d. In accordance with this effect, each time a section of zebrafish retina is scanned, a large volume of the retina is exposed to laser excitation. As the entire retina is labelled with Bodipy FL C_5-Ceramide, the entire exposed volume will be affected by phototoxicity by the excitation. The net result is that with 50 sections per volume, scanned 6 times each, each section in the entire volume is exposed to the equivalent of 50*6 = 300 section scans for each timepoint. In TPELSM, however, each section is only exposed to excitation as many times as the section itself is scanned (i.e. 6 times per timepoint in this case). Thus the thicker the volume (or the more sections scanned), the greater the exposure to excitation in CLSM compared to TPELSM. Additionally, this effect is multiplied by the time for which a volume is scanned. Continuing with the above example, if the volume is scanned 50 times, a particular section will be exposed to 300 * 50 = 15000 scans in CLSM, but only 6 * 50 = 300 scans in TPELSM for the entire time. This is the essence of the advantage of TPELSM over CLSM in long-term time-lapse imaging – the thicker the volume and the longer the time-lapse, the greater the advantage of using TPELSM over CLSM in terms of photodamage, photobleaching and, therefore, unwanted perturbations to the experimental specimen. Since the photodamage caused by TPSLM is mainly related to the two-photon (and three-photon) excitation of molecules and not to other effects such as heating of the tissue by the IR laser (Koester et al., 1999), it will be unlikely to realise any advantage over CLSM in terms of phototoxicity when imaging thin specimens such as cultured cell monolayers.

Pigmentation

Many endogenous molecules in cells are able to absorb light energy and possess characteristic excitation spectra. These include haemoglobin, melanin and water. The near infra-red wavelengths (700-900nm) typically used for TPELSM are known as a cell's optical window as water and haemoglobin absorb light inefficiently at these wavelengths and cells are therefore transparent (Konig, 2000). Although this is an advantage for TPELSM, melanin poses a greater challenge. The excitation spectrum for melanin contains a peak around 400nm but can also be excited by two-photon absorption around 800nm (Hoffmann et al., 2001). Interestingly, the two-photon absorption does not require the simultaneous two-photon absorption described above, but rather a consecutive absorption of two-photons to be excited. This means that a lower flux of photons is required for light absorption by melanin; i.e. it is easier for melanin to be excited by two

photons compared to most other molecules. This is reflected in the brightness of the emitted signal from melanin pigment in the retinal pigment epithelium when imaging the zebrafish retina even at very low laser powers that are insufficient to excite other fluorescent molecules (Fig. 2.12a). IR light absorption by melanin means that the excitation efficiency of the IR laser for structures deeper than the melanin is reduced. In addition, IR light absorption by melanin causes a photothermal effect potentially producing heat that may affect surrounding tissues. As the entire zebrafish retina is layered by a pigmented epithelium, imaging the retina by TPELSM requires some method of removal of the pigment to avoid loss of excitation signal and damage of surrounding tissues by heat. Two methods of suppressing pigmentation were used. The first was to bathe embryos in 1-phenyl-2-thiourea (PTU) (Sigma) before pigment formation to prevent this from occurring. However, there is possibly a short delay in the development of the embryo. Retinal pigment is only delayed by about 12 to 24 hours, while pigmentation in the rest of the embryo can be suppressed for at least one week. If TPELSM excitation is started before the appearance of heavy pigmentation, it seems to be suppressed by the destructive effect of the excitation such that less pigment than expected appears during imaging. However, the effects of this damage on surrounding tissues have not been assessed. A second method was to use *sandy (sdy)* mutant zebrafish. *Sdy* is a recessive mutation in which fish express very little melanin pigment. The structure of the retina seems intact at 7 dpf (Fig. 2.12b), and viable fertile homozygotes can occasionally be raised. The fish are blind to movements and most likely have difficulty in finding enough food to survive past larval stages. For imaging by TPELSM, these are extremely useful as pigmentation is effectively suppressed. Being a recessive mutation and due to the difficulty of raising adults, crosses with GFP-expressing transgenics to produce transgenic pigmentless fish requires two generations of crosses to be done. This is useful once achieved. Pigmentation is not photodamaging when imaging in CLSM (although some absorption does occur), and is therefore an important disadvantage when imaging the zebrafish retina by TPELSM.

In summary, the main advantages of TPELSM over CLSM when imaging zebrafish embryos are as follows:

1. The specimen is only excited focally such that there is less overall photodamage or photobleaching for longer time-lapses and thicker tissue volumes.

2. Light detection is more efficient as scattered emitted light is as useful as unscattered light, especially with the use of non-descanned detectors. This also allows greater depth penetration, and reduced photodamage and bleaching as less power is required for the same signal.

Further Improvements

Although the Leica TCS MP system that was used proved to be adequate for long-term volumetric imaging, further improvements can still be made. An important factor for exciting fluorescent molecules is the power or photon flux delivered to the specimen. The greater the power, the more likely (and the brighter) that fluorescent molecules are excited. The photon flux at the specimen is determined by the output power of the laser, losses in the light path and scattering and absorbance in the specimen.

Why More Power?

The IR laser (Tsunami, Spectra-Physics) is itself pumped by a 5W Millenia V laser (Spectra-Physics). The optics within the cavity of the Tsunami laser provide the range of wavelengths that the laser output can be tuned to. The power of the output depends on the wavelength that the laser is tuned to as shown in the power spectrum in Fig. 2.13. In this setup, maximal power is achieved around wavelengths of 790nm, with the power gradually decreasing with increasing wavelength. Although destructive power levels can already be achieved, this depends on the wavelength as well as the specimen. It is possible that the optimal wavelength of 850nm for eGFP excitation found in my experience, rather than the reported 930nm (Xu et al., 1996), is due to the fact that power levels at 930nm may be too low to produce more emission from eGFP than the higher excitation power at 850nm, regardless of the higher quantum yield or efficiency of the fluorophore at 930nm. Thus, the actual usable range of the laser is also restricted by the power spectrum. For very dense or bright fluorophores, this may not be important. In the case of eGFP and long-term time-lapse experiments, it is always desirable to use the most efficient parameters possible to ultimately reduce the average power required for imaging. Imaging at higher wavelengths could be achieved by increasing the power output of the laser. Increased power may also be required if imaging of deep tissue is required. In the rat olfactory bulb, imaging at 450μm required a power of 290mW at the specimen (Charpak et al., 2001), an order of magnitude greater than the power required for imaging superficial objects.

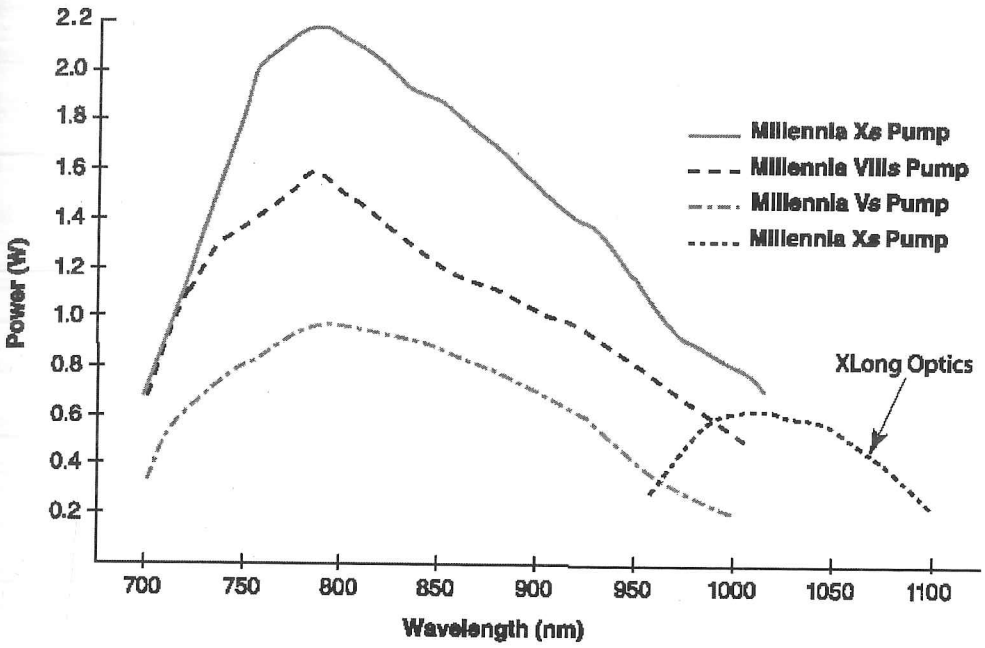

Fig 2.13 ***The power output of the TPELSM laser depends on the wavelength chosen.*** The power spectra show that the most power is available when the laser is tuned to approximately 800nm. Applications in which wavelengths above or below are required may be affected by the lower power output. For example, the optimal excitation wavelength for GFP is reported to be 930nm, but the emission signal will be weaker than at 850nm due to the lower power available for excitation.

Currently, the optimal wavelength for a fluorophore and individual specimen preparations is found by tuning the laser across a short range of wavelengths while the specimen is excited by the laser and observing the emission. The wavelength at which the brightest image is observed is chosen for the experiment. A more objective way to assess the laser power at specimen would be to use a device to make direct measurements of laser power in the back-focal plane of the objective lens. This would be useful to gather consistent data on how much laser power a specimen can withstand before being damaged, how much laser power is required to excite particular fluorophores to useful levels, how much laser power is required at different depths of the specimen and how changes to different parts of the setup affect the power delivered to the specimen.

Laser to Microscope Coupling

One way to increase the power available at the specimen would be to use a more powerful pump laser to provide increased output power, however this is an expensive solution. Alternatively, the coupling between the laser and the microscope could be made

more efficient. This solution is two orders of magnitude cheaper than the 1st for a similar performance gain. The imaging system as I used it consisted of a fibre-optic coupling between the IR laser and the microscope. The fibre-optic coupling enabled some flexibility in a multi-user environment such that the laser could be coupled to an inverted or an upright microscope and moved between the two as required. However, the fibre-optic coupling has two disadvantages. First, its positioning is important in reducing wear and tear. A tight bend in the fibre-optic cable close to the laser output can cause damage to the cable due to the effects of the laser intensity itself. More importantly, the length of the cable increases the length of the light path, such that it is responsible for power losses between the laser output and the objective or specimen. These losses are significant if the laser power becomes limiting. Recently, the coupling between the laser and the microscope was converted to a shorter and safer direct coupling. Reported benefits include a 50% increase in available laser power determined by the need for 3 to 6% ND filters compared to 25% ND filters required previously for similar experiments (J. Skepper, personal communication). The advantages are that there is now a greater flexibility in the range of powers that are available, as a larger range of ND filters can be used, and in the range of wavelengths that are available as increased power can be used for wavelengths that are less efficiently transmitted by the optics within the laser cavity.

Laser Beam Width

Different objectives have different diameter back apertures. In wide-field transmitted or epifluorescent microscopy, uniform filling of the back focal plane by the illumination ensures that excitation light does not enter the objective at skewed angles, and can be adjusted by means of the condenser diaphragm and height for transmitted light, or the epifluorescent light source depending on the objective used. Although uniform filling is not essential for two-photon excitation, a laser beam wider than the back-focal aperture of the objective would result in the loss of laser power as part of the beam is immediately blocked from entering it. Higher magnification lenses have proportionately smaller back-focal apertures so that overfilling the aperture is likely. A method to adjust the width of the beam to the back-focal aperture of the objective being used may result in significant reductions in the loss of laser power and such a method has indeed been implemented in the newer Leica SP2 scan heads.

Femtosecond or Picosecond?

The critical factor for the two-photon effect of the IR laser is that it produces extremely short, high energy pulses that provide the high instantaneous energy levels required at a low average energy non-destructive to the specimen. These pulses range from femtosecond (10^{-15}) to picosecond (10^{-12}) magnitudes. There is some debate as to whether shorter pulses, which have a higher peak power and lower average power, are more efficient for two-photon excitation of biological specimens. However, studies have shown that the length of the pulse does not affect the amount of fluorescence detected or photodamage caused to the specimen as long as relatively low laser intensities are used (Koester et al., 1999; Konig, 2000). For picosecond lasers, this is thought to be <30mW at the focus (Koester et al., 1999). Femtosecond lasers require a lower average power (<8mW) at the focus for the same effect, however we found femtosecond lasers to be more difficult to tune to particular wavelengths and more unstable during long experiments (liable to come out of the mode-locked, pulsing mode). Additionally, fs lasers could not be used with fibre-optic coupling due to lengthening in the pulse width to ps levels as it travelled through the length of the fibre. Therefore, we now use a picosecond laser for experiments.

Non-descanned Detectors

As described above, non-descanned detectors provide a distinct advantage to TPELSM by dramatically increasing the light collection efficiency of the system. Currently, the non-descanned detector in the system used is the same as the regular transmitted light detector for the microscope and cannot be modified for use with filters or a filterwheel. It cannot be used for experiments where different colour fluorophores need to be detected. The presence of multiple non-descanned detectors with modifiable filters would be essential for useful multiple-colour TPELSM experiments. The main limitation to the use of non-descanned detectors is the need for high NA, oil-immersion condensers above the specimen in an inverted microscope (opposite to the objective lens). This will impede on the space available for customised or specialised specimen mounting, manipulation or measurement apparatus.

All of the improvements described above such as direct coupling, non-descanned detectors and adaptable laser beam width are technically feasible (and some have now been implemented to some extent). Even though the advantages provided by TPELSM

over CLSM can already be exploited, these modifications would increase this advantage further. One must remember that two-photon microscopy is not the ultimate answer to the problems with confocal microscopy. It is still limited by photodamage in thinner, non-scattering specimens, the choice of fluorophores and the nature of the specimen itself. Some experiments may still be better suited to CLSM, and it may be a matter of trial and error to determine exactly how much advantage is gained from TPELSM in individual cases.

The Use of Software in Processing 4D Data

This section briefly describes the techniques used in this project to visualise and analyse time-resolved volumetric data. The volume of data generated in 4D experiments is extremely large, and requires enough data storage hardware to be able to save and manage the data, as well as relatively powerful computers and software to make sense of it. The lack of availability of such resources is likely to have limited the popularity of 4D imaging techniques, however the decreasing cost of increasingly powerful hardware and the availability of free or less expensive software is making 4D imaging more feasible. 3D reconstruction of volumes in various guises is used extensively in microscopy due to advances in image acquisition and hardware control (such as focus drives) in direct-held microscopy, and the popularity of optical sectioning techniques such as confocal and two-photon laser scanning microscopy. Time-lapse analysis is also used extensively. Often, if volumes are analysed in time, they are generally time-lapse recordings of small volumes or parts of volumes that can be simplified to 2D images, either by selecting optical sections of interest or by projecting the entire volume onto one 2D image. A combination of 3D reconstruction of large volumes and the visualisation of changes within these volumes over time, however, is more computer intensive and has not yet been used extensively (Bornfleth et al., 1999; Buehler et al., 1999; Mohler, 1999; Thomas and White, 1998).

Sampling for 3D Visualisation

3D impressions of a volume are usually generated from a set of 2D optical sections through that volume. 3D visualisation requires that the volume being visualised is sampled at a high enough frequency in all three dimensions to extract as much spatial information as possible from the volume. According to the Nyquist sampling theorem, the sampling distance needs to be less than half the minimum possible distance between the smallest objects that need to be resolved. Using a 63x lens, which gives a field of view of 158.7μm squared and a pixel resolution of 512 X 512, each pixel or smallest possible sampling distance, is about 0.33μm X 0.33μm. This means that the smallest resolvable object, or distance between objects will be 0.66μm wide in the XY plane of the microscope. In the Z-axis, a similar resolution of 0.33μm per optical section is about half to one third of the depth of field or Z-resolution limits of most objective lenses. Thus, a sampling rate of 0.33μm to 0.5μm per section is around the required Nyquist sampling

rate. Necessarily, a high sampling rate produces a greater volume of data which can become unmanageable for large volumes sampled repeatedly over time, so that sampling rate may need to be compromised. For most experiments in the zebrafish retina, a sampling rate of 1μm per section was chosen, ensuring that all structures greater than 2μm could always be resolved. This was found to be adequate for imaging zebrafish retinal cells and their nuclei that generally have diameters from 3 to 4μm.

Methods of Exploring 3D Data

2D analysis of 3D/4D data

3D and 4D datasets can be explored and analysed by looking at the individual sections that give rise to each volume. Software can be used to arrange the sections into an intuitive sequence, such that one can navigate 'up and down' through a volume, as well as 'sideways' in time, between different timepoints. This approach is not very computer intensive, and is useful for the careful examination of unchanged data. Software can also be used to mark features within the volume that can then be processed for analysis as true 3D features. Another advantage is that datasets that are not amenable to 3D reconstruction, such as those containing too many objects to be easily distinguished in 3D reconstructions, can be analysed using this method. A disadvantage with this method is that large volumes or complex objects and the relationships between them can be difficult to imagine simply by looking at 2D sections.

3D Reconstructions

3D reconstructions of the volume data can be made to gain a visual map of the shape and structure of the volume and its objects that is easier to interpret to the eye. Further advantages of 3D reconstructions are that visual cues, such as the rotation of a volume, allow the relationship between objects to be understood clearly. Features that might be missed on 2D sections may be more prominent on 3D volumes. This enhancement can be due to the movement of a feature noticed only when rotating the volume or, more likely, because a feature that spans multiple sections, but is actually difficult to see on one individual section, is more noticeable due to the combination of more sections encompassing that feature. An example is dendrites and axons that can often be difficult to see in single sections, being only a few pixels wide (Fig. 2.14). Importantly, 3D reconstructions are most useful with datasets containing relatively few, discreet, homogeneous objects. The more crowded a volume and the less discreet and

homogeneous the objects, the more difficult it can be to visualise and understand the volume. Two main techniques used in this project are maximum intensity projections and volume rendering techniques, provided by a combination of free and commercially available software.

Maximum Intensity Projections

One common method for reconstructing 3D volumes is to use Maximum Intensity Projections (MIPs). A view of the volume is projected onto a 2D image that can be imagined to lie opposite the viewer. Each pixel on the 2D screen is generated by an imaginary orthogonal ray passing through the volume onto the screen and the pixel values are determined by the brightest pixel values that each corresponding ray encounters on its way through the volume. This produces a view of the volume in which the brightest objects are most pronounced. Many software products for imaging can produce MIPs. By generating MIPs of a particular volume from different angles, and by combining these in a sequence, movies of rotating volumes can be made. Because MIPs rely on the brightness of objects within a volume, the brightest objects are the most prominent regardless of their depth within the volume. Pixels in a volume can also be weighted according to their depth to generate some sense of depth in the volume, although brightness is still the main criterion for object prominence. Fainter objects lying in the same line of view as brighter objects are easily obscured. Although rotation of the volume can enable objects at different depths to be distinguished, faint objects in crowded areas of a volume can be still difficult to see (Fig. 2.12a).

Volume Rendering

A more computer intensive method of visualising volumes is to render a set of 2D sections into a set of 3D objects in a volume using an imaginary light source and shadows to provide visual cues of depth. In volume rendering, the pixels that are part of the 2D sections are made into clouds of pixels representing the 3D objects. Opacity values can be assigned to the pixels such that objects look solid, and objects closer to the viewer will obstruct objects behind from being seen, much as a viewer's intuitive experience of the world would expect. Pixel brightness is no longer important and faint objects can be made as opaque as bright ones. Only a range of pixels can be considered, such that faint pixels more likely to be noise can be excluded from the rendering. Although volume rendering can be useful in visualising 3D volumes, it is very computer intensive, and creating 3D volumes that can be freely rotated requires relatively powerful hardware and software.

The smooth movement of 3D volumes controlled by the user is very useful in enabling objects to be distinguished. Similarly, for time-lapse datasets, smooth movement between timepoints enables changes in shape, position and relationship between objects to be monitored over time. The addition of the time dimension multiplies the required computational resources, and finding software that can deal smoothly with the visualisation of volumes in a time-lapse context is difficult, perhaps because the need and feasibility for such software has only recently been realised. The analysis of 3D and 4D datasets is also challenging. Because 3D reconstructions are 2D representations of volumes on a display, a reliable method of directly allowing users to select and mark objects within a 3D view is probably extremely difficult to devise using conventional computers and tools. Instead, a useable method is to mark or measure chosen objects within the original 2D sections, and perhaps combine this with the 3D rendering for visualisation purposes. This can be done to some extent in some software packages.
Because time-lapse experiments can provide data about changes occurring in single objects, it is often desirable to be able to track these objects through the time-lapse dataset, for example to compare states before and after particular events. Programs to automatically track objects have been produced but they rely heavily on the ability to easily distinguish objects computationally from the surroundings and are usually based on 2D images, rather than 3D volumes. If distinguishing objects in a volume is difficult to do by eye, it is unlikely that common algorithms, such as those based on edge detection or differences between pixel intensities, would be able to do so easily. Different situations may require algorithms to be specifically adapted for such a task, which would require expert skills in this area in addition to a large investment of time. Tracking objects through time-lapse 3D datasets is possible, but laborious and slow, and is a limiting factor for long-term time-lapse experiments if it is essential to the analysis.
Although many software packages exist that deal with 3D datasets, few are available to deal with 4D datasets. The features of some of those that are available and that I have used are mentioned below.

NIH Image (Free)

Platform: Mac, PC, Java

NIH Image can be used to generate MIPs of volumes rotated around the x-, y- and z-axes at pre-defined angles. This program was used initially for 3D reconstructions,

identification of cell divisions and basic measurements from volumes. This method of visualising 4D data does not necessarily require powerful hardware. (http://rsb.info.nih.gov/nih-image/)

4D Viewer (Free)

Platform: Mac, Java

This program forms part of a set of programs designed to visualise and analyse 4D data. Navigation through 4D datasets in space (i.e. through a stack) and time (across different stacks representing different timepoints) is possible. Basic annotation facilities are provided to keep track of particular features in the dataset. (http://www.loci.wisc.edu/)

Volocity (Commercial)

Platform: Mac and Windows

This program was developed specifically for 4D data analysis. It can produce MIPs and renderings of volumes. It is relatively fast and allows the user to control the position and viewpoint of the volume in real time, and allows navigating through a dataset in time, while in rendering mode. Basic measurements can be made on the section data. Volocity also allows regular and virtual reality (VR) movies to be made from the datasets. Although this program only became available recently, its speed and flexibility has meant that it has been used extensively for many of the experiments described in this thesis. (http://www.improvision.com/)

Vis5d (Free)

Platform: Unix

This program is used to study meteorological data but has been used to look at C. elegans development in 4D (Mohler, 99). It is not easy to use and requires a powerful system to run as well as some experience of Unix or Linux systems to set up. (http://www.ssec.wisc.edu/~billh/vis5d.html)

Leica LCS (commercial)

Platform: Windows

This software is available on most Leica confocal microscopes. 3D renderings and MIPs are one of its many image analysis features, however it is not designed for visualising 4D data. This was occasionally used immediately after data acquisition on the microscope to estimate the quality of the dataset.
(www.leica-microsystems.com)

Conclusion

Combining 3D imaging with *in vivo* time-lapse imaging is a challenging undertaking that has become feasible with new tools such as confocal and two-photon microscopy along with the availability of hardware and software to start making sense of the huge amounts of data that are generated. This chapter has described how some of these tools have helped make the process of 4D imaging possible and the technical factors that can affect the outcome of experiments, mainly based on my own experiences. 4D imaging is now a rapidly developing field, with improvements and innovations being made to both instrumentation and data analysis software. Automation and ease-of-use built into the hardware and software used in 4D imaging are likely to be the most crucial factors for it to gain wider acceptance. Nonetheless, I hope that the work described here shows that 4D imaging is not as difficult as many believe. The ability to visualise the spatial and temporal properties of minute biological events within the larger context of organs or organisms is not as limited by technical reasons as one might expect. Just as the use of fluorescence microscopy, GFP and its derivatives or even 3D imaging have become relatively commonplace in biological research, 4D imaging should be within the reach of most researchers as another tool to help them reveal what often seems hidden.

Fig. 2.7 ***Principles of confocal microscopy.*** **a)** A point source of excitation light, created by placing a pinhole in front the light source is reflected onto the specimen by a dichroic mirror and focused onto a point. Emission light from that point is focused onto the detector pinhole. Scattered out-of-focus emission is not focused onto the pinhole and is therefore prevented from reaching the detector. The rejection of out-of-focus emission is the main cause for the increased signal/noise ratio achieved in confocal laser scanning microscopy. **b)** A point-spread function (PSF), or Airy disc, can be plotted as a graph of light intensity against distance from the centre of the disc, with most of the light (the highest peak) present in the central disc (black graph). Light emitted from a point source will form the point-spread function (PSF) for that point. The detector pinhole acts as a PSF-shaped filter. The net effect of superimposing two PSFs is to multiply them. The resulting PSF (shown in red) is narrower, and higher order peaks are reduced. Since resolution depends on the radius of the PSF (or Airy disc), the narrowing in PSF results in a higher resolution for confocal systems.

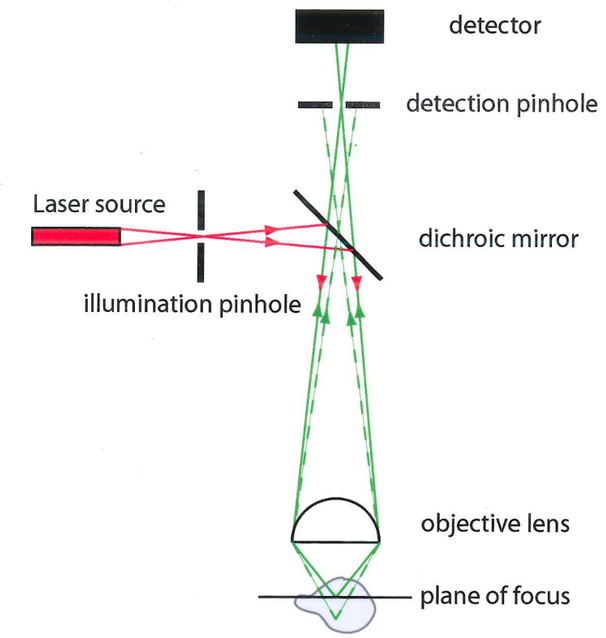

Fig. 2.10 **a)** ***External detectors enhance the detection of emission when using TPELSM.*** The same optical section of GFP expressing cells is imaged by two-photon excitation. A shows the resulting image using a descanned PMT while a' is the resulting non-descanned image. Merging a and a' results in a". The signal/noise ration is noticeably greater in a". Use of non-descanned detectors leads to less excitation power being required and shorter laser exposure times. The overall effect is to reduce phototoxic effects further. **b)** ***A comparison of CLSM and TPELSM in depth.*** A transgenic zebrafish embryo expressing GFP in some cells was stained with Bodipy FL-C5-Ceramide to visualise the cell membranes and imaged in X-Z sections. Bodipy ceramide is brightest when using a 488nm laser in confocal microscopy (b), however GFP labelling could only be seen together with bodipy ceramide under two-photon excitation (red arrowhead; b'). Two-photon excitation or emission is attenuated by the lens of the eye, with little improvement seen on increasing laser power (b' and b"). The signal is also reduced under confocal microscopy, but to a lesser extent. This may be simply be due to the brighter bodipy ceramide signal seen in CLSM.

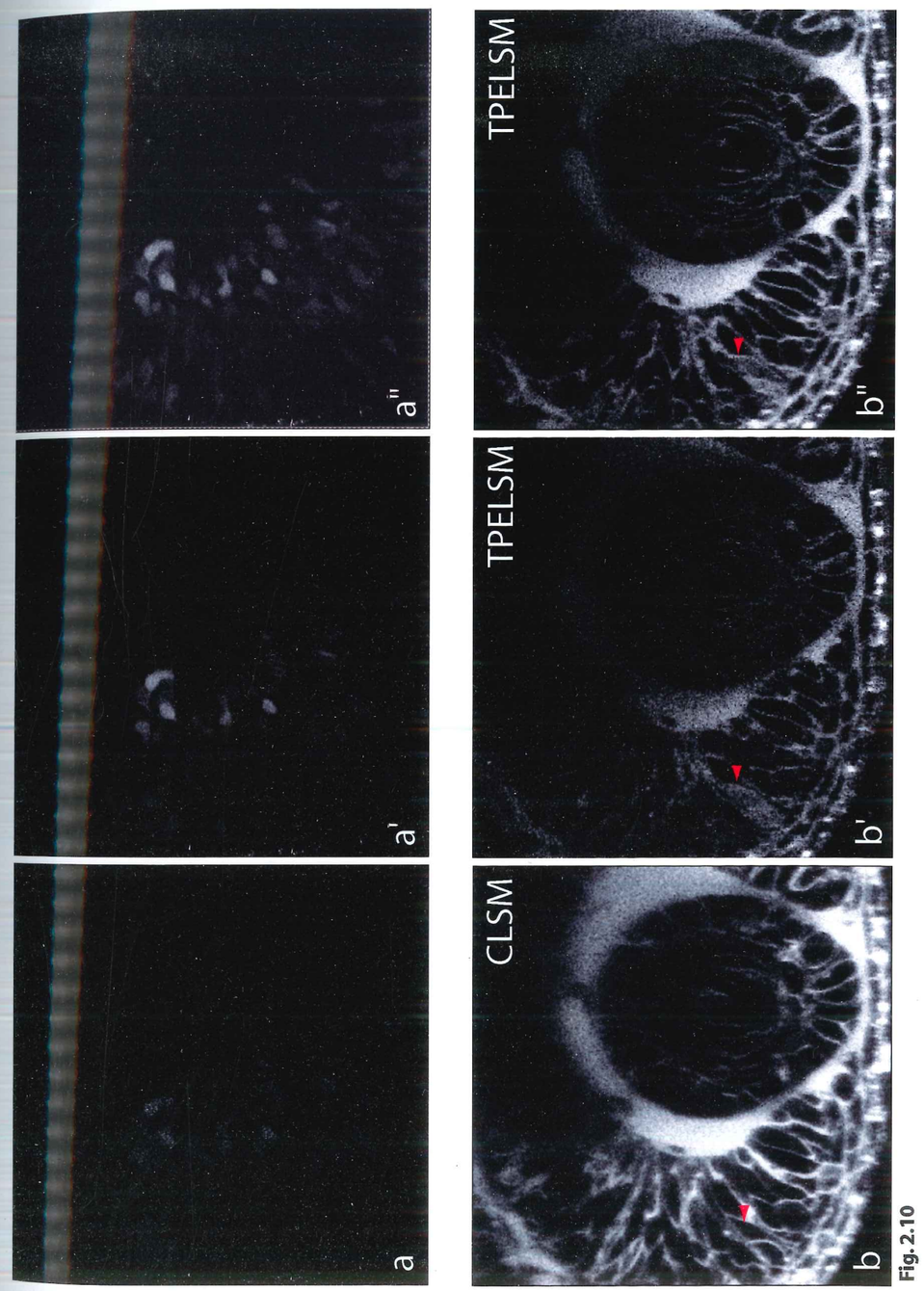

Fig. 2.11 ***Photobleaching and photodamage in CLSM and TPELSM.*** Zebrafish stained with Bodipy-FL-C5-Ceramide were imaged under CLSM **(a)** or TPELSM **(b)** for three hours. After three hours, the retina exposed to CLSM is thinner and more ragged than that exposed to TPELSM, although such a comparison is very subjective. **c)** A plot of average signal intensity per optical section against time for CLSM and TPLSM. The signal under CLSM gradually decreases, most likely due to photobleaching, while the signal under TPELSM remains steady throughout, although of lower intensity. **d)** ***Extent of specimen excitation by CLSM and TPELSM.*** In CLSM, the entire volume of the specimen that the excitation beam passes through is exposed to its phototoxic effects, as the probability of excitation decreases linearly with the distance from the focal point. In TPELSM, the probability of excitation decreases with the square if the distance from the focal point, so that only the focal point itself is prone to phototoxicity and photodamage.

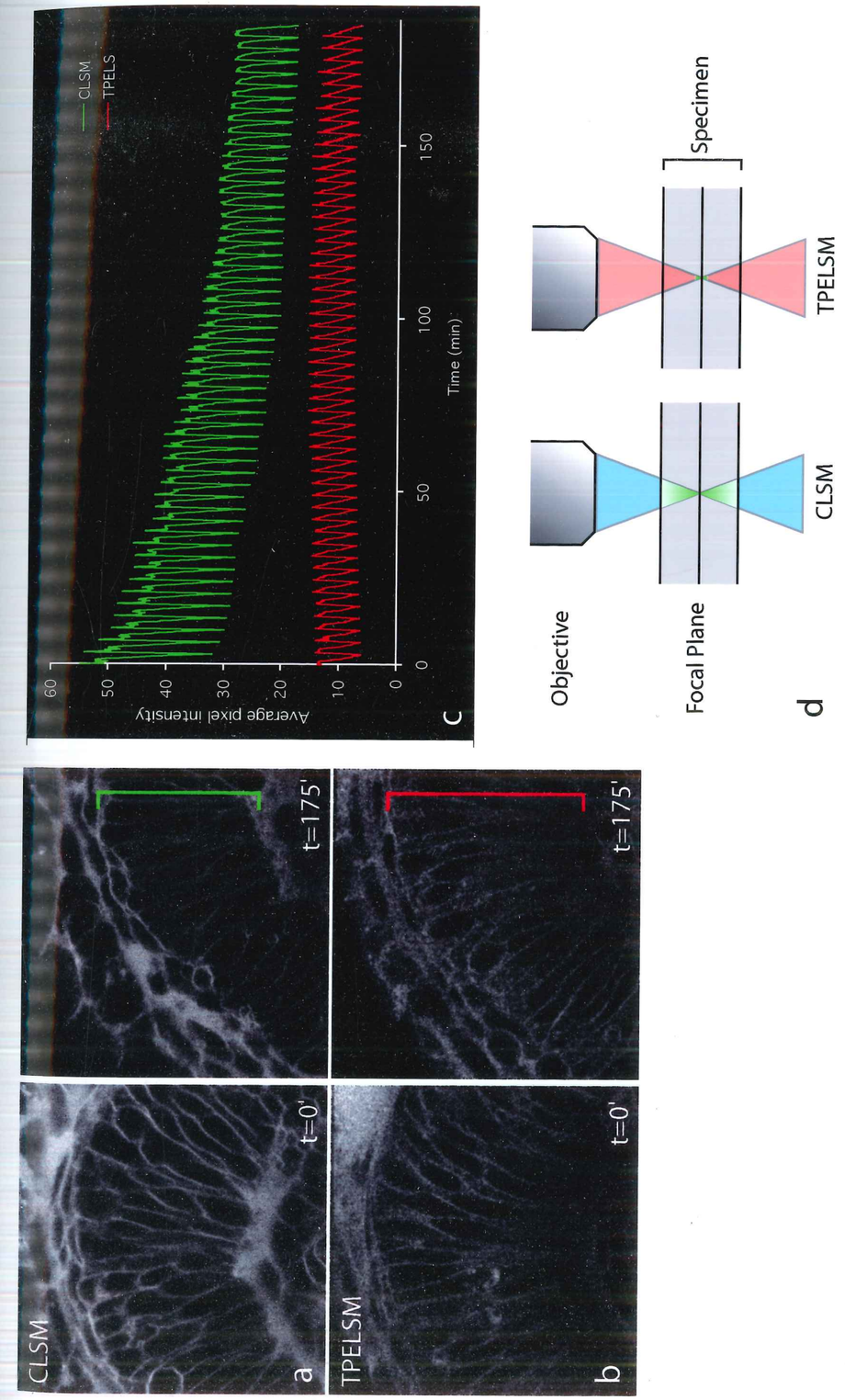

Fig. 2.11

Fig. 2.12 ***Melanin pigmentation hinders TPELSM imaging of the zebrafish retina.*** **a)** Melanin in the retinal pigment epithelium of zebrafish eyes is easily excited to fluoresce by TPELSM. Labelled cells or structures within the retina are obscured by the bright melanin signal. **b)** Methylene blue stained sections from the retinas of seven-day-old wildtype and *sandy* mutant embryos show that although *sandy* mutants lack pigmentation in the retinal pigment epithelium, the structure of the retinal is morphologically intact. This has been exploited for TPELSM imaging by using *sandy* mutants where possible for imaging in order to avoid the problems posed by pigmentation.

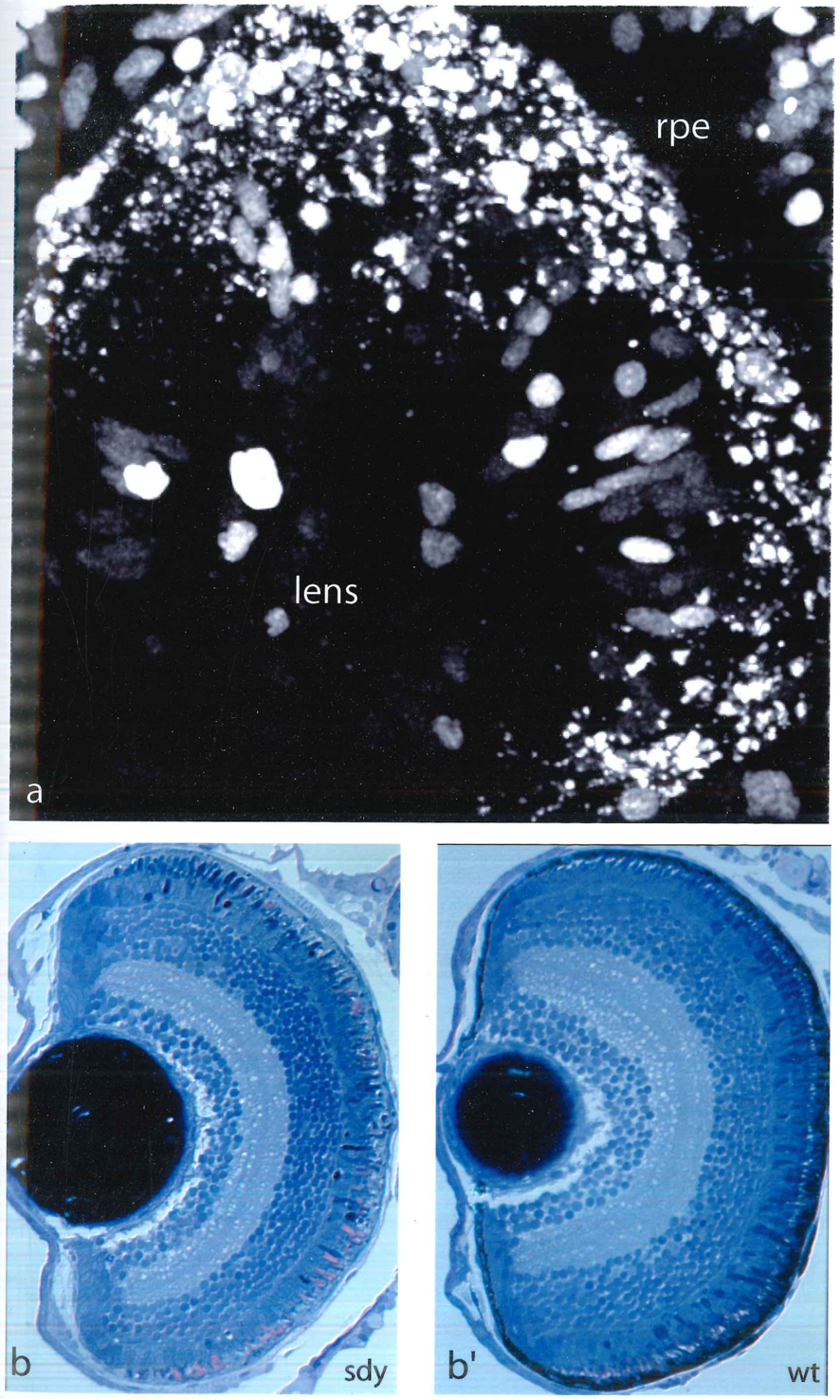

Fig. 2.12

Fig. 2.12 ***Melanin pigmentation hinders TPELSM imaging of the zebrafish retina.*** **a)** Melanin in the retinal pigment epithelium of zebrafish eyes is easily excited to fluoresce by TPELSM. Labelled cells or structures within the retina are obscured by the bright melanin signal. **b)** Methylene blue stained sections from the retinas of seven-day-old wildtype and *sandy* mutant embryos show that although *sandy* mutants lack pigmentation in the retinal pigment epithelium, the structure of the retinal is morphologically intact. This has been exploited for TPELSM imaging by using *sandy* mutants where possible for imaging in order to avoid the problems posed by pigmentation.

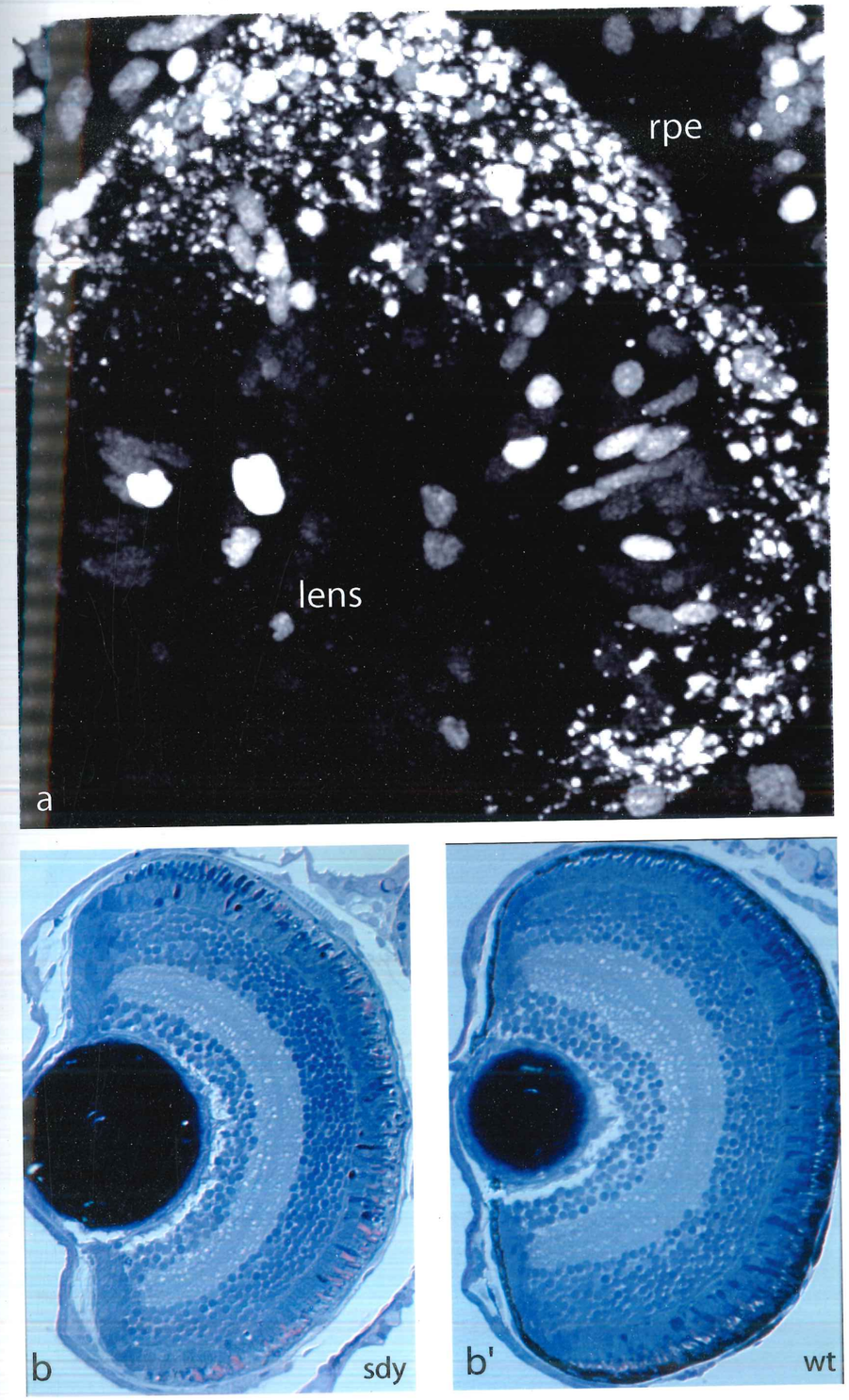

Fig. 2.12

Fig. 2.14 ***3D reconstructions of optical sections.*** **a)** 10 confocal sections, 1μm apart, imaged from a Pax6-GFP expressing transgenic zebrafish. The bright green cells are amacrine cells, whose dendritic network can barely be seen as scattered green spots in the image. **b)** A maximum intensity projection type of 3D reconstruction of the 10 frames in **a** reveals the dendritic network more clearly.

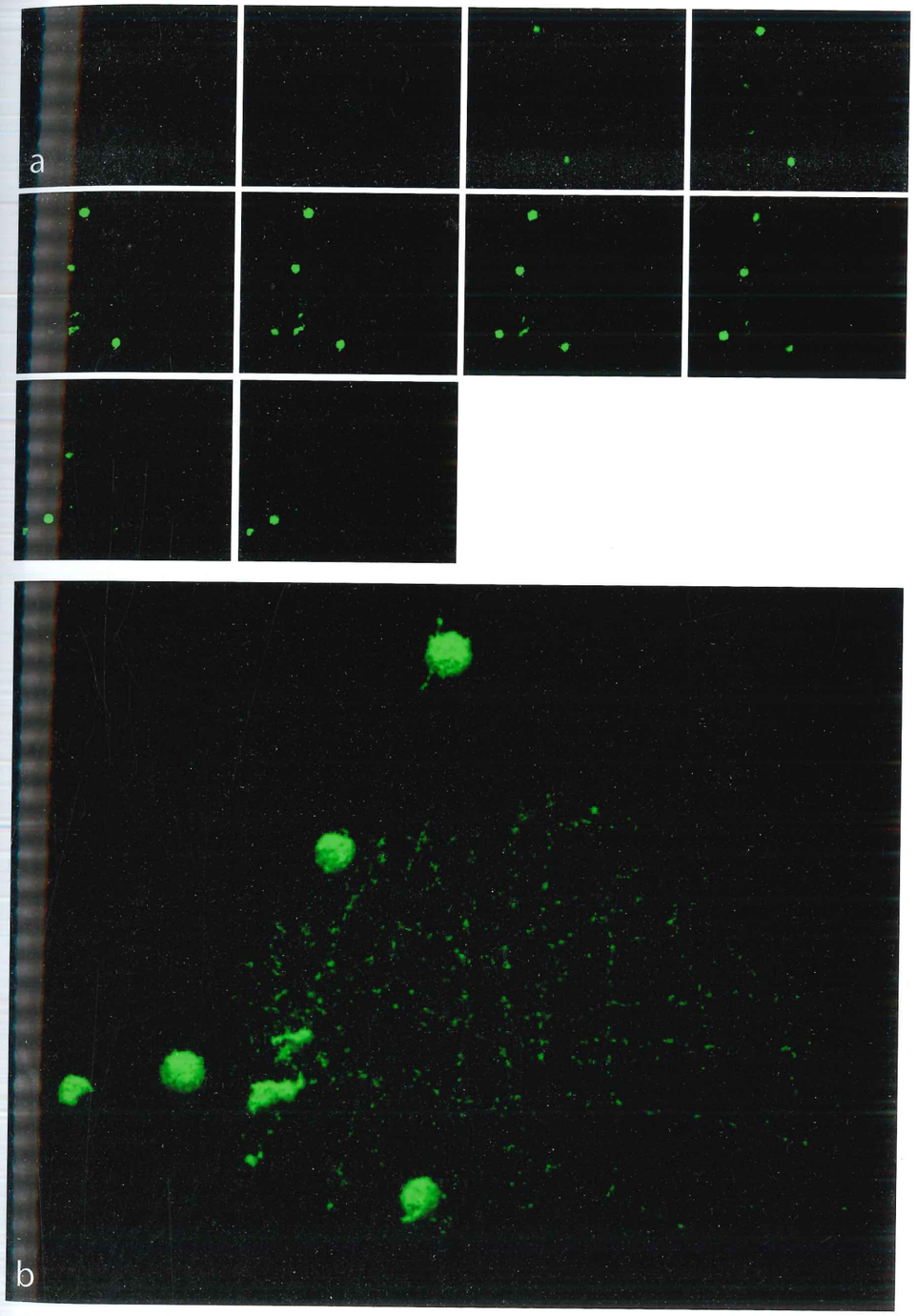

Fig. 2.14

Chapter 3: Cell Division in the Zebrafish Retina

Introduction

The cleavage orientation of cell divisions during vertebrate neurogenesis may be important for the generation of postmitotic cells, as well as maintaining correct three-dimensional tissue morphology during development. The developing zebrafish retina, part of the central nervous system, serves as a useful model to study both of these ideas due to its accessibility to *in vivo* imaging techniques that allow morphogenetic and cellular changes to be charted through time. The development of the zebrafish eye occurs in two phases. The first is a series of morphogenetic changes, starting as an evagination from the neural keel around 11 hours post fertilisation (hpf) and finishing with the formation of the optic cup around 24 hpf (Schmitt and Dowling, 1994). During this early period of morphogenetic change, the level of cell proliferation is low and the length of the cell cycle is transiently increased, while the volume of the retina remains almost constant. Following the morphogenetic changes that transform the solid disc-like mass, continuous with the neural keel, into a cup-shaped and more spherical optic vesicle, an abrupt transition to increased proliferation and shorter cell cycle lengths occurs around 33 hpf, when the retina is ready to grow in volume (Li et al., 2000a; Li et al., 2000b). At the same time, the retina starts its transformation from a morphologically homogeneous neuroepithelium into a tissue consisting of six neuronal and one glial cell types organised into cell-type specific laminae. What changes in cellular division occur at this time that could account for the morphogenetic and neurogenic changes that are taking place?

The orientation in which cells divide has previously been proposed to play a role in morphogenesis. For example, non-random rostrocaudal divisions that correlated with the rostrocaudal extension of the neural plate were demonstrated in the chick and mouse embryo (Sausedo et al., 1997). Non-random orientations of cell division have been found in developing tissues of numerous other organisms such as the zebrafish gastrula (Concha and Adams, 1998) and neural tube (Kimmel et al., 1994), mouse cerebral cortex (Adams, 1996) and rat neural tube (Tuckett and Morriss-Kay, 1985) although they have not always been correlated to tissue morphogenesis. Do non-random orientations of cell division occur in the zebrafish retina and could they play a role in the way it grows?

The orientation of division has also been shown to be important for neurogenesis in the developing nervous systems of vertebrates and invertebrates in the form of asymmetric cell division, where the unequal segregation of cell fate determinants during cell division results in one daughter cell becoming post-mitotic while the other continues to proliferate. Asymmetric cell division is thought to be one mechanism by which the diversity of cell fates in the nervous system could be generated. This diversity is evident from experiments in which lineage tracers injected into single progenitor cells in the developing mouse or Xenopus retina were found distributed amongst multiple postmitotic cell types (Holt et al., 1988; Turner and Cepko, 1987). A few of the clones produced were small clones consisting of three cells of different fates. Such clones could arise from a progenitor cell dividing asymmetrically to produce one postmitotic and one mitotic daughter cell, followed by symmetric division of the mitotic daughter to give rise to two more postmitotic cells. Alternative scenarios for which asymmetric divisions would be unnecessary cannot be excluded. For example, a progenitor cell could divide symmetrically to produce two daughters, which each divide symmetrically to generate four postmitotic cells. One of these could then die to form a three-cell clone.

The extensive study of asymmetric cell division in invertebrates and the identification and expression in the vertebrate CNS of a number of genes homologous to those involved in asymmetric division in Drosophila and C. Elegans has lent credence to the idea that asymmetric cell divisions play a role in neurogenesis in the vertebrate CNS (Lu et al., 2000). In invertebrates, an asymmetrically dividing cell has an intrinsic polarity that allows cell fate determinants to be localised asymmetrically across the cell and allows the cell's mitotic spindle to orientate itself along the same axis such that, after cell division, a different complement of cell fate determinants is located in each daughter cell (Doe and Bowerman, 2001). During development of the Drosophila central nervous system, neuroblasts divide along the apico-basal axis, rather than along a planar axis, to give rise to a Ganglion Mother Cell basally and a neuroblast apically. The apico-basal orientation of division allows cell fate determinants that are segregated asymmetrically along the apico-basal axis within the cytoplasm of the neuroblast to be distributed differentially to the two daughter cells, which results in different cell fates for the daughter cells (Doe and Bowerman, 2001; Lu et al., 2000). Cell fate determinants that get segregated to the GMC after neuroblast division include Numb, which acts by inhibiting Notch protein function in some cell lineages (Spana and Doe, 1996). Numb is localised to the basal cortex of the

neuroblast during prophase (Knoblich et al., 1995), and requires an adapter protein, Partner of Numb, for its asymmetric localisation (Lu et al., 1998). Studies of neurogenesis in the vertebrate central nervous system have shown a minority of cell divisions taking place apico-basally, with the majority orientated in the plane of the tissue. Chenn and McConell (1995) observed apico-basal divisions in DiI-labelled ferret cortical slices by time-lapse imaging while fixed tissue studies of mouse retina and chick and mouse cortex have also shown cells dividing apico-basally (Cayouette et al., 2001; Chenn and McConnell, 1995; Wakamatsu et al., 1999; Zhong et al., 1996). Evidence that these apico-basal divisions may be asymmetric in nature comes from observations of asymmetric expression of vertebrate homologues of Numb or Notch in apico-basally dividing neural progenitor cells. In this regard, however, the studies are somewhat discordant: in mouse cortex and rat retina, m-Numb localises to the apical side of progenitor cells (Cayouette et al., 2001; Zhong et al., 1996), while in chick, c-Numb seems to localise to the basal side (Silva et al., 2002; Wakamatsu et al., 1999). Meanwhile, the protein that Numb potentially antagonises, Notch-1 has been found in the basal daughter of ferret cortex progenitors (Chenn and McConnell, 1995), the apical side of rat cortical progenitors (Johansson et al., 1999), and distributed throughout progenitor cells in the mouse cortex (Zhong et al., 1997) and cultured mouse retinal cells (Cayouette et al., 2001). Whether asymmetric cell divisions occur in the zebrafish retina and how these relate to the orientation of cell division is not yet known. There is some data to suggest that planar divisions can be asymmetric. First, there is a precedent for asymmetric divisions taking place in a planar axis in the Drosophila peripheral nervous system. The Sensory Organ Precursor (pI) for the bristle mechanosensory organ first divides along the antero-posterior axis within the plane of the neuroepithelium. One of its daughter's (pIIa) also divides along the same axis while the other (pIIb) divides apico-basally. Each of these divisions is asymmetric involving the segregation of Numb to one daughter cell (Gho and Schweisguth, 1998). Secondly, the number of apico-basal divisions observed in the ferret cortex (Chenn and McConnell, 1995) and rat retina (Cayouette et al., 2001) appears to be too low to account for the number of neurons that are born around the same time. This suggests that either some proportion of planar divisions needs to be asymmetric, or that most postmitotic neurons arise from symmetric divisions. Finally, a recent study of the chick retina found no correlation between relatively rare apico-basal divisions and the expression of an antigen expressed early in differentiating retinal

ganglion cells (Silva et al., 2002). The antigen was as likely to be expressed in one of the daughters of a cell undergoing a planar division as in the basal daughter of an apico-basally dividing cell. Thus, although apico-basal divisions consistently seemed asymmetric in nature, the apico-basal orientation was not necessary to impart asymmetry on the division.

A different criterion that one would expect asymmetric cell divisions in the developing nervous system to meet is a changing temporal pattern that matches the changes in level of ongoing neurogenesis. In a study of the changing proportions of proliferative and quiescent (or postmitotic) cells over time in the mouse neocortex, Takahashi et al. propose a model of neurogenesis where the proportions of proliferative and postmitotic fractions of cells can be used to predict the proportion of asymmetric divisions at any one time (Takahashi et al., 1996). This predicted proportion shows an increase followed by a decrease, peaking around the time that the proliferative and postmitotic cell fractions are expected to be equal. This model seems to fit to some extent with studies of apico-basal division in ferret cortex, where an increase (but no decrease) in the proportion of apico-basal divisions was seen over time (Chenn and McConnell, 1995) and mouse retina, where an increase and decrease in the proportion of apico-basal divisions was described (Cayouette et al., 2001). The only inconsistency, as mentioned earlier, is that the actual proportion of apico-basal divisions is much less than that predicted by the model. Given this expectation of a temporal pattern, does the level of asymmetric cell division in the zebrafish retina change over time?

Neurogenesis in each cellular layer of the retina is initiated in a wave-like manner starting in an area known as the ventro-nasal patch, adjacent to the choroid fissure (Hu and Easter, 1999). This neurogenic wave progresses around the circumferential axis of the retina in a ventral to nasal to dorsal to temporal direction. It has been demonstrated in terms of markers of differentiated photoreceptors and ganglion cells (Laessing and Stuermer, 1996; Raymond et al., 1995), using BrDU pulse labelling experiments to identify post-mitotic cells (Hu and Easter, 1999) as well as in terms of expression of genes involved in cell fate determination (Masai et al., 2000; Neumann and Nuesslein-Volhard, 2000). Given that neurogenesis occurs in a wave, a wave may also be involved in regulating or initiating neurogenic cell divisions. If so, are orientations or patterns of cell division correlated with these waves or affected in zebrafish mutants in which these waves are disrupted?

In an attempt to answer some of these questions, *in vivo* time-lapse imaging has been used. The zebrafish is especially suited to this sort of experimentation due to its relative transparency and speed of development. Using two-photon excitation of fluorescent probes, 3D representations of almost the entire zebrafish retina can be obtained over a long period of time due to the lower levels of photodamage that normally result from laser scanning microscopy (Piston, 1999). An advantage for the study of morphogenesis is that measurements of the specimen can be taken with the knowledge that no artefact will have been introduced from fixing, staining or mounting the specimen. Furthermore, because time-lapse data is being used, relative changes in morphogenesis can be observed in single specimens. In addition to long-term changes in the behaviour and orientation of dividing cells, shorter-term changes in morphology during cell division can also be studied. Of particular interest is the issue of the basal process by which neuroepithelial progenitor cells are attached to the basal side of the retina. During the cell cycle in the vertebrate retina, the nucleus undergoes interkinetic nuclear migration, which involves movement of the nucleus within a neuroepithelial cell that spans the entire retina or ventricular zone. At mitosis, the nucleus always migrates to the apical side of the tissue where the cell divides. Recent time-lapse studies of cortical glial cells showed that the basal process seemed to remain in place during mitosis of radial glial cells (Miyata et al., 2001; Noctor et al., 2001). This may relate to reports of cultured neuroblasts in the developing superior cervical ganglion of the rat that can divide after having elaborated axonal processes (Wolf et al., 1996). In such cases, the process persists and is inherited by one of the daughter cells. By imaging retinal progenitor cells *in vivo*, we show that the basal process does persist during mitosis. This also raises questions about the fate of the basal process at mitosis. We have tried to determine whether one daughter cell or both daughter cells can inherit the basal process, and whether any pattern of inheritance of the basal process might bear any relation to asymmetric cell division.

Methods and Materials

Fish

Fish were maintained at 26.5°C. Embryos were raised at 28.5 °C and staged in hours post fertilisation (hpf). Embryos used for imaging were of wildtype strains (Ab, wik) or homozygous for the *sdy*^{tk20} mutation. Wild-type embryos were treated with 0.003% PTU (Sigma) from 11 hpf to 24 hpf to delay pigment formation in the eye. *Sdy* embryos fail to develop melanophores and do not require PTU treatment to prevent pigmentation. Because PTU treatment is less effective in the retina after about 48 hpf, *sdy* embryos are better suited to long-term imaging. Embryos carrying the *sonic you* (*syu*^{t4}) mutation (a gift from S. Wilson, UCL) were used in experiments to study the role of the neurogenic wave (see introduction). Retinal ganglion cells expressing GAP-GFP, a membrane tagged version of eGFP, were visualised using transgenic fish that express the GAP-GFP gene under the control of the zebrafish Brn3c promoter (a gift from Tobias Roeser, UCSF). Both *syu* and Brn3c-GAP-GFP fish were also treated with PTU for imaging experiments.

Bodipy-Ceramide Labelling

Bodipy-FL-C_5-Ceramide (D-3521, Molecular Probes) stock solutions were made using DMSO to a concentration of 6.25μg/μl. Prior to labelling, a 5μl aliquot was further dissolved in 150μl of embryo medium containing 0.01M HEPES buffer. 15 to 20 embryos were bathed in the solution in darkness at 28.5°C for 4 to 8 hours. The embryos were rinsed thoroughly in embryo medium and dechorionated prior to mounting as described below.

Plasmids

A number of plasmids were used as *in vivo* markers of cell membranes or nuclei for studies of cell division. GAP-GFP (S-H. Kim et al, 1998), which consists of eGFP preceded by a palmitoylation signal from GAP43 targeting it to the cell membrane, was subcloned into pCS2+ for use as a cell membrane marker. pEYFP-mem and pECFP-mem (Clontech), which contain the same palmitoylation site as GAP-GFP, were used as YFP or CFP based membrane tags. GAP-DsRed was made by triple-ligating the palmitoylation sequence from GAP43, created by using overlapping primers, the DsRed fragment from pDsRed1-N1 (Clontech) and the pCS2 plasmid linearised at EcoRI and AflIII sites. H2B-GFP (BD Pharmingen) was used to label cell nuclei. H2B-GFP is a fusion protein of

human Histone 2B and eGFP driven by an EF-1α promoter in the mammalian vector, pBOS. GAP-GFP, pEYFP-mem, pECFP-mem, GAP-DsRed and H2B-GFP were injected as supercoiled plasmids into cells of 1 – 8 cell stage embryos at concentrations of around 10ng/μl in 0.25% Phenol Red. Pon-GFP is a fusion construct of eGFP and the C-terminus of Drosophila Partner of Numb, which localises to the same place as endogenous Partner of Numb, although is not dependent on the endogenous protein (Lu et al., 1999). Pon-GFP RNA was synthesised by *in vitro* transcription from a Pon-GFP fragment amplified by PCR and injected into 1 – 8 cell embryos at 100ng/μl. The Pon-GFP PCR product had to be used for RNA synthesis, as no convenient sites existed to linearise the Pon-GFP DNA plasmid. Pon-YFP and Pon-CFP constructs were made by ligating PCR products for the pon C-terminal fragment from Pon-GFP and eYFP or eCFP fragments from eYFP-mem or eCFP-mem. The resulting ligation products were inserted into pCS2.

In vivo *Imaging*

Injected embryos were screened at 24 hpf under a fluorescent dissecting stereo-microscope (Leica MZ FLIII) for those with strong eGFP expression in the retina. Chosen embryos were mounted in 0.2% agarose at pH 7.4, containing 0.04% MS-222 and 0.01M HEPES onto a no. 0 coverslip that served as the bottom of a 35mm petri dish. Embryos were also orientated such that the lateral side of the eye was closest to the coverslip. Acetate rings were used as spacers and another no. 0 coverslip was placed on top. The petri dish was placed in a heated stage at 28.5°C on an inverted microscope (Leica DMIRBE).

eGFP fluorescence in the specimens was imaged using a Leica TCS SP two-photon laser scanning microscope. A picosecond-pulsed Ti:Sapphire laser (SpectraPhysics Tsunami, 5W) was tuned to a wavelength between 850nm and 885nm and focused onto the specimen using a Leica 63x, 1.2 NA water immersion objective with a long working distance (225μm). Emission between 500nm and 550nm was detected using a non-descanned transmitted light detector. For long-term time-lapses, optical sections 1 μm apart were taken through a volume of the retina up to 120μm in depth and Kalman averaged two to six times. Time points were between 10 and 30 minutes apart. For higher-resolution imaging, 0.4μm optical sections were taken through volumes about 15μm deep every three to four minutes. Image data was acquired and stored as TIF files using Leica TCS NT or Leica LCS software.

Visualisation

To visualise the acquired data as time-resolved volumes, images were processed on a Macintosh computer using Object Image (http://simon.bio.uva.nl/object-image.html), a program based on NIH Image (http://rsb.info.nih.gov/nih-image/) or Volocity (Improvision, UK). NIH Image macros for 4D visualisation (LOCI, University of Wisconsin-Madison) were adapted to produce maximum intensity projections (MIPs) for each volume (or time point) rotated through 360° around the X- and Y-axes at 10° intervals. All projections in each dataset were assembled into Quicktime movies using 4D Turnaround software and viewed using 4D Viewer (LOCI, University of Wisconsin-Madison). The software allows the user to view the MIPs generated from each time point, and therefore 'rotate' the volume as well as step through the data in time. LOCI software is available at http://www.loci.wisc.edu/4d/native/4d.html. With Volocity, each time point was volume rendered and could be viewed from any angle while being viewed as part of a time-lapse series. Colour highlighting of particular features in time-lapse images was done using a combination of Object-Image, Volocity and Adobe Photoshop.

Definition of Retinal Axes

In order to analyse the orientation of cell divisions in the retina, we defined three orthogonal axes in the retina. The first is the apico-basal or radial axis, which is perpendicular to any given point on the surface of the retina, and runs between its apical and basal sides. Orthogonal to the radial axis are two axes that run within the plane of the retinal surface itself. By considering the retina as an ellipsoid body much like a globe, with the lens at one pole and the optic nerve head at the other, we can define a central-peripheral axis analogous to lines of longitude or great circles on a globe and a circumferential axis analogous to lines of latitude running orthogonal to the central-peripheral axis (Fig. 3.4a).

Analysis of Orientation of Cell Division (Zebrafish)

In order to check if cells divided apico-basally or radially, we analysed the orientation of cell division in the apico-basal direction with respect to the apical surface. To measure this orientation, maximum intensity projections of each time point of interest were rotated around the X- or Y-axis into a position that revealed the closest relationship between the nuclei and the apical surface. The apical surface was marked as the contour formed by any labelled pigment epithelial cells. The difference in orientation between a line joining

the centres of the two cells or nuclei (equivalent to the mitotic spindle axis) and an estimated tangent to the apical surface was measured in terms of an acute angle between 0° and 90°. An angle close to 0° represented a cell division parallel to the apical surface, while an angle closer to 90° represented an apico-basal division.

To measure the orientation of cell division within the apical or retinal surface, the mid-point of the 'spindle axis' joining a pair of daughter cells was determined and a line was drawn from the centre of the lens to the mid-point, to be taken as the 0° reference. Such a line is simply a projection of a central-peripheral line on the surface of the retina. The orientation of this line was compared to the orientation of the spindle axis and measured. An angle of 0° indicated a division in the central-peripheral axis while 90° meant a division in the circumferential axis. For daughter cell pairs that were aligned with the z-axis of the volume, and therefore impossible to distinguish in the lateral view of the eye, the whole volume was rotated by 90° around the X- or Y-axis. The measurement procedure was then followed as described above.

Analysis of Orientation of Cell Division (Rat)

We studied the orientation of cell division in the retina of Sprague Dawley rats. Animals were killed at embryonic day 16 (E16), postnatal day 0 (P0), or P4. The eyes were removed, and the retinas dissected free from surrounding tissue in cold HBSS. Retinas were flat-mounted (vitreous side down) on a microscope slide and fixed with 4% paraformaldehyde for 1 hour at room temperature. They were then rinsed three times in PBS and counterstained with propidium iodide (5μg/ml in PBS + 25U RNase A) to visualize nuclear morphology. They were examined with a laser scanning confocal microscope (BIO-RAD MRC 1024), and z-series in 1μm steps were acquired in the central and peripheral regions of the retina.

To determine the orientation of cell divisions within the retinal surface, a line was drawn from the optic nerve head to the periphery of the retina (equivalent to the central-peripheral axis), and another line was drawn perpendicular to the first to serve as the 0° reference line. The angle between this reference line and the spindle axis was taken as the angle of division. An angle of division of 0° would correspond to a mitotic spindle aligned along the circumferential axis of the eye, whereas an angle of 90° would correspond to a mitotic spindle aligned along the central-peripheral axis of the eye. To be

consistent with the fish data, however, we used the complementary angles to those of the rat results so that an angle of 0°, for example, became 90° (circumferential) and an angle of 90° became 0° (central-peripheral).

Analysis of the Basal Process

To visualise the basal process of a neuroepithelial cell during mitosis, zebrafish embryos were injected with GAP-GFP, which labels cell membranes, and their retinas were imaged as described above ('Visualisation'). A short time series of a volume of interest containing a dividing cell was rendered using Volocity (Improvision, UK). This allowed us to freely rotate the volume and attempt to determine whether the basal process could be seen. Looking at time points before and after mitosis also helped to identify the basal process. For basal processes that could be seen, we also described which area of the cell's surface the basal process emanated from, since a decentralised basal process could be inherited asymmetrically after mitosis depending on the cleavage plane of the cell. We defined its position in terms of the central-peripheral and circumferential axes mentioned above. On the basal aspect of the cell, the position of the process could be described in relation to the cell's pole as 'lateral' or 'central' in the circumferential axis and as 'central' or 'peripheral' in the central-peripheral axis.

Results

I. There are no apico-basal divisions in the zebrafish retina

To study the behaviour of dividing neuroepithelial cells in the developing retina, zebrafish embryos were stained with Bodipy-FL-C_5-Ceramide, a fluorescent dye that is distributed in the interstitial space between cells. Imaging by confocal laser scanning microscopy allowed the outline of all retinal cells to be visualised over time. Dividing cells could be clearly identified (Fig. 3.1), however labelling of every cell in the retina made tracking the morphology and position of individual cells extremely difficult. Nonetheless, analysis of images of dividing cells provided two avenues for further investigation. First, no divisions were noticed with a cleavage plane parallel to the ventricular surface. Secondly, mitotic cells were found that seemed to retain a process to the basal side of the retina as indicated by an increased intensity of signal compared to the plasma membrane of neighbouring cells. In order to label fewer cells in the retina so that these could be visualised more clearly, we imaged zebrafish embryos injected with DNA encoding GFP based fusion proteins. H2B-GFP, a fusion protein of Human Histone 2B and eGFP localises to the chromatin in nuclei (Kanda et al., 1998). When injected into zebrafish embryos, it is an extremely effective label for studying cell divisions as changes in chromatin arrangement during mitosis can be seen easily in time-lapse movies. Embryos were imaged in 10 to 15 minute intervals for a minimum of 10 hours starting at 27.5 hpf up to 45 hpf, a time period encompassing the beginning of neurogenesis in the retina (28 hpf) and the birth of all retinal ganglion cells, as well as most inner nuclear layer cells in the central retina (Hu and Easter, 1999). Each time-point consisted of a volume that was reconstructed and could be rotated around any axis as described in the Materials and Methods section. The angle of orientation was initially analysed with respect to the apico-basal axis and the retinal or apical surface (Fig. 3.2). An orientation of 0° represents a division that occurred parallel to the tangent plane of the apical surface at the point of division, while an orientation of 90° is characteristic of a division orthogonal to this plane, i.e. an apico-basal cell division. Surprisingly, no cell divisions occurred at orientations greater than 40°at any of the time-points analysed (Fig. 3.3a). 70% of the observed cell divisions (n=131) were orientated by 10° or less towards the retinal surface. The rest were orientated by larger angles. The first postmitotic cells in the

zebrafish retina are ganglion cells born around 28 hpf, with the peak rate of neurogenesis between 33 hpf and 48 hpf (Nawrocki, 1985). However, the distribution of orientations of cell divisions remained the same regardless of time, as revealed by cumulative plots of orientations at different time periods (Fig. 3.3b). If some postmitotic cells in the zebrafish retina are indeed born of asymmetric cell divisions, the lack of apico-basal divisions would indicate that these asymmetries occur in a planar orientation.

II. The orientation of cell division shifts from a central-peripheral to a circumferential axis over time

To look for signs of asymmetry in planar retinal cell divisions, the orientation of divisions parallel to the apical surface was characterised with respect to the central-peripheral axis. Considering the retina as a thickened shell of an ellipsoid body, a central-peripheral axis would be equivalent to lines of longitude or great circles drawn on its surface (green in Fig. 3.4a), with the centre of the lens as one of the poles and the optic nerve head as the opposite pole. In a 2D projection of the ellipsoid as seen from the optic nerve head pole, as is done when making flat-mount preparations of the retina, these lines would look like radial lines emanating from the centre. Perpendicular to the central-peripheral axis is a circumferential axis equivalent to lines of latitude on a globe (red in Fig. 3.4a). In our analysis, an orientation of 0° represents a cell division along the central-peripheral axis, while an orientation of 90° represents a division along the circumferential axis (Fig. 3.4b-e). Fig. 3.5a depicts the cumulative distribution of orientations of division in relation to these two axes and its change over time. Before 30 hpf, when neurogenesis is just beginning in the retina, 68% of cell divisions (13/19) were orientated at <45°. However after 40 hpf, by which time all retinal ganglion cells have been born and inner nuclear layer cells have started to become postmitotic (Hu and Easter, 1999), only 18% (2/11) cells divided at <45°. In fact, all remaining cells from this time period divided at an orientation greater than 60° from the central-peripheral axis. The distribution of orientations before 30 hpf was significantly different from the distribution after 40 hpf. The gradual shift in the distributions of orientations over time is evident. The proportion of cell divisions occurring along the circumferential axis, therefore, increases over time at the expense of central-peripheral axis divisions. Two possibilities are considered further to explain the temporal change in orientation of divisions. First, the retina undergoes morphogenetic changes including an abrupt increase in volume from 33 hpf (Li et al., 2000b). Different orientations of cell divisions may contribute differently to the growth of

the retina in the appropriate proportions for each dimension during this time. Alternatively, the increase in circumferential cell divisions in the retina may reflect an increase in the number of asymmetric cell divisions, which would provide a basis for the increase in rate of neurogenesis that occurs over the time period studied. We considered the possibility, therefore, that circumferential divisions represent asymmetric divisions. To test this idea it was necessary to follow the daughter cells through subsequent divisions (see section V). In one case of a circumferential division, we were able to trace both resulting daughters and found that both of them divided again – i.e. a symmetrical division by the limited definition that these daughters share the phenotype of remaining in the cell cycle. While it is not possible to draw general conclusions from a single case, clearly not all circumferential divisions are asymmetric.

III. The distribution of orientation of cell divisions also shifts over time in the developing rat retina

We performed a similar analysis for planar orientations of retinal progenitor cell divisions using fixed rat retinas from 3 different time-points in development (E16, P0 and P4). During E16 and P0, there was no difference between central-peripheral and circumferential divisions (52.5% vs. 47.5% and 55% vs. 45% respectively). However, during P4, 73% of cells divided circumferentially, while only 26% of cells divided along the central-peripheral axis (Fig. 3.5c). The distribution of orientations of cell divisions during P4 is similar in tendency to the distribution of cell division orientations in zebrafish aged between 35 and 45 hpf. In the rat retina, rods, Müller cells and bipolar cells are predominantly born after P0 (Young, 1985) while in zebrafish, cells from the inner nuclear layer including Müller cells and bipolar cells are born between 38 and 48 hpf. The correspondence in shifting proportions of cell division orientation between zebrafish and rat models implies that the change towards circumferential divisions is important in the development of the vertebrate retina.

IV. Orientation of division in syu *mutants*

The circumferential axis is also the axis along which the neurogenic waves of the retinal ganglion cell and inner nuclear layers, characteristic of the zebrafish retina, spread (Hu and Easter, 1999). Initiated within the ganglion cell layer at 28 hpf in an area adjacent to the optic fissure known as the ventro-nasal patch, the wave travels over 10 hours along

the circumferential axis to the temporal side of the retina. Similarly, the neurogenic wave in the inner nuclear layer is initiated at 38 hpf in the ventro-nasal patch and ends in the temporal retina after 10 hours. One signalling molecule that is expressed in a spatio-temporal pattern characteristic of the neurogenic wave is Sonic Hedgehog (Shh), which has a role in initiating retinal ganglion cell differentiation (Neumann and Nuesslein-Volhard, 2000), as well as a later role in inhibiting excess retinal ganglion cell differentiation (Zhang and Yang, 2001). A correlation between the spread of Shh activity, and hence neurogenic activity, along the circumferential axis of the retina and the increase in circumferentially orientated cell divisions would provide further evidence for such divisions tending to be asymmetric. In the *sonic you (syu)* mutant, Sonic Hedgehog expression is reduced and the wave of expression does not spread, resulting in a failure of normal retinal ganglion cell differentiation. To check if the distribution of orientations of cell divisions was changed due to the disruption of the wave of differentiation, H2B-GFP was injected into *syu* mutants, and orientations of cell divisions in the retina analysed as described above. In terms of the apico-basal orientation of cell divisions, the majority of divisions occurred parallel to the retinal epithelial surface, as in the wildtype. However, a few apico-basally orientated divisions were observed (data not shown). These may reflect disruption of the normal process of retinal progenitor cell division due to the mutant nature of the embryos, as opposed to a representation of asymmetric cell divisions, since none were observed in wildtype embryos. The gradual shift in proportion from central-peripheral to circumferential divisions that is seen in the wildtype retina is absent or delayed in *syu* (Fig. 3.5c). The difference in the temporal change of proportions of cell division orientations between wildtype and *syu* embryos is consistent with the hypothesis that circumferential cell divisions tend to be asymmetric, and that the lack of Sonic Hedgehog secretion delays the expected increase in asymmetric neurogenic divisions. However, we cannot rule out the hypothesis that the failure of the retinal ganglion cell layer to form properly affects the morphogenesis of the growing retina. Indeed, the retina of *syu* mutants is less organised and slightly smaller than the wildtype retina. It is also possible that in *syu* there is simply a delay in growth relative to the wildtype retina, and that this delay causes a consequent delay in the change of proportions of cell division orientations observed.

V. Retinal ganglion cells followed from division

In an attempt to follow cell divisions leading to neurogenesis, transgenic zebrafish expressing GAP-GFP under the control of the promoter for the Brn3c transcription factor, in which retinal ganglion cells could be identified by the expression of membrane-tagged GFP, were used. GAP-GFP expression driven by Brn3c is first seen at 45 hpf, about 17 hours after the first ganglion cells are actually born. Due to the membrane binding nature of the GFP, the cells and their axons can be visualised, however cells are difficult to distinguish from each other as all cells in the retinal ganglion cell layer are labelled. The optic tract from the retinal ganglion cells to the optic tectum is clearly delineated (Fig. 3.6). Transgenic embryos were injected with H2B-GFP DNA to label a random population of nuclei in the retina, and imaged in three dimensions by time-lapse TPLSM from 27 hpf to at least 50 hpf at 15 to 30 minute intervals. The large resulting time series were then studied starting at a timepoint when GAP-GFP staining could clearly be seen, thus identifying cells that had been stained by GAP-GFP and also had nuclear H2B-GFP staining. These cells were followed back through the time-lapse series until the division that led to the birth of the cells could be identified. The siblings of the identified cells were also followed forward in time as far as possible. A cell division could be labelled asymmetric if the sibling to the identified retinal ganglion cell was to divide again (and therefore not destined to undergo neuronal differentiation in that cell cycle), or symmetric if the sibling also underwent differentiation to become a retinal ganglion cell, as seen by GAP-GFP labelling. However, of 39 cells tracked, only one retinal ganglion cell could definitely be traced back to its originating cell division. The division occurred circumferentially at 33 hpf and gave rise to a retinal ganglion cell and a sibling that underwent apoptosis by 55 hpf (Fig. 3.7). Due to the death of the sibling, its fate remains unknown and this division cannot be defined in terms of symmetry. In all other cases, cells could not be traced back to a division for a number of reasons – three cells had already divided before the beginning of the experiment and could not be identified, give cell nuclei were actually lens cell nuclei that were identified because they divided within the lens area instead of the ventricular surface, although their close apposition to the ganglion cell layer led to their mistaken identification as retinal ganglion cells. The rest of the retinal ganglion cells (29 cells) could not be traced back through the time series due to loss of the cell nuclei from the field of view, or inability to distinguish the cell nucleus at particular timepoints from those of other close neighbours. A few cells that divided early

in the experiments were tracked forward through the time series in case any of the resulting daughters differentiated as retinal ganglion cells, as the time of cell division (around 28 hpf) would be consistent with the birth of the earliest cells to become RGCs. Of these, one cell divided circumferentially to give rise to siblings that both underwent circumferentially oriented mitosis at 34 hpf and 37 hpf – a symmetrical division (Fig. 3.8a-c). In two other pairs of siblings, also from circumferential divisions, one daughter remained near the ventricular surface while the other lay close to the retinal ganglion cell layer, although without expressing GAP-GFP by the end of the time series (Fig. 3.8d-e). These may speculatively represent asymmetrical divisions if the cells that remained close to the ventricular surface are assumed to remain in the cell cycle.

VI. Partner of Numb, a potential molecular marker for asymmetric division

Partner of Numb (Pon) is an adaptor protein required for the asymmetric localisation of Numb in asymmetric divisions in Drosophila neuroblasts. A Pon-GFP fusion protein has been used to label the asymmetric distribution of Partner of Numb *in vivo* in Drosophila neuroblasts (Lu et al., 1998; Lu et al., 1999; Roegiers et al., 2001). RNA for the Pon-GFP fusion protein was injected into zebrafish embryos in an effort to visualise Pon-GFP as a molecular marker for asymmetric divisions in the retina. Although Pon-GFP RNA was expressed, expression levels were low and difficult to detect by TPLSM (Fig. 3.9a). The expression was diffuse within neuroepithelial cells, perhaps with some concentration in the nuclei, similar to the expression pattern seen in Drosophila interphase cells (Lu et al., 1999). However, in the few mitotic cells that could be seen, the staining remained diffuse and was not localised to either the basal or apical side of the cell (Fig. 3.9b). Pon-GFP RNA was also injected along with GAP-GFP DNA, which would label the cell membranes, to localise the Pon-GFP signal accurately with respect to the cell membrane. Two problems presented themselves with this approach. The weakness of the Pon-GFP signal compared to the GAP-GFP signal meant that it was difficult to judge whether Pon-GFP was being adequately expressed. Secondly, both constructs were based on GFP, and could therefore not be distinguished by any means other than the cellular compartment in which they might be expressed (the cell membrane vs. the cell cytoplasm or nucleus). A few cases were observed where a signal from within the cell cytoplasm, forming a structure distinct from the cell membrane and located in the basal side of the cell, could be visualised during cell division (Fig. 3.9c and 3.10a). This structure was distributed

asymmetrically to only one of the two daughter cells resulting from the mitosis. The structure can be seen during mitosis, and seems to be distinct from the space occupied by the cell nucleus. Its segregation to only one daughter cell is intriguing, and may represent a Pon-GFP signal. This structure was not seen when imaging the retinas of zebrafish injected with GAP-GFP alone. Although this may be indicative of an asymmetric division and can be seen in both circumferential (Fig. 3.10a) and central-peripheral divisions (Fig. 3.9c), no significance has currently been attached to the presence of the structure, as it cannot be positively identified as either Pon-GFP or GAP-GFP and is seen infrequently. Attempts were made to produce different colour combinations of GAP- and Pon- fusion proteins in order to be able to distinguish between the two definitively. GAP-YFP, GAP-CFP and GAP-DsRed fusion constructs were made successfully. Pon-YFP and Pon-CFP constructs were also made and shown to be identical to Pon-GFP when sequenced, except for the short nucleic acid sequence that governs the spectral properties of the fluorescent protein. The GAP-DsRed construct was made using a sequence encoding the DsRed1 construct from Clontech (BD Biosciences, Palo Alto, CA). This version of the tetrameric DsRed has a greater tendency to form protein aggregates than later variants, resulting in a punctate staining pattern (Bevis and Glick, 2002). Although GAP-DsRed labelled cell membranes when injected as DNA or RNA into zebrafish embryos, the punctate pattern made the cell outlines difficult to visualise. Cell membranes in GAP-YFP or GAP-CFP injected embryos could be visualised, however neither Pon-YFP, nor Pon-CFP could be imaged effectively by TPLSM. There may be a number of reasons for this. The expression level of Pon constructs was known to be low (as noted by the use of Pon-GFP constructs) and CFP has a lower quantum yield than GFP that would make it more difficult to image. YFP has been shown to be optimally excited by TPLSM at wavelengths closer to 950nm (K. Svoboda, pers. comm.), a wavelength at which the TPLSM system used cannot provide adequate power for imaging weak fluorophore expression. Pon-YFP and Pon-CFP signals could not be usefully imaged using CLSM either, indicating that expression levels were probably too low. Injecting higher concentrations of DNA or RNA of the constructs or the use of higher laser powers to image them were lethal to the embryos and did not provide an advantage in imaging. Although some imaging experiments using Pon-GFP in combination with GAP-GFP indicated the possibility of asymmetric segregation of a marker in planar cell divisions, the identity of the marker could not be confirmed as Pon-GFP due to the unexpected

pattern of the signal (resembling the nuclear membrane) and the low number of cases seen. Further experiments, perhaps with optimised versions of DsRed now available, will be required to confirm or exclude a potential role for Partner of Numb in vertebrate asymmetric division.

VII. The basal process persists during mitosis

Miyata et al. recently showed that when radial glial cells in the developing mouse cerebral cortex divided, the membranous process that anchored the glial cell to the basal or pial side of the cortex persisted through the division. They also suggested that this process was more likely to be asymmetrically inherited by the neuronal progeny of the radial glial cell (Miyata et al., 2001). To follow the basal process through the division of retinal neuroepithelial cells, a membrane targeted eGFP construct (GAP-GFP) was used to visualise cell membranes. These time-resolved experiments revealed that the basal process does indeed persist during cell division. Out of 81 cell divisions observed between 27 hpf and 48 hpf, 77 cells had a basal process that clearly persisted throughout the division. In the other four cases, the presence or absence of the basal process could not be determined due to low signal intensity. Dividing cells also had an 'apex', a slight protrusion that the basal process emanated from, which could be seen in all 81 cases. There were no clear cases where the basal process was seen to actually retract during cell division. The most likely possibility, therefore, is that all dividing cells in the zebrafish retina retain a basal process. Most of the cytoplasm seems to end up in the mitotic cell body at the apical side so that the basal process itself becomes extremely thin. If labelled neighbours do not surround the dividing cell, the basal process can be seen clearly in 3D reconstructions of the volume (Fig. 3.10a). If the cell is surrounded by labelled neighbours however, the persistence of the membrane is indicated by a higher intensity at the expected position along the cell membrane of adjacent cells. After metaphase, the basal process becomes more visible again as cytoplasm moves back into it. The position of the basal process at this time is almost identical to that of the process prior to cell division, indicating that the basal process persisted and retained its structure during the division. In many cases, the time elapsed between mitosis and the process being refilled with cytoplasm is very short, on the order of 15 minutes. Occasionally, as the nucleus and cytoplasm of a cell shift to the apical side in preparation for cell division, a small volume of cytoplasm will fail to move from the basal process into the soma. It becomes trapped in a bubble-like swelling of the basal process at some distance from the main body of

cytoplasm. After cell division, the stray cytoplasm always joins one of the two daughter cells produced, confirming the existence of a continuous connection between at least one daughter cell and the stray cytoplasm and thus, the persistence of the basal process (Fig. 3.10b).

VIII. Inheritance of the basal process after cell division

By time-lapse analysis, we noticed that, in some cases, the basal process seemed to be inherited by one of the two daughter cells. Similar to the report of asymmetric inheritance of the basal process in mouse radial glial cells (Miyata et al., 2001), we addressed two questions. Firstly, how exactly is the basal process of a dividing cell inherited by its daughter cells? And secondly, if only one of the two daughter cells inherited the basal process, was this event correlated in any way to any other asymmetry in such a division? Of the 77 cells whose basal process could be seen, 54 (70%) divided such that only one daughter cell clearly inherited the basal process. For each of these cases, we found that the basal process or the apex that it emanated from was already positioned slightly off-centre with respect to the basal pole of the cell prior to mitosis (Fig. 3.11). By rotating a rendering of the prophase cell around its apico-basal axis, the position of the process was determined in relation to the central-peripheral and circumferential axes of the retina. A basal process positioned off-centre in one axis results in an asymmetry of inheritance if the cleavage plane of division is in the other axis. The position of the basal process could be consistently used (71.5% of the time for 54 cells) to predict which daughter cell, if not both, would inherit the process given a certain orientation of division. This shows that the basal process does not have to split two ways nor is it always inherited by just one daughter cell. In fact, its position at prophase and the orientation of division will determine how it is inherited. Within 15 or 20 minutes of mitosis, the daughter cell that did not inherit the process usually rejoined its sibling's basal process with its basal apex lying adjacent to it.

Observed

		Axis	
		Central-peripheral	Circumferential
Inheritance	asymmetric	22.00	15.00
	symmetric	18.00	20.00

Expected

		Axis	
		Central-peripheral	Circumferential
Inheritance	asymmetric	19.73	17.27
	symmetric	20.27	17.73

Table 1. *The number of observed and expected cell divisions that are oriented along the central-peripheral or circumferential axes and resulted in symmetric or asymmetric inheritance of the basal process.* The chi-squared test for independence between the orientation of cell division and the mode of inheritance of the basal process shows that the two factors are independent of each other (p=0.29).

Since an asymmetry in the position and inheritance of the basal process was seen, developing retinas labelled with GAP-GFP were analysed for the orientation of cell division along with the asymmetric inheritance of the process (Table 1) as well as for temporal differences in the proportion of cells whose basal process is asymmetrically inherited.

Asymmetric inheritance of the basal process and the planar orientation of cell division were found not to correlate with each other (p=0.29) and are, therefore, independent of each other. Similarly, the proportions of cell divisions that led to asymmetric inheritance of the basal process did not change significantly over time, at least between 26 hpf and 48 hpf, indicating that inheritance of the basal process is not regulated by the same processes that regulate the temporal changes in cell division orientation. We were unable to follow both daughters of a cell whose basal process had been inherited by only one daughter to determine whether or not both daughters were capable of dividing again.

Discussion

The present study attempts to address the question of how cell divisions take place in the vertebrate central nervous system by taking advantage of the zebrafish retinal model. Direct visualisation of the retina *in vivo* has allowed us to avoid the issues involved with maintaining structural and physiological integrity of specimens while analysing the movement and changes in morphology of neural progenitor cells. A model of a cell dividing in the zebrafish retina that summarizes much of this data is shown in Fig. 3.12.

Time-lapse analysis has revealed changes in cell division patterns that correlate temporally to an expected transition from symmetric to asymmetric divisions (Cayouette et al., 2001; Chenn and McConnell, 1995). The current study clearly confirms the persistence and occasional asymmetric inheritance of the basal process of neuroepithelial cells during cell division. Yet, we were unable to furnish any direct evidence that the orientation or asymmetry of basal process inheritance was causally connected with a cell division in which one daughter differentiated while the other remained in the cell cycle.

I. Orientation of Cell Division

We initially analysed the orientation of cell division with respect to the apico-basal axis and the ventricular surface of the retina by imaging zebrafish with their nuclei labelled by the transient expression of H2B-GFP. The current model for asymmetric cell division in the vertebrate cortex and retina holds that cell divisions occurring along the apico-basal axis are asymmetric, with the basal daughter cell becoming a post-mitotic neuron or a Müller glial cell. Evidence for this comes from time-lapse studies of dividing cells in the neuroepithelium of the ferret cortex (Chenn and McConnell, 1995) as well as antibody staining of Numb, an asymmetrically segregated cytoplasmic cell fate determinant, in chick, mouse and rat progenitor cells (Cayouette et al., 2001; Silva et al., 2002; Wakamatsu et al., 1999; Zhong et al., 1996) and Notch, a potential target for Numb in mouse, rat and ferret progenitor cells (Chenn and McConnell, 1995; Johansson et al., 1999; Zhong et al., 1997). We were surprised by our result that no apico-basal divisions take place in the zebrafish retina. This is in contrast to recent studies of asymmetric division in rat and chick, which showed that apico-basal cell divisions do take place in the retina during neurogenesis, albeit at a relatively low frequency (Cayouette et al., 2001; Silva et al., 2002). A number of reasons could explain this apparent discrepancy. Not all

cells are labelled when an embryo is injected with H2B-GFP DNA, so it is possible that the rare occurrences of apico-basal divisions were simply missed. However, in the rat retina, 3% of divisions were found to be apico-basal at a time point when the frequency of apico-basal divisions was at a minimum. From the data presented here the chance that no apico-basal divisions are found if 3% are expected is less than 0.05 (chi-squared test). The likelihood that none are found when 10 to 20% of divisions are expected to be apico-basal (the peak proportion in rat) (Cayouette et al., 2001) is much lower still ($p<0.0001$).

In the study of apico-basal divisions in the rat retina, the authors found that m-Numb was expressed in the apical daughter of an apico-basal division, while Notch was expressed throughout the progenitor cell and therefore in both daughter cells (Cayouette et al., 2001). The proposed model is that m-Numb inhibits Notch in the apical cell but lack of inhibition in the basal cell allows Notch to promote the differentiation of the basal cell into a Müller glial cell. This would be consistent with the low frequency of apico-basal divisions in the rat retina being responsible for only one cell type. The present study covers part of the time, until 45 hpf, when Müller glial cells, which lie in the inner nuclear layer, are expected to be born (38 to 48 hpf) (Hu and Easter, 1999). Assuming that about 5-10% of cells will become Müller cells (McFarlane et al., 1998; Ohnuma et al., 1999), one would expect the same proportion of recorded divisions to be apico-basal according to the proposed model. Since 50 divisions were recorded in this time period, five of these should give rise to Müller glial cells, yet we noticed no apico-basal divisions during this period. The probability of observing none when the expectation is five is 1.8%, therefore it is unlikely that in the zebrafish retina apico-basal divisions are responsible for generating Müller cells. Although species differences could be called upon to explain the lack of apico-basal divisions in the zebrafish retina compared to other vertebrates, it is more likely that asymmetric cell divisions, if they do exist, do not take place along the apico-basal axis of the fish retina.

Asymmetric divisions may also be manifest in a different way from apico-basal divisions. If cells in the neuroepithelium possess some planar polarity, cytoplasmic cell fate determinants could segregate asymmetrically along the planar axes, parallel to the ventricular surface. In the Drosophila peripheral nervous system, asymmetric divisions have been shown to take place in the plane of the neuroepithelium along the anterior-posterior axis. The first division of the Sensory Organ Precursor lineage is an asymmetric division of the pI cell in the a-p axis, with the polarity of pI mediated by Frizzled

signalling. pIIa, one of pI's daughters, also divides along the a-p axis although its polarity is controlled by a different mechanism (Bellaiche et al., 2001; Gho and Schweisguth, 1998). Given the presence of homologous proteins in vertebrates of many of the proteins involved in planar cell polarity in Drosophila (Huttner and Brand, 1997; Knoblich, 2001; Lu et al., 2000), similar mechanisms may mediate a planar polarity in zebrafish retinal cells. In the chick retina, about 15% of divisions observed were apico-basally oriented and asymmetric. However, 35% of planar divisions were also observed to be asymmetric, as determined by the expression of c-Numb or RA4, an antigen expressed early in differentiating retinal ganglion cells.

The potential for a planar polarity in the neuroepithelial cells led us to analyse the orientation of cell divisions within the planar surface. Two orthogonal axes running along the retinal surface were defined – a central-peripheral axis and a circumferential axis. We found, in both zebrafish and rat, that the proportion of cells dividing in the circumferential axis increased over time at the expense of divisions orientated with the central-peripheral axis, and that this increase represented a significant change. The cell divisions are therefore not orientated randomly but show a particular bias. Time-lapse imaging of mitotic spindles in the ventricular zone of rat cortical slices showed that although the spindles spin around just prior to M-phase, they spend most of their time in two orthogonal orientations parallel to the ventricular surface, finally stabilising in one of the two orientations for mitosis (Adams, 1996). This would suggest that the orientation of cell divisions during cortical neurogenesis is regulated within the plane of the ventricular zone. In the retina, the change in trend of division orientation over time could be due to two different phenomena: it could be part of the morphological changes of growth that the retina goes through, including an associated increase in the volume of space in which the cells can divide, or it could reflect the transition from symmetric to asymmetric divisions that would be expected with increasing levels of terminal neurogenesis.

If circumferential divisions are asymmetric cell divisions, the neurogenic wave could be the basis for a signal spread along the circumferential axis that provides a planar polarity to dividing cells. A few cell fate determining genes, such as *ath5* and *sonic hedgehog* have been identified that are expressed in the same pattern as the neurogenic wave and are involved in the differentiation of retinal ganglion cells (Kay et al., 2001; Masai et al., 2000; Neumann and Nuesslein-Volhard, 2000). Since the wave itself spreads along the circumferential axis of the retina, one can speculate that the later increase in proportion of

divisions orientated along the circumferential axis is related to the advent of the neurogenic wave and hence to the differentiation of cells. More circumferentially orientated divisions could be asymmetric in nature compared to central-peripheral axis divisions, with one cell being exposed to a higher concentration of a signalling protein that propagates the neurogenic wave. In *syu* zebrafish embryos, the expression of Shh is abolished, affecting the production of retinal ganglion cells but not of cells in the inner nuclear layer or photoreceptor layer. The increase in circumferential divisions is either absent or delayed in these mutants. This difference may correspond to the absence of asymmetric cell divisions that would normally give rise to retinal ganglion cells.

The model that circumferential divisions are likely to be asymmetric is supported by correlational evidence, but direct evidence is lacking. Attempts were therefore made to trace retinal ganglion cells and their siblings from their final mitosis to differentiation. Transgenic zebrafish expressing GAP-GFP under the control of the promoter for the Brn3c transcription factor were used to positively identify retinal ganglion cells as those expressing GAP-GFP. These transgenic embryos had also been injected with H2B-GFP DNA to label a random population of nuclei in the retina, and imaged from 27 hpf to at least 50 hpf, a period in development when retinal ganglion cells are born and differentiate. Brn3c expression was itself first seen about 17 hours after the first ganglion cells are actually born. A few cells with nuclei labelled by H2B-GFP and also expressing GAP-GFP due to Brn3c activity (or lying very close to GAP-GFP expressing cells) were traced back in time to the division that gave rise to them, while the other sibling resulting from that division was followed forward. So far, these experiments have shown one case of a circumferential division that led to one cell differentiating while its sibling underwent apoptosis. Two cases of circumferential divisions where one daughter remained close to the ventricular surface while the other was positioned close to the retinal ganglion cell layer on the basal side of the retina were seen, although neither could be positively identified as differentiated retinal ganglion cells. The above data are not inconsistent with the hypothesis that circumferential divisions are asymmetric. However, in this study we also found one example of a circumferential division where both daughters divided again. Thus, although there is correlational evidence suggesting that circumferential divisions are asymmetric, we can say with certainty that circumferential divisions are not always asymmetric in nature with respect to remaining in or leaving the cell cycle. No retinal ganglion cells were traced back to central-peripheral divisions. Although a possibility, it

is unlikely that central-peripheral divisions would never give rise to differentiated retinal ganglion cells. The number of cells successfully traced was too low to make a definite statement on this point. To understand the relationship between the orientation of cell division in the retina and asymmetric cell division in vertebrates, it will be important to continue these types of studies in which the progeny of CNS neuroblasts can be definitively followed either to their eventual determined fate or another cell division. Such studies, although only beginning, impose substantial experimental challenges that can only be overcome with improvements in long term time-lapse microscopy and the creation of zebrafish transgenic lines expressing fluorescent markers that label specific cell types soon after their birth.

Time-lapse studies in which cells are followed from their birth to their fate could be complemented by studies in which molecular markers can be seen to segregate asymmetrically across cells. The experiments with Pon-GFP represent an initial attempt at finding a suitable *in vivo* marker for vertebrate asymmetric division during neurogenesis. Although a few cell divisions were seen in which labelled structures or organelles were segregated asymmetrically, these organelles were not identified. In Drosophila neuroblasts, Pon-GFP is expressed diffusely in the neuroblast cytoplasm and the cell nucleus until mitosis, when it is localised to the basal cell cortex for segregation into the basal Ganglion Mother Cell (Lu et al., 1999). Although Pon-GFP expression is almost identical to endogenous Pon expression, it also differs in that Pon-GFP can also be seen diffusely expressed in the nuclei of interphase cells, a localisation attributed to GFP itself. It is unlikely that this is the expression seen in these cases, as the organelle does not always resemble a nucleus (Fig. 3.9c) and is distinct from the space presumably occupied by the nucleus during mitosis (Fig. 3.9e, 3.10a). The bright outline of the organelle suggests that it has a membrane labelled by GAP-GFP (Fig 2.9d), or may represent an interaction between pon-GFP and GAP-GFP, but it may also be the result of internalisation of GAP-GFP labelled membranes. If the molecules from the labelled organelle were segregated symmetrically as would be expected from a cell nucleus, similar labelled organelles would have been seen in both daughter cells. However, this is clearly not the case. Although it is difficult to attach great significance to these observations due to the low frequency of such occurrences, they do indicate that some mechanism for asymmetric segregation of parts of the cell can exist in planar divisions in the zebrafish retina. The use of alternative Pon constructs with different spectral

properties from the membrane label failed to shed light on the possible role of Pon in asymmetric division in the zebrafish retina. Further work in this area, either using Pon-DsRed constructs (which would allow effective spectral separation from GAP-GFP,) or the use of other potential markers such as Numb-based reporter constructs, should allow for the process of asymmetric segregation to be visualised in the zebrafish retina *in vivo*.

An alternative set of explanations for the shifting trend of orientation of division is that the cell divisions are co-ordinated with the growth and morphogenesis of the retina. The retina undergoes a large increase in its volume around 33 hpf, before which the volume is almost constant after optic cup formation at 16 hpf (Li et al., 2000b). This coincides with the transition to more circumferential cell divisions. Perhaps circumferentially orientated divisions are required for the accelerated increase in retinal volume. We compared observed changes in retinal dimensions to expected changes in retinal dimensions that were estimated from the changes in proportions of orientations of cell division within an equatorial, rectangular patch of the retina. Given the greater proportion of circumferential divisions seen at later time-points, we expected a greater increase in the circumferential dimension of the retina compared to the central-peripheral dimension (6.8% vs. 1.7%). In fact, we found that at later time-points, the retinal surface increased less in the circumferential axis than it did in the central-peripheral dimension (3.5% vs. 7.6%). These figures do not support the hypothesis that orientation of cell division drives the change of shape of the eye. The reverse may, in fact, be indicated; i.e. that overall changes in the growth and morphogenesis of the retina allow more cells to divide circumferentially rather than in the central-peripheral axis. This could provide an alternative explanation for the absence or delay of circumferential divisions in the *syu* mutant – the lack of retinal ganglion cell production could affect the morphogenesis of the retina, in turn affecting the orientation of divisions. The analysis of cell division orientation in zebrafish mutants with small eyes yet well preserved retinal structure, such as *out of sight* (Malicki, 2000), might help uncover possible relationships between orientation of cell division and morphogenesis.

II. The Basal Process

Neuroepithelial cells span the entire width of the retina. In order to divide into two cells, the nucleus and most of the cytoplasm of a cell will migrate to the apical surface of the retina and round up for mitosis. From reconstructions of cells from E13 mouse retinal

sections visualised by electron microscopy, Hinds and Hinds were able to build a sequence of morphological stages that a neuroepithelial cell would presumably pass through as it differentiated into a retinal ganglion cell (Hinds and Hinds, 1974). They found one instance of a cell in mitosis that no longer had a process connecting it to the basal side of the retina. They concluded that the basal process must retract or degenerate during mitosis and grow back as the cell moved into interphase or differentiated. However, recent time-lapse studies in embryonic mouse cerebral slices have shown that the basal process persists during the mitosis of radial glial cells (Miyata et al., 2001; Noctor et al., 2001). Our time-lapse analysis of membrane labelled cells has also shown that, in all clear cases, the basal process of neural progenitor cells persists through mitosis. Although it becomes extremely thin and barely visible, its position does not change significantly immediately before and after mitosis. In addition, there have been cases where part of the cell's cytoplasm failed to migrate into the metaphase cell body, yet rejoined the cytoplasm of one of the daughter cells, now in interphase, shortly after mitosis. Even though the basal process could not always be seen clearly in some of these cases, the stray cytoplasm rejoining the cell must entail some connection persisting between the cell body and the cytoplasm. Since the stray cytoplasm was always basal to the rest of the cell, this connection was probably the basal process itself, which did not degenerate. This supports our conclusion that the neuroepithelial cell retains its connection to the basal side of the retina. Because the basal process is obscured if many cells neighbouring a dividing cell are labelled, we cannot exclude the possibility that the basal process does retract in some cases, although no clear case of this happening was seen in this study. The persistence of the basal process during mitosis brings up the interesting question of asymmetry of inheritance of the basal process. In the cases where the basal process was clearly inherited by only one daughter cell, it was also found asymmetrically positioned on the basal surface of the mitotic cell. Generally, the daughter that did not inherit the basal process would either promptly grow its own process along its sibling's process, or simply join the sibling's process. We could not distinguish between these two alternatives by laser scanning microscopy, nor could we determine if the non-inheriting sibling did not grow a basal process at all. The fact that the non-inheriting cell joined its sibling implies either some sort of recognition between the two siblings or a persisting physical link between the two. The importance of such a link becomes evident when one considers the structure of the retina as a collection of radial units similar to

those in the cortex (Dowling, 1987; Rakic, 1995). Cells of a clone can be physically kept together by the persisting basal process of at least one cell acting as a scaffold for other cells in the clone. This would result in the radial pattern of cells seen when single progenitor cells are marked with lineage tracers (Holt et al., 1988; Turner and Cepko, 1987; Turner et al., 1990). This also provides further support for the idea that the tangential migration and dispersal of retinal cells that is seen when labelling clones of cells is an event that affects cells post-mitotically, perhaps after their migration to particular laminae, rather than as neuroepithelial cells.

Another suggested hypothesis for the role of the basal process during differentiation of retinal cells is that the process itself will become the axon of a retinal ganglion cell or part of the dendritic tree of a horizontal cell, while cells that did not have a basal process after division would become photoreceptor cells or amacrine cells (Hinds and Hinds, 1974; Hinds and Hinds, 1979) The basal process extends from the neuroepithelial cell from a structure seemingly analogous to the axon hillock. In terms of cell differentiation and the basal process, two hypotheses present themselves: as the cell differentiates, its basal process must start retracting from the basal surface. Alternatively, the daughter cell that does not inherit the basal process could start to differentiate without having to grow its basal process all the way to the basal side of the retina. Interestingly, Miyata et al suggest that the neuronal progeny of radial glial cells tend to inherit the basal process (Miyata et al., 2001). This would allow migration of the neuronal cell body to its correct lamina, as well as establish the basis for the cell's axon. Our cell tracing experiments showed one division in which the daughter cell that did not inherit the basal process at mitosis was found to divide again 18 hours later. Furthermore, this daughter cell always remained closer to the apical surface while its sibling, that did inherit the basal process was positioned more basally soon after division. This sibling's fate remained unknown, although we were able to exclude an equation between non-inheritance of the basal process and terminal cell differentiation. We also found two divisions, mentioned earlier, where one daughter cell remained near the ventricular surface while its sibling migrated close to the retinal ganglion cell layer. However, since these cells were labelled with a histone rather than a membrane tag, we were unable to ascertain if there was the expected asymmetry of basal process inheritance in these cases. Future studies using similar time-lapse strategies should reveal the fate of the basal process in cells undergoing asymmetric or terminal divisions.

Asymmetric inheritance of the basal process was found to be independent of orientation of cell division. If asymmetric inheritance of the basal process were, in fact, a physical sign of asymmetric division, this would support a hypothesis where the planar orientation of division is not an indicator of asymmetry, but rather plays a role in retinal morphogenesis. The only certainty is that the two factors, basal process inheritance and planar orientation of division, are not both involved in asymmetric cell division since they do not correlate with each other. Imaging of accessible specimens such as the zebrafish embryo, using live imaging techniques that allow longer and more intensive visualisation times, are making direct evidence for asymmetric division and correlation to either orientation or basal process inheritance more attainable. Preliminary work in which cells are tracked from division to differentiation have produced modest results. Nonetheless, future studies using transgenic zebrafish that express fluorescent proteins in specific cell types and zebrafish mutants in which neural cell proliferation, morphogenesis, and differentiation are disrupted will certainly shed light on these issues.

Fig. 3.1 ***Time-lapse analysis of cell division in the zebrafish embryonic retina.*** This specimen, stained with Bodipy-FL-C_5-Ceramide, shows the outline of all cells in the retinal neuroepithelium (ne). The ventricular or apical surface is adjacent to the retinal pigment epithelium (pe), and the basal surface is adjacent to the lens (le). **a)** Low magnification view of the entire retina using confocal microscopy. A white box frames an area equivalent to that shown in **b-d. b-d)** These frames are confocal sections five minutes apart at the same position in the same specimen. A cell division can be seen clearly (arrowhead). The arrow points to a possible basal process, inherited asymmetrically by one daughter cell, as indicated by the intense signal at the area where it emanates from the dividing cell.

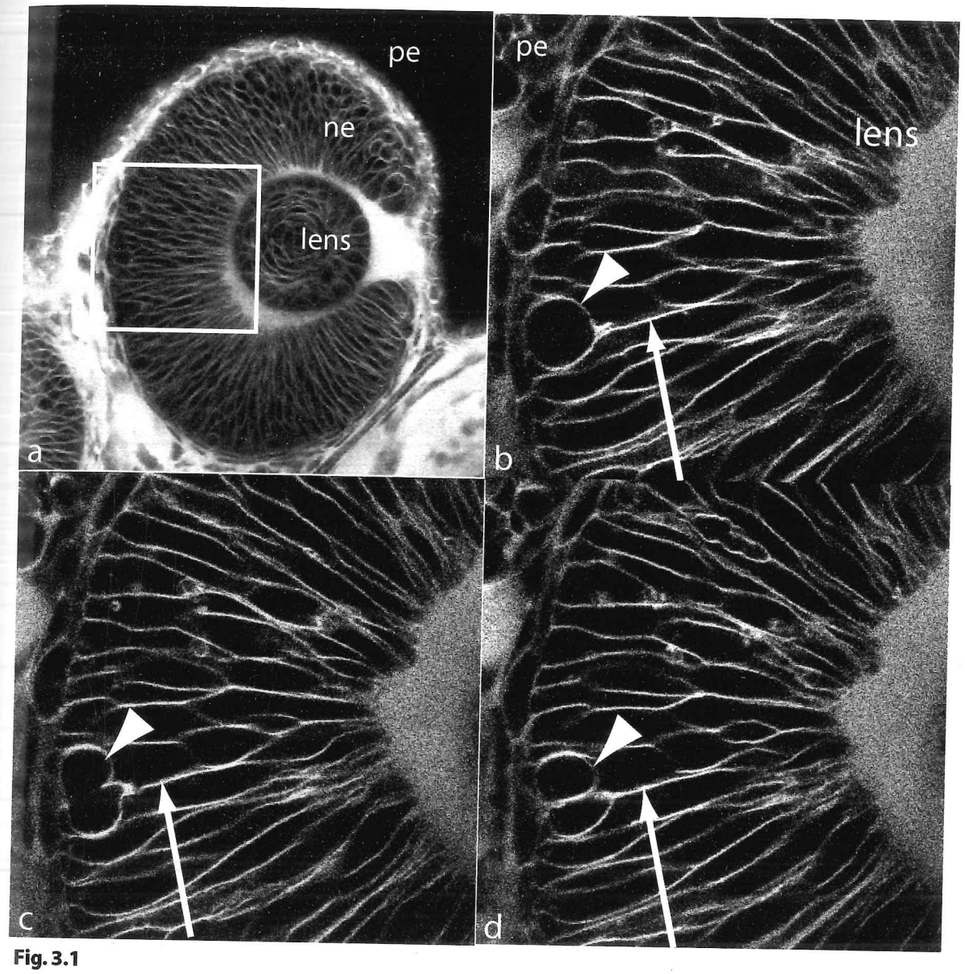

Fig. 3.1

Fig. 3.2 ***Retinal neuroepithelial cells divide parallel to the retinal apical surface.*** Three-dimensional reconstructions of parts of retinas from zebrafish injected with H2B-GFP DNA are shown 10' (**a-a', b-b'**) apart. Nuclei of dividing cells are highlighted in green. White dashed lines represent the apical surface of the retina. The orientation of cell division is measured as the orientation between a line joining the centre of the daughter nuclei and a tangent to the closest part of the apical surface.

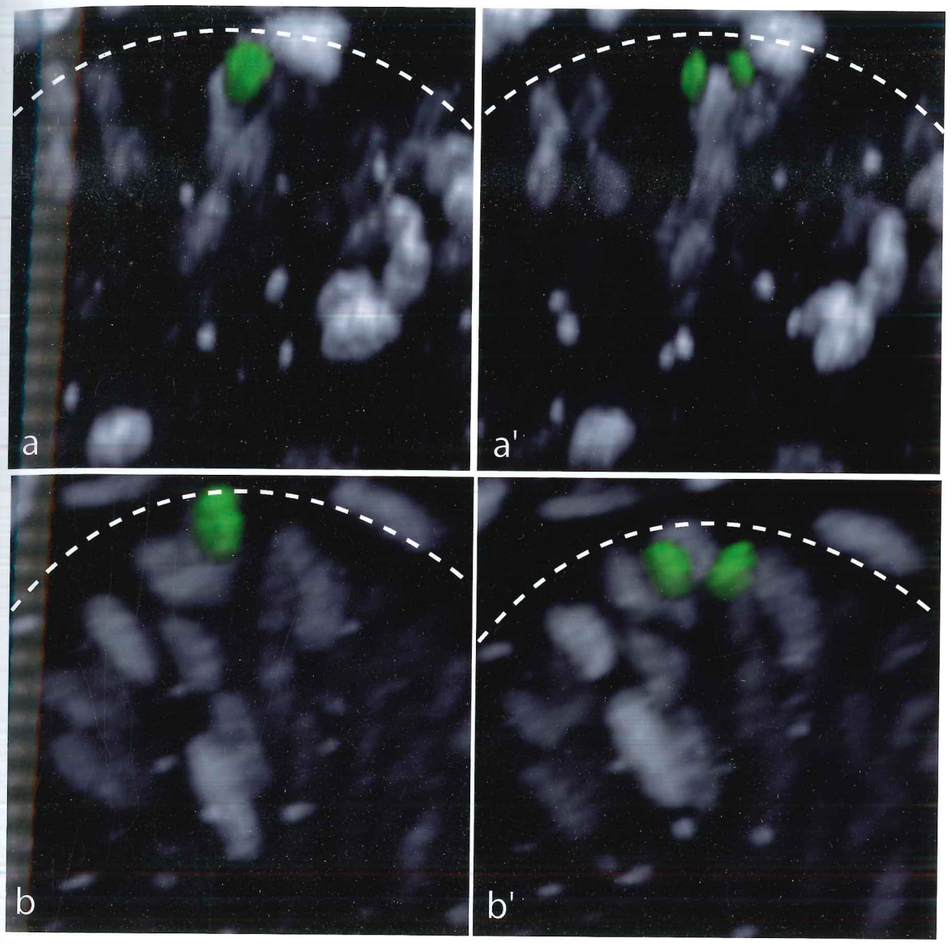

Fig. 3.2

Fig. 3.3 ***Orientation of cell division with respect to the apico-basal axis and retinal surface.*** **a)** An angle of 0˚ represents a cell division parallel to the retinal surface. An angle of 90˚ represents a cell dividing along the apico-basal axis. All divisions observed tended towards the retinal surface, with most divisions almost parallel to the surface. No apico-basal divisions were observed. **b)** Cumulative plot of orientations with respect to the apical retinal surface of all observed cell divisions (n=131) over 4 time periods. There is no significant change in distribution of orientations between the time points.

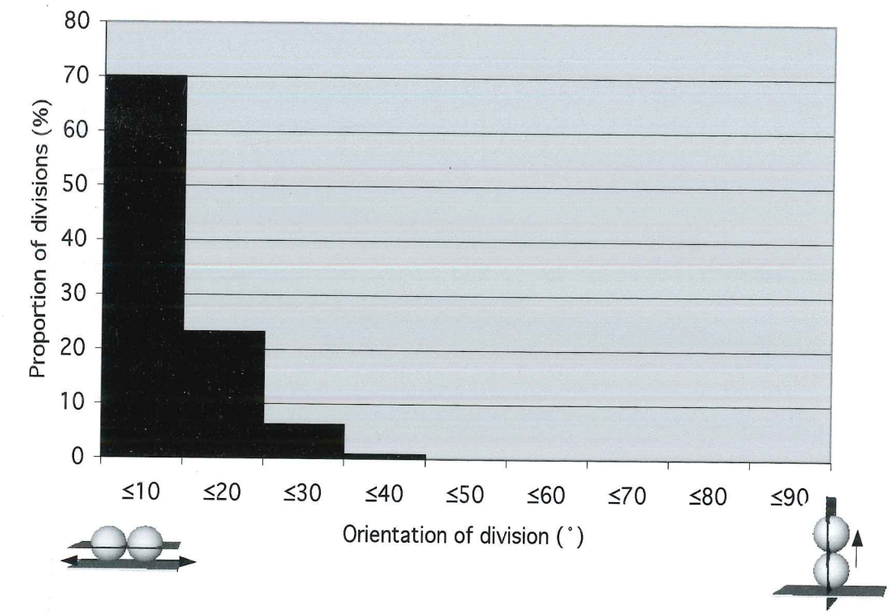

a

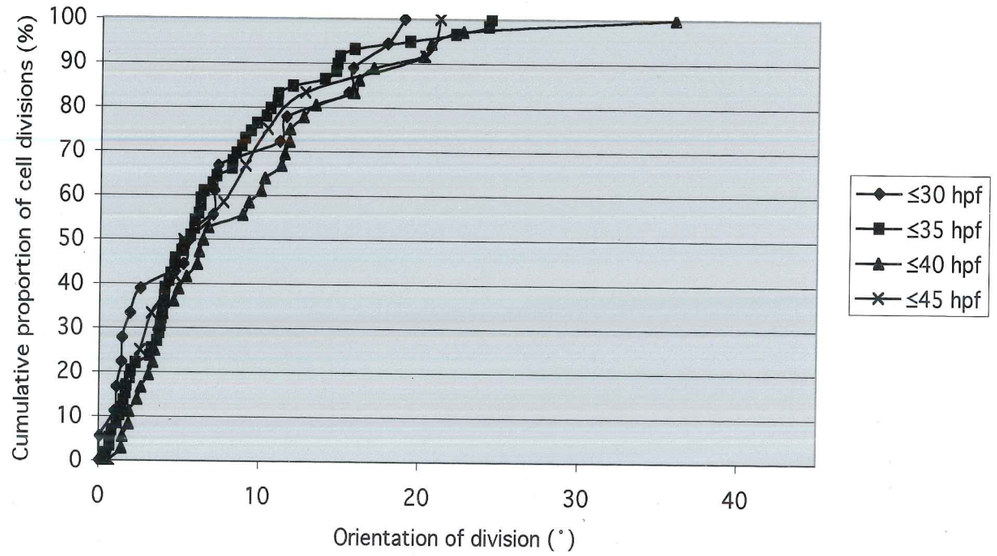

b

Fig. 3.3

Fig. 3.3 ***Orientation of cell division with respect to the apico-basal axis and retinal surface.*** **a)** An angle of 0˚ represents a cell division parallel to the retinal surface. An angle of 90˚ represents a cell dividing along the apico-basal axis. All divisions observed tended towards the retinal surface, with most divisions almost parallel to the surface. No apico-basal divisions were observed. **b)** Cumulative plot of orientations with respect to the apical retinal surface of all observed cell divisions (n=131) over 4 time periods. There is no significant change in distribution of orientations between the time points.

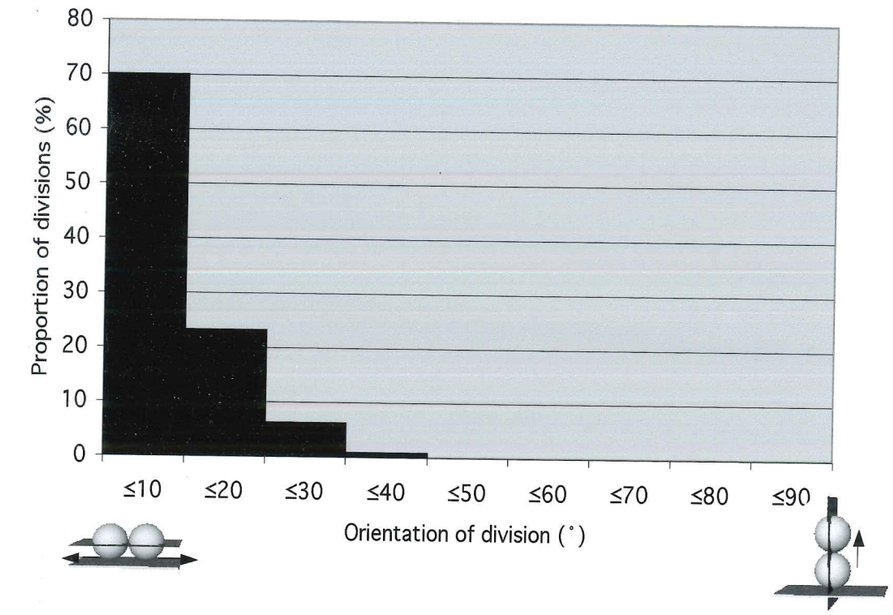

a

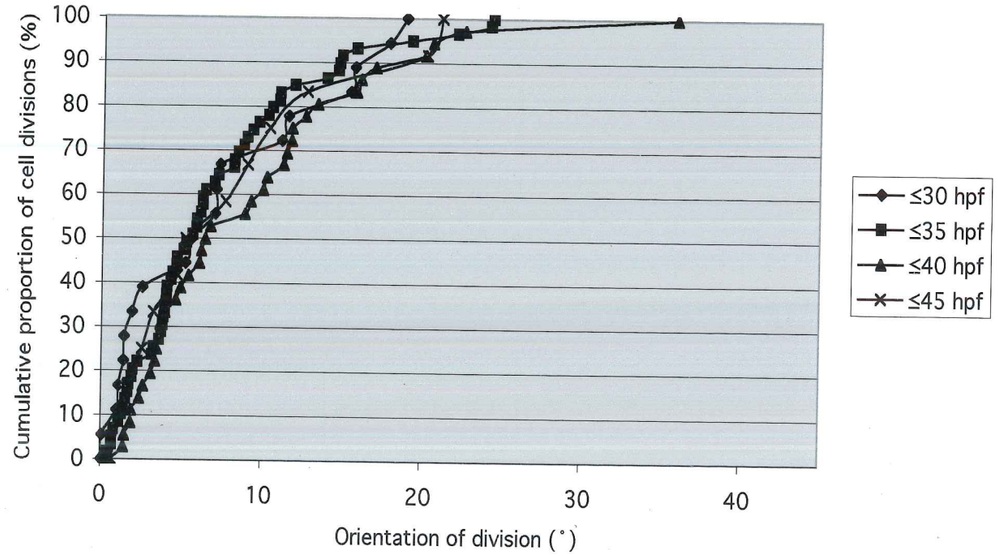

b

Fig. 3.3

Fig. 3.4 ***Analysis of cell divisions orientated parallel to the apical surface.*** **a)** Three-dimensional representation of the zebrafish retina as an ellipsoid body covered by a grid formed from two axes, the central-peripheral axis (green) and the circumferential axis (red). Also shown are cells dividing along both the axes. The orientations of cell divisions were measured with respect to the central-peripheral axis. **b-e)** Zebrafish. Examples of central-peripheral divisions (0˚) highlighted in green and circumferential cell divisions (90˚) highlighted in red. The central-peripheral axis is represented by the yellow dashed line. The retina itself is outlined in white. The highlighted cells are magnified in the insets. **f)** Rat. Example of a central-peripheral division (0˚) highlighted in green and a circumferential cell division (90˚) highlighted in red. The yellow broken lines represent the circumferential axis.

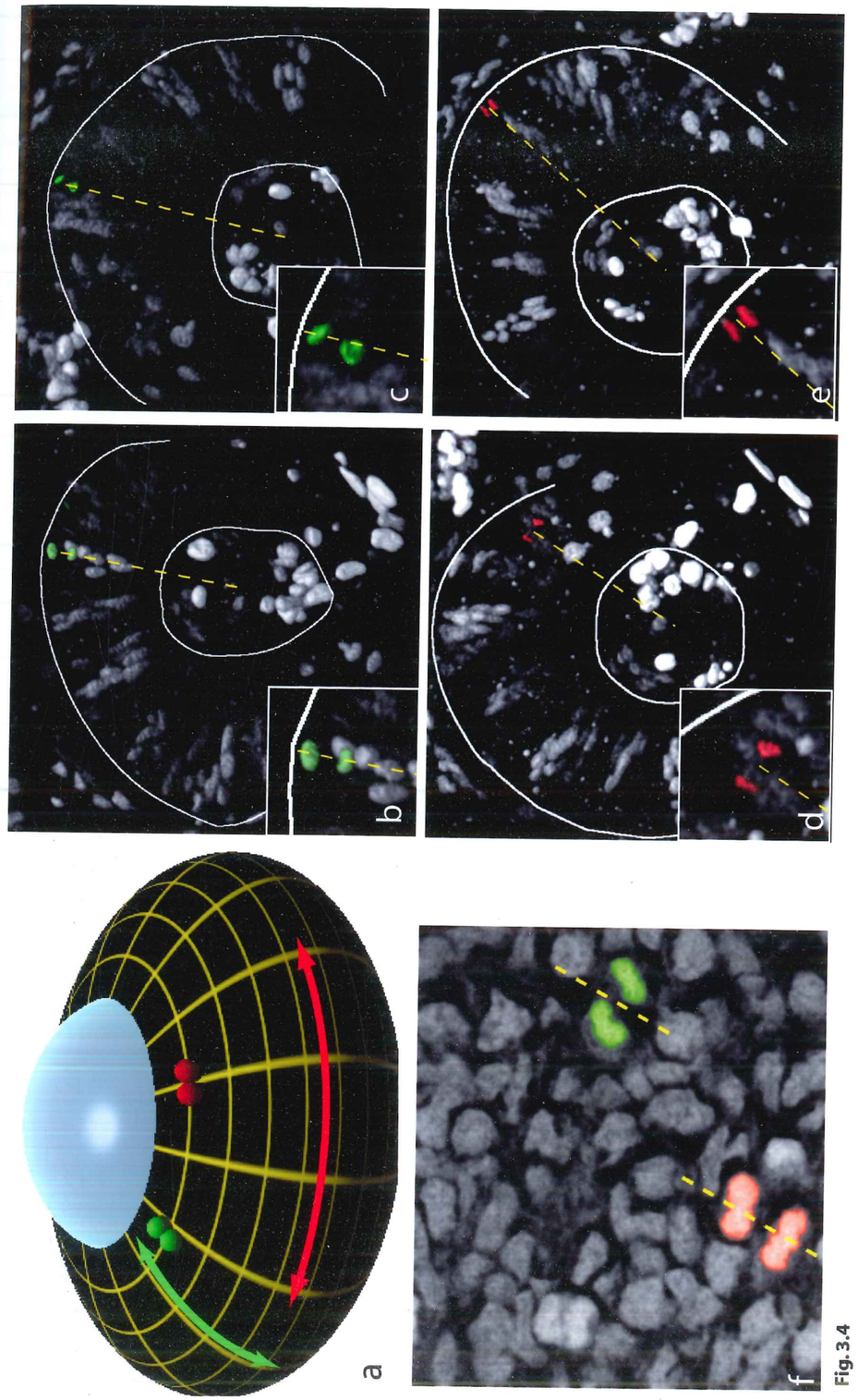

Fig. 3.4

Fig. 3.5 ***Cumulative distributions of orientations of cell divisions parallel to the retinal surface over time.*** The dashed lines represent 45˚ thresholds. **a)** In zebrafish, earlier distributions contain a greater proportion of central-peripheral (<45˚) divisions, while later distributions contain more circumferential (>45˚) divisions. The ≤30 hpf and ≤45 hpf distributions differ significantly as determined by the Kolmogorov-Smirnov test ($p<0.01$). **b)** In *sonic you* embryos, there is no significant difference between the distributions of cell division orientations over time. **c)** In the rat retina, the distribution of orientations of cell divisions at P4 tends towards circumferential divisions compared to the distributions at E16 or P0.

A

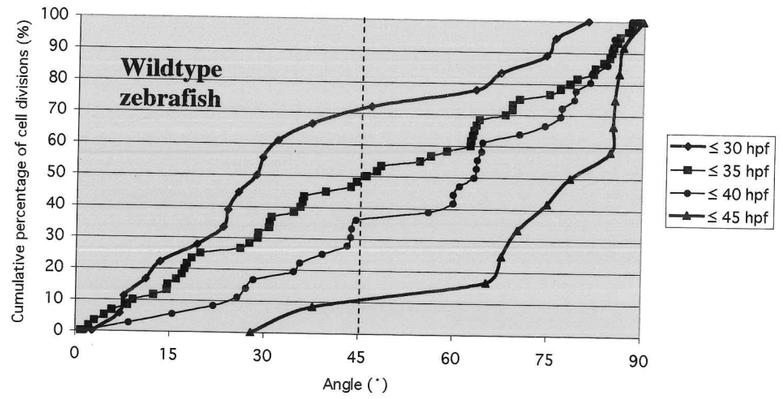

B

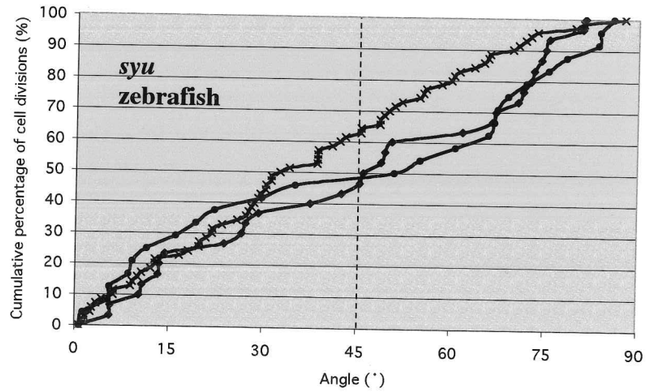

C

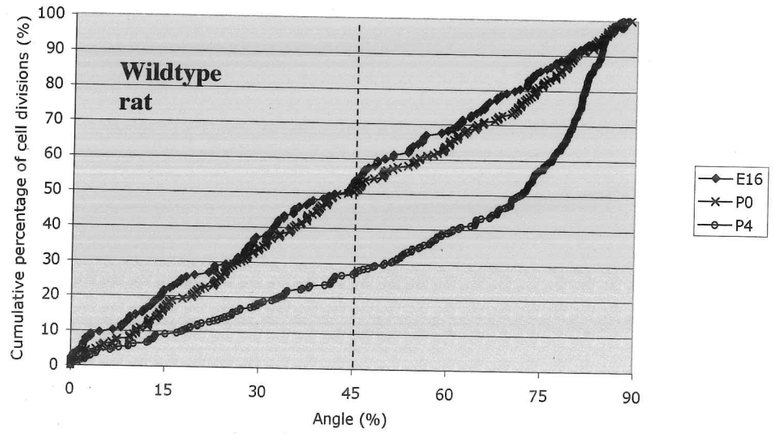

Fig. 5

Fig. 3.6 ***Brn3c-GFP transgenic zebrafish.*** 2dpf Brn3c-GFP transgenic zebrafish express GAP-GFP, which labels cell membranes, under the control of the promoter for the Brn3b transcription factor, targeting GAP-GFP to retinal ganglion cells (RGCs). The use of membrane-targeted GFP enhances RGC axonal processes. **a)** Dorsal view of an embryo under a fluorescent dissecting microscope using filters optimised for GFP emission. The entire optic tract from the RGCs in the retina to the axonal projections in the contralateral tectum, situated dorsally, can be seen clearly (arrowheads). Wild-type zebrafish are thought not to have ipsilateral retinal projections to the tectum. Brn3 transcription factors are also expressed in sensory cells originating in cranial ectodermal placodes (Artinger et al., 1998). These are represented by brightly labelled areas outside the optic tract (arrows). These may be the otic and lateral line placodes. **b)** 3D reconstruction of Brn3 expressing neurons in ectodermal placodes superimposed on a transmitted light view of the region, visualised by CLSM using a 20x water immersion objective. Bundles of otic and lateral line sensory cells surrounding or lying in the otic vesicle are labelled by GFP. y (yolk sac), r (retina), o (otic vesicle). **c)** Antero-lateral view of a 3D reconstruction of the optic tract visualised by CLSM using a 20x water immersion objective. The RGC layer of the retina closest to the objective lens and the tectal projections from the contralateral retina are brightest, although the entirety of the retinal projection can be seen from the closest side. The contralateral RGCs can barely be seen due to the depth at which they lie compared to the objective lens (255μm). As the axons exit the retina, a branch point in the optic tract (arrow) can be seen lateral to the chiasm (arrowhead). Although the target for these axons cannot be seen, they may join an equivalent point on the contralateral side**. r (retinal), t (tectum). d)** Optical section through the RGC layer, showing RGC membranes labelled by GFP, visualised by TPLSM using a 63x water-immersion objective. l (lens), or (outer retina) **e)** 3D reconstruction of the ganglion cell layer and RGC axons as they exit the retina, visualised by TPLSM using a 63x water-immersion objective. Axon tracts can be seen clearly, as they form the optic nerve (arrowhead).

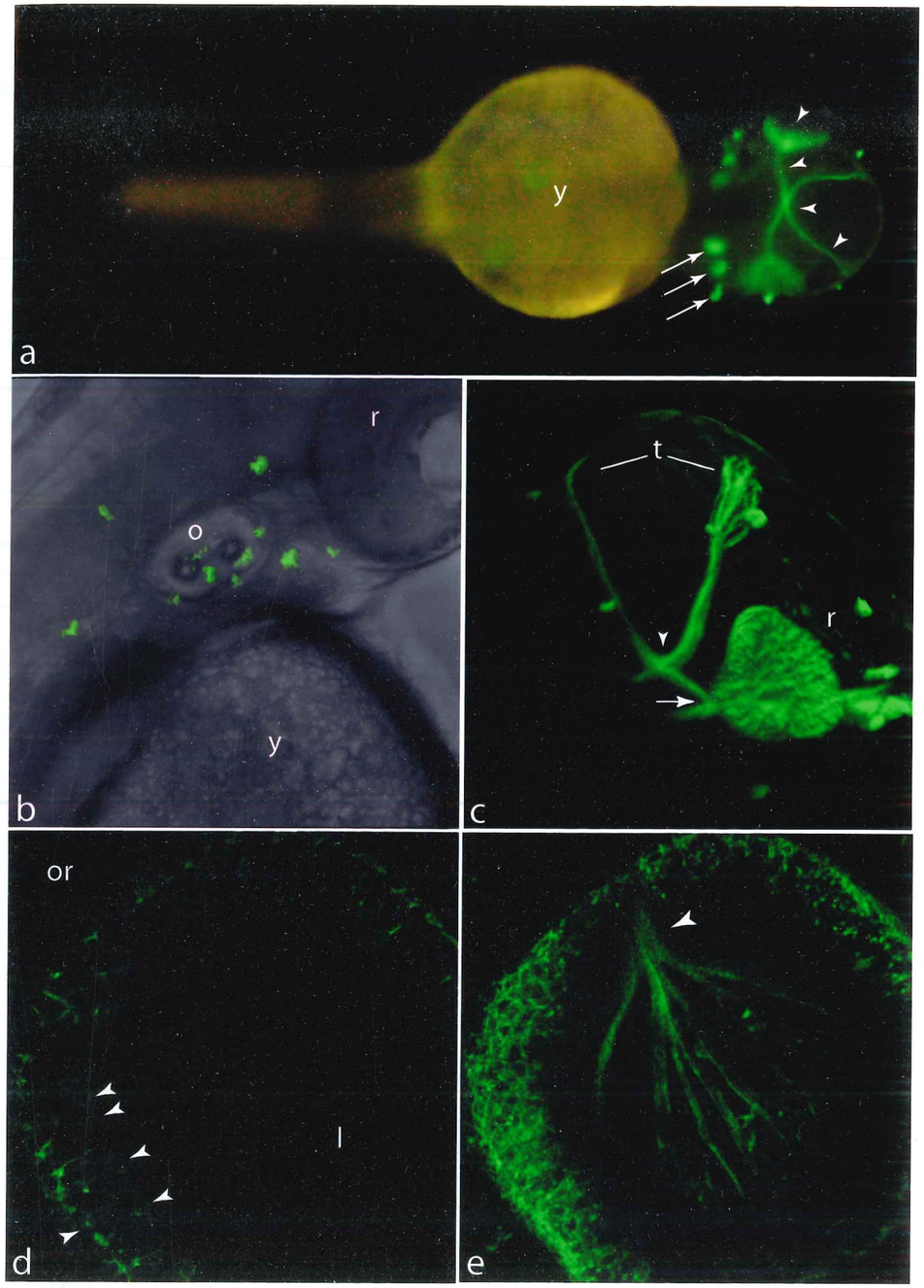

Fig. 3.6

Fig. 3.7 ***Tracing RGCs back to their final division.*** A retinal ganglion cell in a 2dpf Brn3c-GFP zebrafish injected with H2B-GFP is traced back to its final division, and the fate of its sibling is recorded by tracing it forward in time. Nuclei labelled by H2b-GFP are used to track cell movements. In all figures, the retinal pigment epithelium (rpe) is below, while the lens is above. **a)** A combined trace from all timepoints between 30 hpf and 62 hpf of the retinal ganglion cell (green). Its sibling (red) and their parent cell (yellow) are shown. The trace gives some indication of direction of movement (arrows) and change in cell shape over time, in the XY-plane. It does not take into account specimen drift during the experiment, and is therefore not in scale with the width of the typical retina. Tracing begins at 30 hpf, and the parent nucleus (yellow trace) migrates to the ventricular surface to divide at 33 hpf (yellow nuclei in **b**). Both daughters migrate away from the ventricular surface. One undergoes apoptosis at 55 hpf (red trace, and red cell in **c**), while the other is confirmed to be a retinal ganglion cell by the surrounding Brn3c-driven GFP expression (green trace and green cell in **d**). **b)** The nuclei of daughters of the cell being traced are highlighted in yellow in anaphase at 33 hpf. **c)** The apoptotic body of one of the two siblings (red trace in a) is highlighted in red at 55 hpf. **d)** The retinal ganglion cell resulting from the division at 33 hpf is highlighted in green at 61 hpf, surrounded by Gap-GFP labelling. Denser GAP-GFP lab can be seen closer to the lens, where retinal ganglion cells have been established for longer. The optic nerve (on) is also evident deep to the retinal ganglion cell layer (arrow).

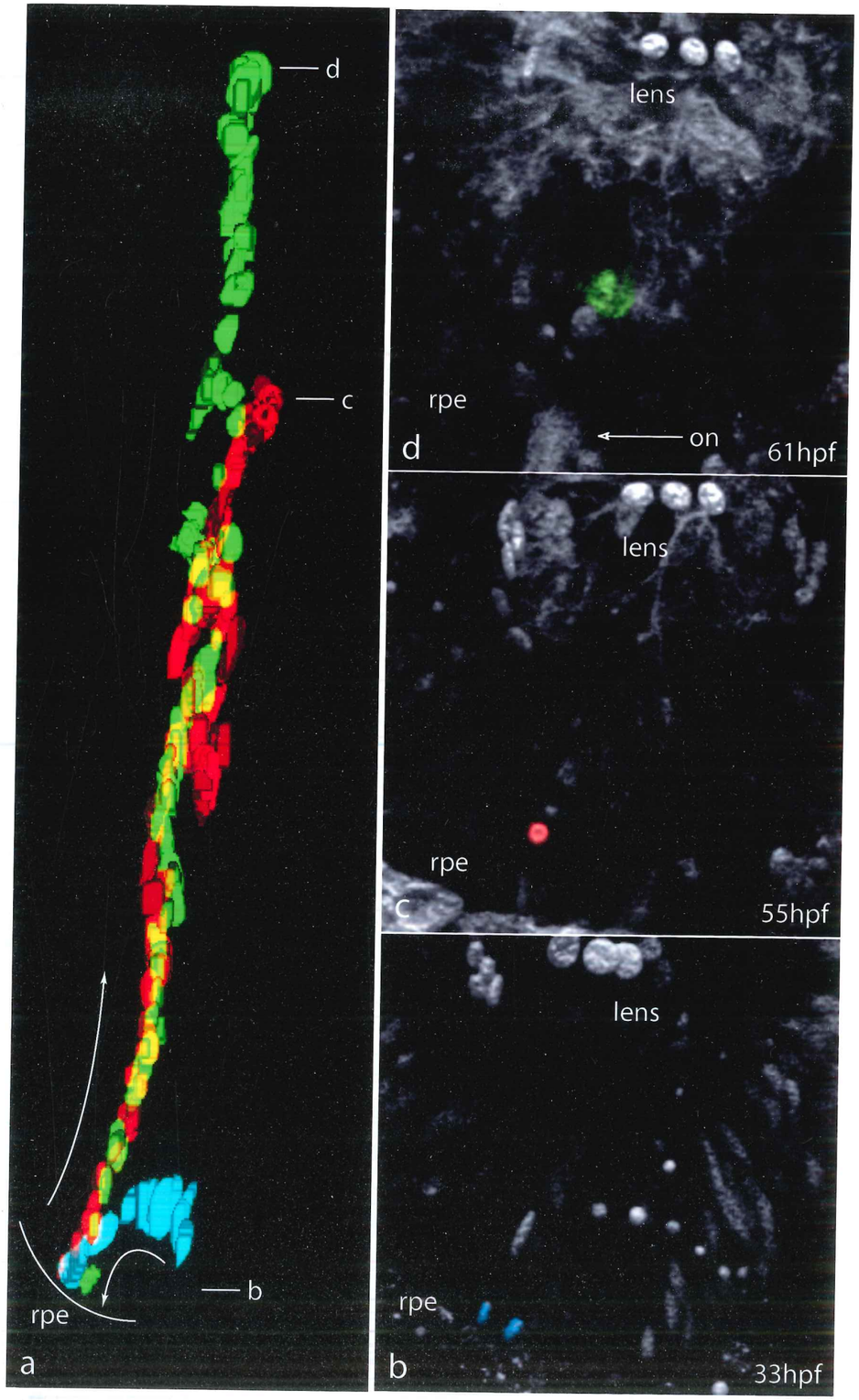

Fig. 3.7

Fig. 3.7 ***Tracing RGCs back to their final division.*** A retinal ganglion cell in a 2dpf Brn3c-GFP zebrafish injected with H2B-GFP is traced back to its final division, and the fate of its sibling is recorded by tracing it forward in time. Nuclei labelled by H2b-GFP are used to track cell movements. In all figures, the retinal pigment epithelium (rpe) is below, while the lens is above. **a)** A combined trace from all timepoints between 30 hpf and 62 hpf of the retinal ganglion cell (green). Its sibling (red) and their parent cell (yellow) are shown. The trace gives some indication of direction of movement (arrows) and change in cell shape over time, in the XY-plane. It does not take into account specimen drift during the experiment, and is therefore not in scale with the width of the typical retina. Tracing begins at 30 hpf, and the parent nucleus (yellow trace) migrates to the ventricular surface to divide at 33 hpf (yellow nuclei in **b**). Both daughters migrate away from the ventricular surface. One undergoes apoptosis at 55 hpf (red trace, and red cell in **c**), while the other is confirmed to be a retinal ganglion cell by the surrounding Brn3c-driven GFP expression (green trace and green cell in **d**). **b)** The nuclei of daughters of the cell being traced are highlighted in yellow in anaphase at 33 hpf. **c)** The apoptotic body of one of the two siblings (red trace in a) is highlighted in red at 55 hpf. **d)** The retinal ganglion cell resulting from the division at 33 hpf is highlighted in green at 61 hpf, surrounded by Gap-GFP labelling. Denser GAP-GFP lab can be seen closer to the lens, where retinal ganglion cells have been established for longer. The optic nerve (on) is also evident deep to the retinal ganglion cell layer (arrow).

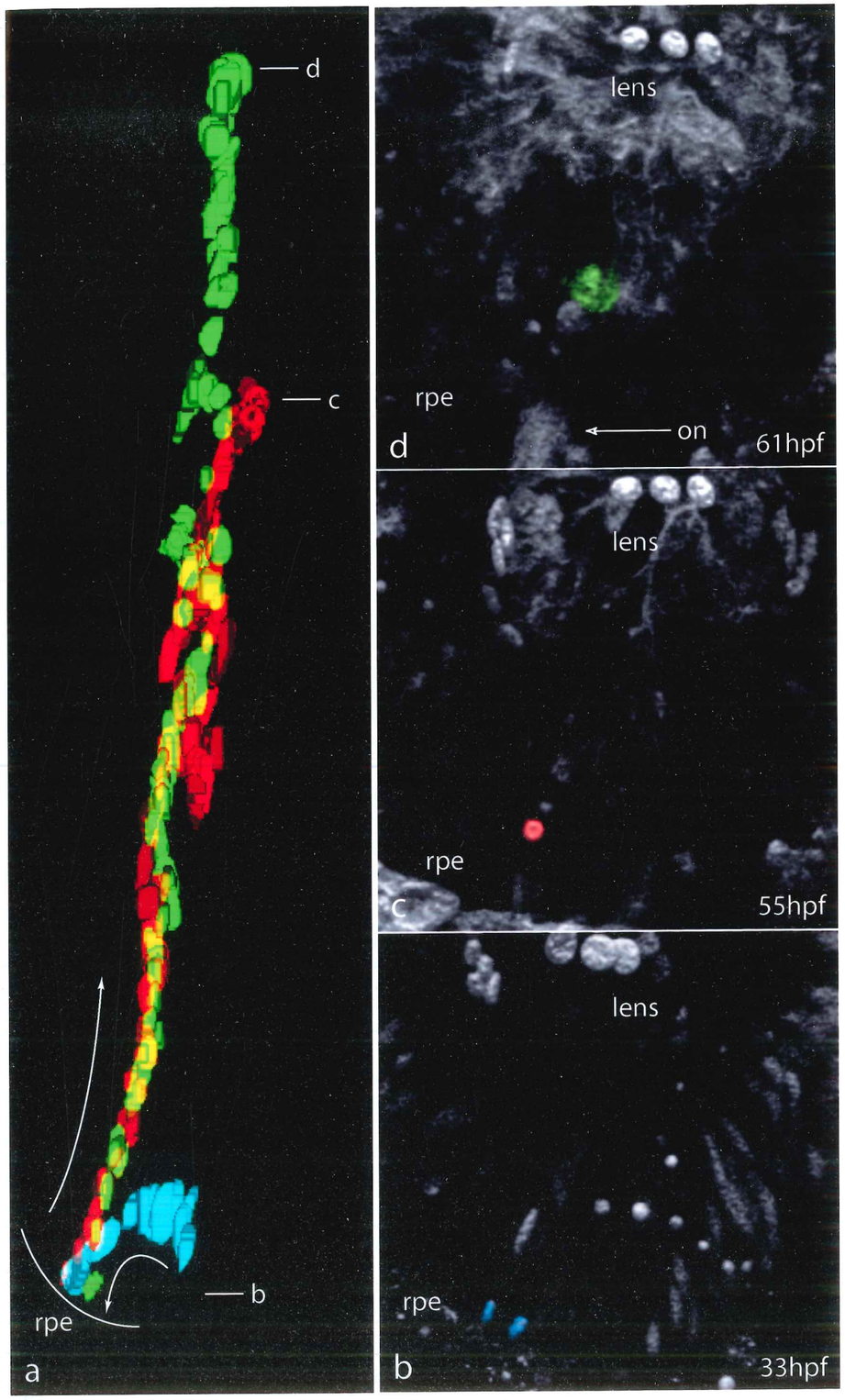

Fig. 3.7

Fig. 3.8 ***Tracing cell divisions forward in time in 1dpf Brn3c-GFP embryos injected with H2B-GFP.*** In all figures, the retinal pigment epithelium is to the left and the lens to the right. **a)** A circumferential division at 25 hpf (highlighted) was determined to be symmetrical as both daughters from the division also divided, at 35 hpf (highlighted in **b-b'**) and 40 hpf (highlighted in **c-c'**). **d)** Another cell that divided at 25 hpf circumferentially gave rise to one daughter that remained near the ventricular surface (arrowhead in **e**), and one whose nucleus migrated closer to the retinal ganglion cell layer, (double arrowhead) as seen by the more diffuse GFP signal and presence of the optic nerve **(on),** by 48 hpf.

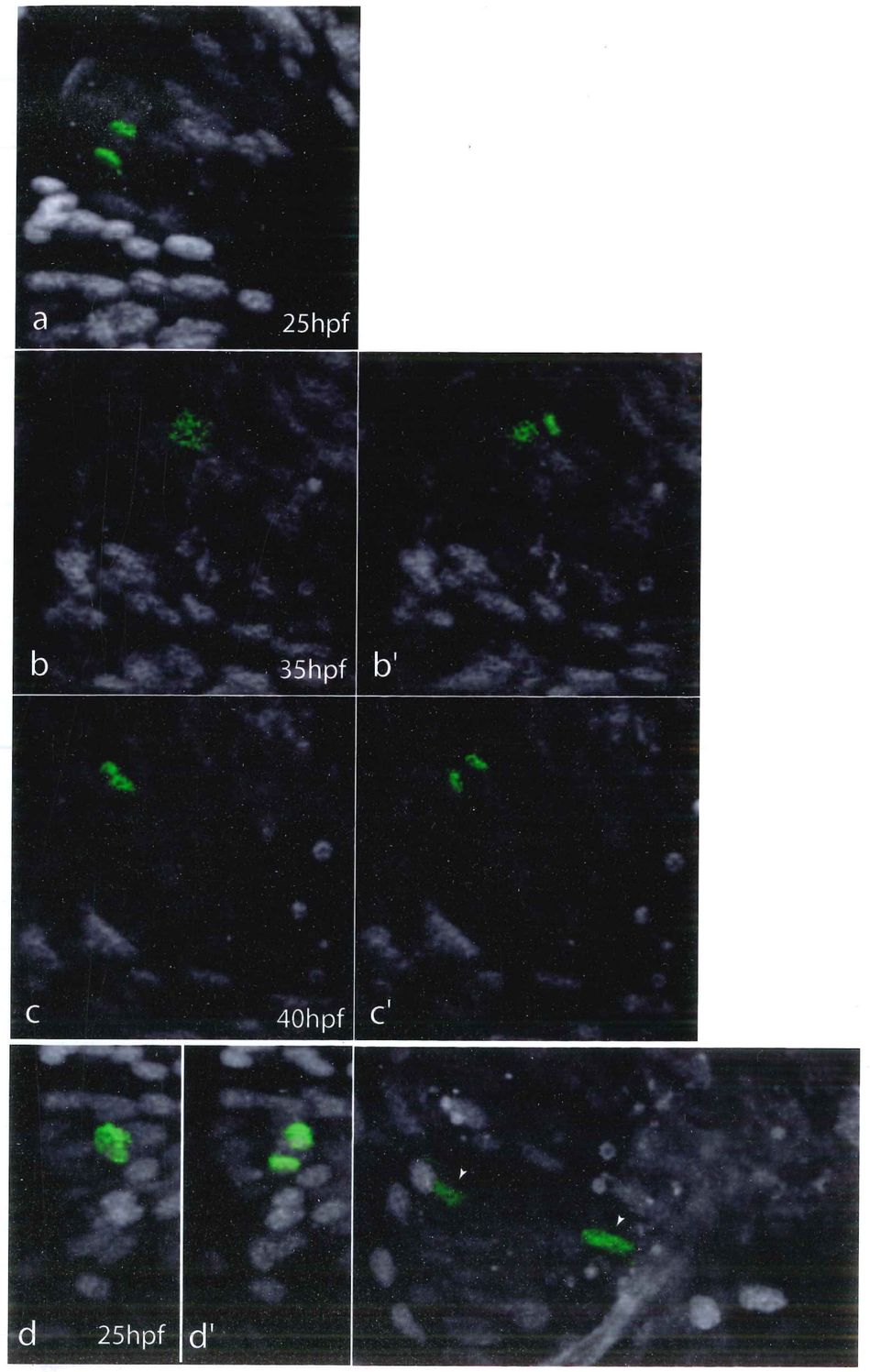

Fig. 3.8

Fig. 3.9 ***Pon-GFP labelling in the retina.*** **a)** 3D projection of the retina of a 1dpf embryo injected with Pon-GFP RNA. The Pon-GFP signal is visible with increased gain and contrast enhancement, but diffuse throughout the neuroepithelial cells with some concentration in the cell nuclei. **b)** Time-lapse series of a mitotic cell in the retina of a 1dpf embryo injected with Pon-GFP. The localisation of Pon-GFP in mitotic cells (arrows) is initially diffuse. Pon-GFP may be localised in the cell cortex after division (arrowheads) but examples are difficult to find. **c)** 3D reconstruction of a time-lapse series of a mitotic cell from the retina of a 1.5dpf zebrafish injected with Pon-GFP RNA and GAP-GFP DNA. A structure within the mitotic cell, possibly labelled by GAP-GFP, is segregated asymmetrically after cell division (arrows). See also Fig. 3.10a. **d, e)** Optical sections taken through dividing cells from Pon-GFP / GAP-GFP injected retinas. The structure within the dividing cells can possess both GAP-GFP-like outline labelling (arrowhead in **d**) and Pon-GFP-like diffuse labelling (arrowhead in **e**). The structure lies away from the nuclear positions (open arrowheads in **e**).

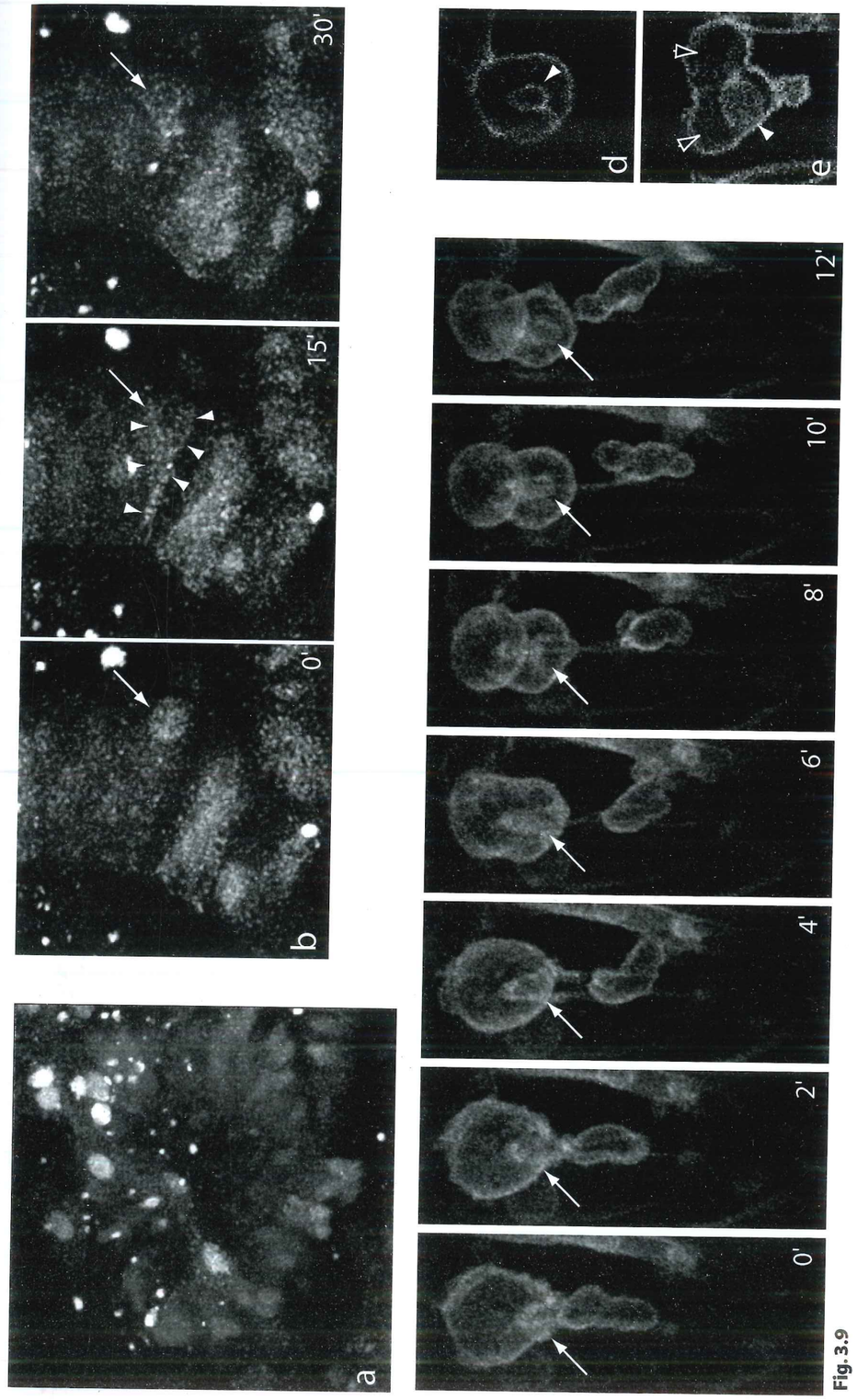

Fig. 3.10 ***Persistence of the basal process during cell division in vivo.*** The highlighted cell is labelled with GAP-GFP to label the membranes. **a)** The time-lapse series shows the cell dividing, while the basal process (arrows) remains in place during the entire event. In preparation for division, the nucleus and all the cytoplasm move to the apical side of the retina. After division (t=40'), the cell on the left seems to have inherited the basal process while the cell on the right seems to be growing a new process along side its sibling (red arrowheads). White arrowheads denote an 'organelle' that is asymmetrically inherited during this division by the cell on the left. The open arrowhead points to the space expected to be occupied by the daughter cell nucleus, distinct from the organelle itself. **b)** Evidence for the basal process during cell division. The highlighted retinal cell expresses GAP-GFP. As the cell divides, some cytoplasm is left behind (arrow) in the basal process at M-phase (t=20'), while the rest is resorped into the cell body. The stray cytoplasm rejoins one of the daughter cells after division, so it must have remained connected via the basal process (arrowheads) during cell division. In addition, the basal process was inherited by the right-hand cell, as this cell is the only one to merge with the stray cytoplasm.

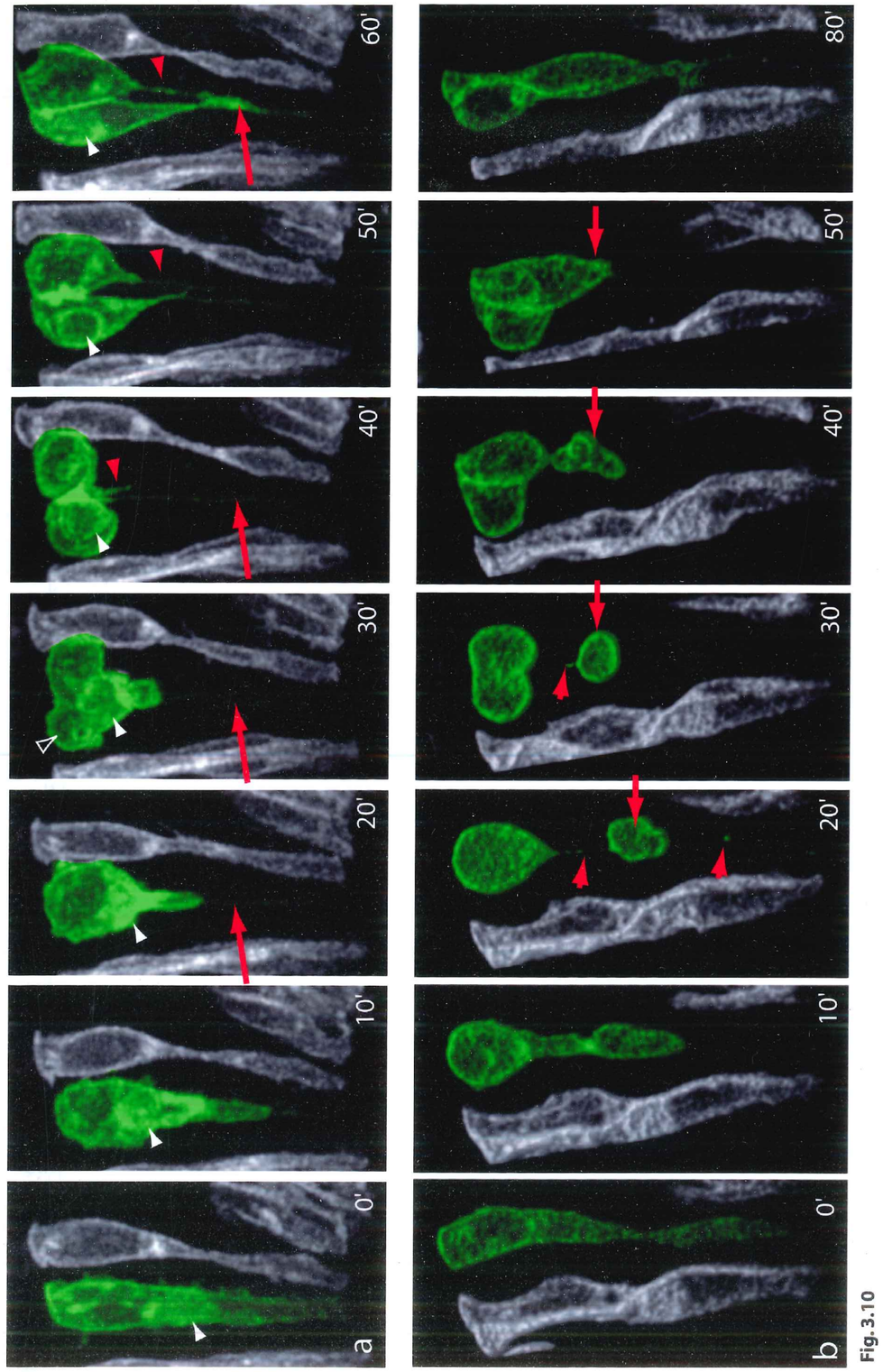

Fig. 3.10

Fig. 3.11 ***Asymmetric inheritance of the basal process.*** A single neuroepithelial cell in **a** divides into two unequal siblings (**a' and a''**), the larger one inheriting the basal process. The dashed lines denote the cleavage plane. Even before mitosis, the basal process can be seen to 'belong' to the half of the cell that will inherit it. The arrow points to the smaller sibling. Ectopic cytoplasm (arrowhead) remains in the basal process during division and rejoins the cytoplasm of the larger sibling.

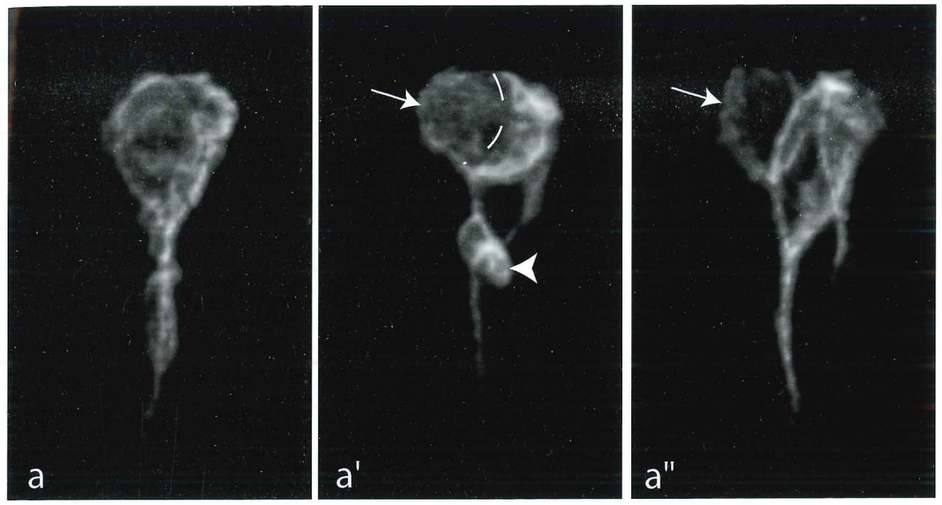

Fig. 3.11

Fig. 3.11 ***Asymmetric inheritance of the basal process.*** A single neuroepithelial cell in **a** divides into two unequal siblings (**a' and a''**), the larger one inheriting the basal process. The dashed lines denote the cleavage plane. Even before mitosis, the basal process can be seen to 'belong' to the half of the cell that will inherit it. The arrow points to the smaller sibling. Ectopic cytoplasm (arrowhead) remains in the basal process during division and rejoins the cytoplasm of the larger sibling.

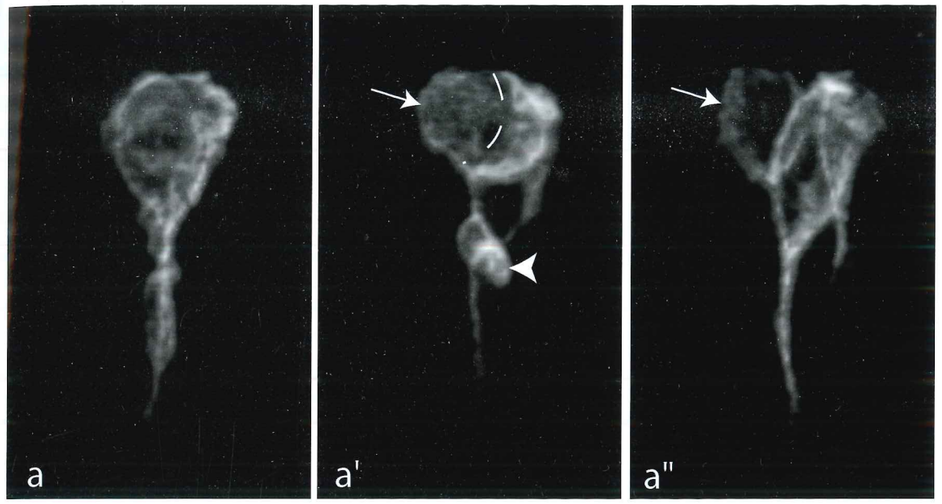

Fig. 3.11

Fig. 3.12 ***Sequence of events for some cell divisions in the developing zebrafish retina.*** Prior to division, a cell's nucleus and cytoplasm collects at the apical surface of the retina, allowing the cell to round up for mitosis. However, a connection is maintained with the basal surface of the retina through a basal process. At division, the slightly asymmetric position of the basal process permits one of the daughter cells to inherit it and maintain the position at which this cell continues its progression through the cell cycle or at which this cell migrates into the retina following differentiation. Its sibling may grow a new basal process alongside the first cell, thus maintaining a spatial relationship between the siblings in a radial column.

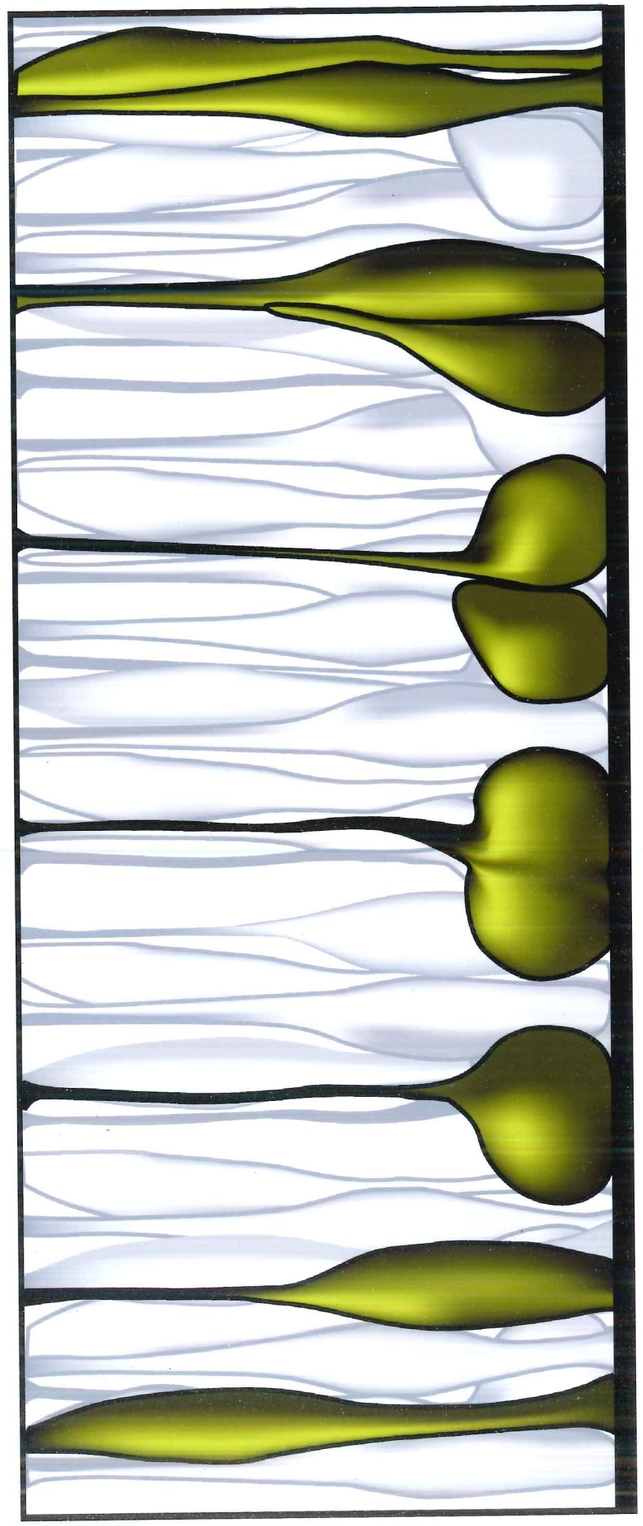

Fig. 3.12

Chapter 4: The development of retinal cell mosaics

Introduction

The vertebrate retina is structurally very well organised, with seven major cell types arranged into three cellular layers and each cell type belonging to a specific layer (Fig. 1.1). Rod and cone photoreceptors are found in the outer nuclear layer. These synapse in the inner plexiform layer with bipolar cells and horizontal cells located in the inner nuclear layer. Bipolar cells transmit signals to ganglion cells in the ganglion cell layer as well as amacrine cells found in the inner nuclear layer and, possibly, displaced amacrines in the ganglion cell layer (Hinds and Hinds, 1978). Retinal ganglion cells are the output cells of the retina whose axons form the optic nerve. Glial cells known as Müller glial cells are located in the inner nuclear layer, although their processes delineate the inner and outer limiting membranes or edges of the retina. A striking feature of the organisation of retinal cells is the columnar appearance of the cells and the circuits that they form. So conspicuous is this cellular organisation that Ramón y Cajal's work on golgi staining of retinal slices allowed him to conjecture about the function of the neuronal circuitry in the retina by studying only the anatomy of the tissue (Ramâon y Cajal, 1995). This organisation has a functional basis as the retina plays an important role in partially processing visual stimuli in terms of various features such as contrast, direction of motion, colour and so on, information which is then sent to visual centres in the brain. Information about stimuli flows from the photoreceptors to ganglion cells and is processed in between. The retina can therefore be seen as a collection of columnar or vertical processing units, each consisting of some cells of each type, perhaps based around single Müller glial cells, with horizontal cells and amacrine cells forming connections between these units (Dowling, 1987). In terms of the development of radial units, each may originate from single or few progenitor cells. Labelling single progenitor cells in the Xenopus and rodent retina using retroviral vectors results a few days later in clones of labelled cells arranged in a radial pattern across the retina (Holt, 1989; Turner and Cepko, 1987; Turner et al., 1990). In addition, work described in the previous chapter showed that retinal progenitor cells retain a process attached to the basal surface of the retina during cell division that may enable a guiding scaffold for migrating daughter cells to be maintained. This is analogous to the radial unit hypothesis proposed to explain the development of the mammalian cortex (Rakic, 1995). According to this hypothesis,

progenitor cells give rise to related neuronal cells that migrate vertically into the cortex along shared radial glial fibres. In fact, radial glial cells themselves may be the progenitor cells that give rise to the cells that will be part of the radial unit (Malatesta et al., 2000; Noctor et al., 2001).

Along with this vertically oriented organisation, various degrees of order are also found between cells in the vertebrate retina in a horizontal direction. Known as cell mosaics, cells of the same subtype can be found arranged in ordered planar arrays. Retinal cell mosaics have been noticed since the mid-19th century and have since been shown to exist in most animal models including cat (Wassle et al., 1981), rabbit (Scheibe et al., 1995), frog (Shamim et al., 1999), fish including zebrafish (Cameron and Carney, 2000; Larison and Bremiller, 1990), chick (Galli-Resta and Novelli, 2000), rat (Galli-Resta et al., 1997), mouse (Galli-Resta, 2000), primate (Wikler et al., 1997) as well as in human retina (Curcio et al., 1991). The order present in some of these mosaics has been demonstrated computationally by comparing the distribution of cells in an array to simulated uniform and random distributions of cells and showing that the actual cell distributions could not be generated randomly (Cameron and Carney, 2000; Galli-Resta, 1998; Galli-Resta et al., 1999; Galli-Resta et al., 1997; Scheibe et al., 1995). However, the introduction of a simple, minimum distance rule, where cells are not allowed to approach each other by a minimum distance and have an exclusion zone around them, is enough to generate mosaics that are similar to actual retinal mosaics (Galli-Resta, 1998; Galli-Resta et al., 1999; Galli-Resta et al., 1997; Scheibe et al., 1995). An interesting result from similar studies is that ordered mosaics are only produced by cells of the same subtype, and that arrays of different cell subtypes are generally independent of each other, even when the cell subtypes are located in different retinal laminae and related to each other by synaptic connections (Cameron and Carney, 2000; Rockhill et al., 2000). An exception was a study of blue cones and blue cone bipolar arrays in the macaque retina that showed a higher than expected probability of finding a blue cone above a blue cone bipolar (Kouyama and Marshak, 1997). These cell types are related anatomically, forming synaptic connections, as well as genetically, sharing common gene-regulatory machinery (Chen et al., 1994; Chiu and Nathans, 1994). The general independence of different cell arrays, yet the orderliness within these arrays, raises questions as to how this regularity arises. Presumably, a regular array of equivalent radial units would have led to a greater

positional dependence between the mosaics of different cell subtypes, so that a model where laminar arrays is a consequence of radial unit arrays is unlikely.

The study of retinal cell mosaics is limited by the markers that are available for different cells. Most studies have used antibodies specific to antigens found in the different cells in mature retinas. The discovery of a number of markers that labelled specific cell types during retinal development enabled the study of the formation of retinal cell mosaics (Galli-Resta et al., 1997; Larison and Bremiller, 1990; Raymond et al., 1995). Postmitotic cells in the developing retina were found to already be part of ordered mosaics. Galli-Resta et al. used an antibody to Islet-1 to label two populations of amacrine cells, one that migrated to the inner nuclear layer and the other to the ganglion cell layer ('displaced amacrine cells'). They found that although migrating Islet-1+ cells were not regularly spaced, the incomplete arrays that they formed were as regular as the arrays in adult retinas. Thus, the minimum distance rules that are thought to govern the arrays in the mature retina seem to be present during the development of these arrays. As new cells are added to an array, mechanisms must be in place for the existing members of the array to accommodate the new arrivals, rather than the whole array rearranging itself after all its component cells have matured. Two mechanisms that could account for the accommodation of new cells are the shuffling of cells established in the array to ensure that a minimum distance is maintained or, perhaps, the controlled death of cells that cannot fit into the mosaic properly.

The support of a model involving the movement of cells within an array to maintain its regularity requires evidence for the tangential movement of postmitotic cells. In fact, experiments using transgenic mice in which the lacZ gene encoding the β-Galactosidase enzyme was incorporated into the X-chromosome have provided reinforcement for this model (Reese et al., 1995). In female heterozygous mice, the phenomenon of X-inactivation ensures that a random 50% of their cells have the lacZ gene inactivated. This occurs around embryonic day 8.5 (E8.5), long before the onset of neurogenesis in the mouse retina, which means that 50% of progenitor cells, and thus 50% of clones of cells have active lacZ and can be stained biochemically. If progenitor cells gave rise to cells that only migrated radially, then blue (stained) and white (unstained) columns would be seen in sections of the retina defining the clonal boundaries with no intermingling of cells; i.e. blue cells in white columns or vice-versa. However, Reese et al. noticed that some cell types, namely cone, horizontal, amacrine and ganglion cells, could be found in

regions composed of different clones; i.e. blue stained cells were found in white columns. Other cell types (rods, bipolars and Müller glial cells) were never found in clones of the opposite colour. Tangential migration of these cells had been dismissed as artefactual in experiments where single or very few progenitor cells had been labelled retrovirally (Turner et al., 1990). The low frequency of such events occurring in these experiments can be explained by the low likelihood of a particular cell type being labelled since few clones were being targeted and cells were labelled after the onset of neurogenesis. Further analysis of retinal clones in X-inactivated mice showed that all cells of a cell type that migrated did so tangentially—tangential migration is a universal phenomenon for each cell type—and that the distance of migration was very short, ranging from 40 to 140μm depending on the cell type. In simulations where the minimum distance rule mentioned above is imposed upon randomly distributed cells, these cells form regular two-dimensional arrays. Two features of the simulations stand out: all cells are found to move and only by short distances. The same features are observed when new cells are added to such simulations (Eglen et al., 2000). Both are features found in tangentially migrating cells of the X-inactivated retinal clones. Finally, the timing of tangential migration of a cell was found to be related to the timing of its differentiation rather than the timing of its birth. For example, tangentially dispersed horizontal cells were only found after they had matured from a radial, bipolar shape to their classic horizontal morphology, despite the passage of more than a week since their birth (Reese et al., 1999). Interestingly, not only do these experiments provide evidence for the existence of tangential migration of cells but they strengthen the case further for tangential migration being involved in the formation of mosaics—the cell types shown to undergo tangential migration are all cell types for which retinal mosaics have been found. Tangential migration of rod cells was not observed in X-inactivated mice, yet, regular rod mosaics have been found in the retinae of ground squirrels in which rods make up only 14% of retinal cells (Galli-Resta et al., 1999). They are found at lower densities than in the mouse in which rods outnumber other retinal cells by 20:1. Thus, it is possible that the very high density of rods in mice masks any spatial ordering or even that such ordering is not required. Ground squirrels are diurnal, not nocturnal, animals so the heightened sensitivity provided by densely packed rods is not essential but regularity in spacing may enable the most efficient use of rods. Incidentally, since tangential migration is tightly correlated to cell type, a model where a mitotic cell within a clone might undergo tangential migration

in the ventricular zone prior to giving rise to a set of neurons is unlikely – a greater variety of cell types would have been expected outside their clone of origin.

Evidence for the involvement of cell death in the formation of retinal mosaics is less compelling. There have been few studies looking directly at the effect of cell loss on the regularity of retinal cell arrays. Limited existing studies were conducted in mammals (rat and cat) in which high levels of apoptosis eliminate significant numbers of retinal cells, mainly retinal ganglion cells, during retinal maturation. A study of α-ganglion cell mosaics in the cat retina showed that these increase in regularity between one month post-natally and adulthood. The loss of 20% of α-ganglion cells that occurs during this time is sufficient to account for the increased regularity provided it occurs selectively. This was determined by computer simulations in which random cell distributions become more regular after the targeted removal of 20% of cells (Jeyarasasingam et al., 1998), On the other hand, Galli-Resta et al. studied cholinergic amacrine cell mosaics in the rat retina and find that the loss of 20% of cells by apoptosis that occurs between P4 and P12 has no effect on the regularity of the amacrine cell mosaics (Galli-Resta and Novelli, 2000). However, this study was done after the amacrine cell mosaics had been established, when no new cells were being added to the mosaic from the ventricular zone. Thus, it does not shed any light on whether cell death might be a mechanism required to enforce regular spacing between cells during the assembly of mosaics.

As many different retinal mosaics can be simulated from randomly distributed cells provided only with an exclusion zone or minimum distance rule (Cameron and Carney, 2000; Galli-Resta et al., 1999; Galli-Resta et al., 1997), the question arises as to how this rule is enforced. Local cell-cell repulsive interactions would be enough to account for such a rule, as no rules other than an exclusion zone around individual cells are required to generate regularity even in a large array, and the exclusion zones themselves are generally only a few cell diameters wide (Galli-Resta, 2000; Galli-Resta and Novelli, 2000; Galli-Resta et al., 1999; Galli-Resta et al., 1997). The analysis of exclusion zones has also shown that even if two cells within an array occur closer to each other than the exclusion zone, their effect on other cells is not additive. Instead, the same minimum distance rule is enforced independently on neighbouring cells. This suggests that diffusible factors are unlikely to provide repulsive cues as their combined effect would be additive (Galli-Resta, 2000). Contact-mediated repulsive or inhibitory cues with a range beyond the cell body, as required by wider exclusion zones, could be provided via the

dendritic trees of the cells in a retinal mosaic. An imaging study of retinal ganglion cells in the ferret retina demonstrated that during retinal development ON-type α-ganglion cells only made dendritic connections with other ON-type α-ganglion cells but never with OFF-type α-ganglion cells or β-ganglion cells, even before full morphogenetic maturation of these cells had been achieved (Lohmann and Wong, 2001). In addition, there was a degree of overlap between the dendritic trees of two neighbouring cells, but this overlap was short and remained constant over time. Since α- and β-ganglion cells of ON- or OFF-types form independent mosaics, this study supports the role of the dendritic trees in maintaining a minimum distance between cells of the same subtype. The functional importance of cell dendrites in arrays was demonstrated in a series of experiments in which microtubules that form the core of neuronal processes were reversibly disrupted in arrays of rat ganglion cells, cholinergic amacrine cells and horizontal cells (Galli-Resta et al., 2002). Molecular and pharmacological means were used to affect the rigidity of the microtubule component of the neuronal cell cytoskeleton in these arrays. With disruption, the arrays lost their regularity, forming clusters in some areas and leaving open spaces in others. They also lost their tendency to remain in monolayers, as cells would scatter slightly in all three-dimensions. About 24 hours after treatment, its effect would wear off, and cells would resume positions forming regular monolayered arrays. Although the treatments would affect microtubules, they would not break connections already formed between cells. Thus, each array was described as analogous to a tense net, which would get wrinkled by the disruption of the rigid links between cells. The effect of the disruptive treatments could only be seen during the time that these arrays were thought to form. Treatment after the establishment of an array, for example at P6 for the cholinergic amacrine cell mosaics, had no effect on array regularity. Again, the independence of different arrays in the retina was evident when some treatments penetrated the retina only superficially, affecting the ganglion cell array but not the amacrine cell arrays. Thus, in the mammalian retina, the formation of retinal cell mosaics seems to involve local cell-cell interactions, mediated for example by the dendritic trees of amacrine and horizontal cells. It also seems to involve tangential cell movement once cells have migrated to their respective layers in order to maintain the regularity of a mosaic. The role of cell death is not confirmed.

In the zebrafish retina, a number of cell mosaics have been shown to exist. Cone photoreceptor cell mosaics are tightly packed and obvious arrays that can be seen in the

adult zebrafish as well as during retinal development (Larison and Bremiller, 1990). In contrast, amacrine cell, interplexiform cell and retinal ganglion cell mosaics have been studied in the adult (Cameron and Carney, 2000). Cone mosaics in zebrafish have been carefully characterised (Larison and Bremiller, 1990) and consist of four types of cones: two single cones that are UV and blue wavelength sensitive and a double cone pair consisting of red and green wavelength sensitive cells. The rows of cones are such that single cones alternate with double cone pairs, and that blue and red cones are adjacent while green and UV cones are adjacent. Thus, the order within a row is blue, red, green, UV, green, red, blue and so on (Fig. 4.1).

In such mosaics, cells are adjacent and within range of local cell interactions such as those involving cell adhesion molecules or lateral inhibitory cues. Very little is known about how the zebrafish cone photoreceptor mosaic is formed. Photoreceptor cells are among the last sets of cells to be born in the zebrafish retina. Post-mitotic photoreceptors

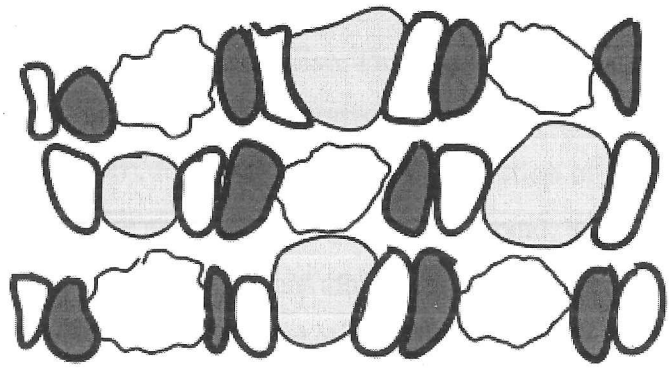

Fig. 4.1 ***Diagram of the cone mosaic found in the adult zebrafish retina.*** Four different cone types are arranged in a lattice such that double cone pairs (bold) are always adjacent to single cones. Red cones (dark) are adjacent to blue cones (ragged) and green cones (small, unshaded) are adjacent to UV cones (light). (adapted from Larisson, 96)

seem to be generated between 48 and 58 hpf, starting with cells near the ventro-nasal patch and followed by neighbouring cells such that a circular wave of photoreceptor differentiation is seen making its way around the retina (Hu and Easter, 1999), similar to the wave of ganglion cell differentiation that is evident earlier (Laessing and Stuermer, 1996; Neumann and Nuesslein-Volhard, 2000). The order in which cone photoreceptors differentiate in a given area of the retina has been determined by studying in-situ hybridisation patterns of the four opsins (Robinson et al., 1995). UV cones differentiate first, followed by blue cones, and finally the double cone pair of which the green member

differentiates before the red. Histological sections show the presence of a uniform layer of morphologically undifferentiated photoreceptor cells in the outer nuclear layer, before characteristics of cone photoreceptors can be identified. However, this is seen at 48hpf when UV opsin staining can already be seen. Thus, it is not known whether cone photoreceptor subtypes are determined before or after they reach the outer nuclear layer. A number of scenarios can be envisaged to explain the formation of a cone mosaic. If cones are not determined by the time they reach the outer nuclear layer, the determination of a subset of cells as UV cones could be followed by the induction of neighbouring cells into the other cone subtypes, such that a strict mosaic pattern is maintained. Comparisons can be made to Drosophila, where the apparently crystalline structure of the retina, composed of about 800 hexagonal ommatidia, begins with the differentiation of regularly and precisely spaced cells in the eye imaginal disc as the R8 photoreceptors. Each ommatidium will contain an R8 photoreceptor, which will then trigger induction cascades to recruit the other photoreceptors and support cells that will also be part of the ommatidium from neighbouring undifferentiated cells (Frankfort and Mardon, 2002). The differentiation of R8 cells occurs at the front of a wave, known as the morphogenetic furrow that sweeps across the imaginal disc. This has been compared to the wave of differentiation that sweeps around the zebrafish retina in all three cellular layers (Hu and Easter, 1999; Jarman, 2000). Furthermore, the differentiation of the R8 cell depends, amongst other genes, on the activity of hedgehog and atonal, both of which have vertebrate homologs (sonic hedgehog and ath5) that are involved in the differentiation of retinal ganglion cells in zebrafish (Kay et al., 2001; Masai et al., 2000; Neumann and Nuesslein-Volhard, 2000). Lateral inhibition pathways involving Notch are responsible for the regular spacing of R8 photoreceptors and have been shown to affect the determination of vertebrate retinal cells including ganglion cells (Austin et al., 1995) and photoreceptors (Rapaport and Dorsky, 1998). Given the striking similarities between the two systems, cell determining signals similar to those required for the formation of Drosophila ommatidia may play a role in the establishment of the cone mosaic in the zebrafish retina. An alternative scenario is that the subtype of cone photoreceptors is determined before the outer nuclear layer is reached, and that signals between the cells enables them to find their correct place in the mosaic. Since the cells are very close to each other, this could involve differential cell adhesion enabling like cones to repel each other and particular sets of unlike cones to attract each other with greater affinity than

other sets. Theoretical models of cone mosaic formation using rules simulating differential cell adhesion properties or cell determination signals have produced conditions under which such interactions could produce zebrafish cone mosaics. They also and show that the conditions for a differential cell adhesion model are less strict than those required for a cell determination model of cone formation but these have not been tested experimentally (Mochizuki, 2002; Takesue et al., 1998; Tohya et al., 1999). Both models do suggest the need for short-range interactions between cells to create cone mosaics.

Programmed cell death could also play a role in the refinement of zebrafish mosaics. Apoptosis occurs in the developing zebrafish retina, albeit at a much lower rate than in mammalian retinas (Biehlmaier et al., 2001). There seem to be a number of waves or peak periods of apoptosis in the central retina. The first at 36hpf occurs before many cells have differentiated but once the retina itself has been established as a separate layer in the optic vesicle (Cole and Ross, 2001). Another between 3 and 4dpf occurs specifically in the ganglion cell layer and the inner nuclear layer, starting in the ganglion cell layer. Levels of apoptosis peak around 1.1% and rapidly reduce to less than 0.2% thereafter. Finally, around 7dpf, levels of apoptosis peak at 1.1% in the outer nuclear layer, where the photoreceptors reside, gradually settling down over the following days. Apoptosis levels are low but consistent throughout the life of the zebrafish in the ciliary marginal zone, a zone of continuous growth in the periphery of the retina (Biehlmaier et al., 2001). The significance of the apoptosis of retinal cells is still unclear, but it may play a number of roles. For example, apoptosis may refine retinal circuitry such that cells that are unable to form local synapses are removed by apoptosis (Oppenheim, 1991). The laminar specificity in the timing of apoptosis suggests that apoptosis follows on from the differentiation and maturation of the neurons as differentiation occurs in sequence from the inner to the outer retinal laminae. It is therefore equally plausible that apoptosis in the zebrafish retina actually helps to refine cellular mosaics in the different layers by removing cells that do not fit in.

The imaging studies presented in this chapter examine the suitability of *in vivo* time-lapse imaging of the developing zebrafish retina for investigations in the formation of cellular mosaics. For example, can cells be observed migrating tangentially, and across what distances? Can the events that take place during the tangential migration of postmitotic neurons be characterised, if these even take place? Cells could migrate short distances by

translocation of the nucleus within the cell's dendritic tree if connections have already been established, or by frank migration determined by the repulsive cues from surrounding cells. Can cells be seen to insert into a mosaic as they migrate radially from the ventricular zone? Finally, can cell death be observed during mosaic formation and might its role be determined? Although many of these questions remain unanswered, this preliminary foray into the study of cellular mosaics *in vivo* may prove to be a useful step forward.

Methods and Materials

Fish

Fish were maintained and raised as described in Chapter three. Pax6-gfp fish (a gift from Tobias Roeser, UCSF) were used for most experiments. These are transgenic fish expressing a green fluorescent protein (m5GFP) under the control of a quail Pax6 promoter and a retina specific enhancer sequence. Tg220 (a gift from Tobias Roeser, UCSF) and shh-gfp (a gift from Carl Neumann, Max-Plänck Institute for Developmental Biology, Tübingen) transgenic embryos are also described. Tg220 embryos express a membrane-tagged GFP under the control of the same promoter-enhancer complex as Pax6-gfp fish while shh-gfp express GFP under the control of a promoter from the sonic hedgehog gene. For imaging, embryos were treated with 0.003% PTU (Sigma) from 11hpf to 24hpf to delay pigment formation in the eye. Pax6-gfp transgenic adults were also crossed with *sdy* adults. *Sdy* is a recessive mutation where homozygous embryos fail to form pigment in the retinal pigment epithelium until at least 4dpf, although retinal development and structure is preserved. 50% of offspring from Pax6-gfp x *sdy* crosses, the F1 generation, will carry a single allele of the *sdy* mutation. As it is not known how many copies of the Pax6-gfp gene have been inserted into the genome of Pax6-gfp fish, nor where these have inserted (personal communication, Tobias Roeser), the proportion of offspring expected to inherit the Pax6-gfp gene is not know. However, a majority of offspring were found to express GFP with variable strengths. F1 fish were in-crossed to identify pairs whose offspring included *sdy* homozygous embryos that also expressed GFP, which were then used in imaging experiments. The use of *sdy* embryos avoided the need for treatment with PTU. *Sdy* embryos could be identified as lacking pigmentation at 24hpf, prior to mounting for imaging.

Imaging

Specimens were screened at 24hpf under a fluorescent dissecting microscope (Leica MZ FLIII) for those with strong GFP expression and pigmentless retinas. For sectioning, embryos were fixed in 4% paraformaldehyde, embedded in OCT, and frozen prior to sectioning on a cryostat.

For *in vivo* time-lapse imaging, specimens were mounted as described in Chapter One. Early experiments were carried out under a Leica TCS-NT confocal laser scanning

microscope, using a Leica 63x, 1.2NA, long-distance, water-immersion objective. A 488nm line from an Argon laser was used for GFP excitation, while emission was detected using a descanned PMT detector. Volumes between 50 and 100μm were scanned every 10 to 30 minutes in 1μm sections. Each section was Kalman 4 to 6 times. Later experiments were carried out under a Leica TCS-SP two-photon laser scanning microscope. The IR excitation laser ('Tsunami', Spectraphysics) was tuned between 750 and 790nm, while emission was detected between 500 and 560nm, either using a descanned PMT detector or a non-descanned PMT detector when this became available. Each section was Kalman averaged 2 (using a non-descanned detector) to 6 times (using a descanned detector). Image data was acquired using Leica TCS NT or Leica LCS software and stored as TIF files.

Visualisation and Analysis

Time-lapse data in the form of image files was processed and visualised using the software Object-Image (based on NIH-Image) or Volocity (Improvision, UK) as described in Chapter 3. To determine nearest neighbour distances between elements in the volume scanned at particular timepoints, elements were selected manually in Object-Image or semi-automatically in Volocity and the x-, y- and z- coordinates for each element were recorded. The distance (d) between two elements with co-ordinates (x1,y1,z1) and (x2,y2,z2) was calculated as follows:

$$d = \sqrt{(x_1 - x_2)^2 + (y_1 - y_2)^2 + (z_1 - z_2)^2} \qquad (14)$$

Intercell distances and displacement of cells between timepoints were calculated using this formula and the required cell coordinates. For all statistical analyses, populations were assumed to come from normal populations as the Gaussian distribution of cells in a cell mosaic has been shown previously (Cameron and Carney, 2000). The relationship of dying cells to distance between the cell and its nearest neighbour was made by plotting cumulative frequency curves of cell death frequency against intercell distance. Curves for dying cells and surviving cells were compared by the log-rank test whose null hypothesis is that the two distributions are identical. Comparisons between two populations were made using the unpaired t-test, unless otherwise stated.

Results

I. Pax6GFP zebrafish express GFP in neuroepithelial cells and amacrine cells

Pax6 is a transcription factor normally expressed in neuroepithelial cells in the early neural retina and in ganglion and amacrine cells in the differentiated retina (Hirsch and Harris, 1997). Pax6GFP zebrafish are transgenic fish whose genome has incorporated the gene for m5GFP driven by a quail Pax6 transcription factor promoter and retina-specific enhancers such that GFP is only expressed in a subset of Pax6 expressing retinal cells. GFP is initially expressed in the cytoplasm of a subset of neuroepithelial cells, detected at least at 24hpf. This expression varies in intensity (Fig. 4.2a), and is thought to be in a subset because some cells are clearly delineated. If all cells had been labelled, the close juxtaposition of neuroepithelial cells would have made distinguishing individual cells more difficult. By 7dpf, this expression is restricted to amacrine cells in the inner nuclear layer as determined by their position within the neural retina (Fig. 4.2b). The sparsity of labelled cells suggests that only a subset of amacrine cells express GFP (Kay et al., 2001). The labelled cells could be classified as stratified cells as they seem to project dendrites to a single layer in the interplexiform layer (Dowling, 1987). However, the presence of different strata of GFP-expressing cell bodies in the inner nuclear layer indicates that more than one subtype may be labelled (Fig. 4.2c). It is not known whether the expression of GFP in neuroepithelial cells correlates to a future cell fate as a GFP-expressing amacrine cell as a direct progression from neuroepithelial cell to amacrine cell has been seen by time-lapse imaging in only one case (Fig. 4.2d). However, this is unlikely given the large number of labelled neuroepithelial cells in the retina. Additionally, Pax6 is itself not required for the differentiation of most amacrine cells as Pax6 deficient neuroepithelial cells tend to differentiate as amacrine cells at the expense of other cell types (Marquardt et al., 2001). Thus, GFP expression driven by Pax6 in neuroepithelial cells should not be a marker for amacrine cell differentiation *per se*. It is more likely that GFP expression is extinguished in most neuroepithelial cells as these give rise to other differentiated cell types, but remains or returns in amacrine cells. Amacrine cells in zebrafish are thought to be born between 38 and 48hpf as part of the inner nuclear layer (Hu and Easter, 1999). By time-lapse *in vivo* microscopy, amacrine

cells were noticed before 48hpf. However, most time-lapse experiments were conducted after 48hpf when GFP-expressing neuroepithelial cells were not found in the central retina or could be avoided.

II. Amacrine cell mosaics in the retina

Time-lapse imaging of the retina of Pax6GFP embryos was undertaken to visualise the behaviour of differentiated amacrine cells in the context of mosaic formation and maintenance. We sought to answer the question: do differentiated amacrine cells move tangentially or undergo apoptosis within the amacrine cell layer during the establishment of amacrine cell mosaics? The total number of amacrine cells imaged varied between experiments, ranging from 8 to 47, with a mean of 31.4±2.85 (mean±SEM; n=5). Whether the cells formed mosaics of regularly spaced elements was not obvious by sight. The regularity of cell mosaics can be compared by examining the distributions of distances between neighbouring cells (Galli-Resta and Novelli, 2000). Increasing regularity is indicated by a narrowing distribution of intercell distances. In the mosaics

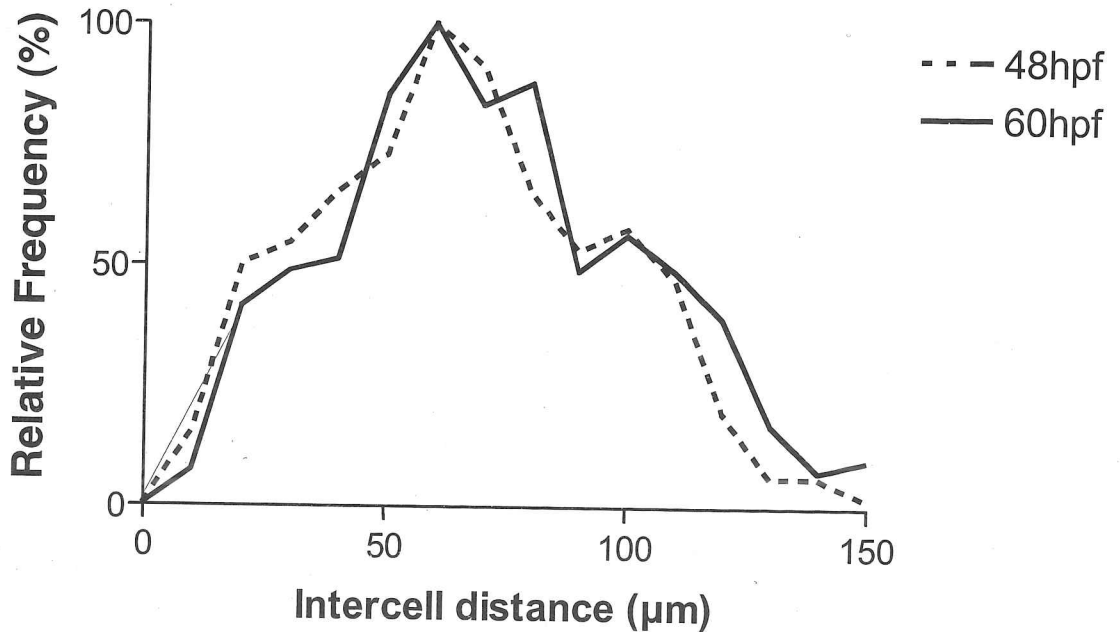

Fig. 4.3 ***The distrbution of intercell distances at 48hpf and 60hpf.*** The normalised distributions of intercell distances at 48hpf and 60hpf have significantly different means (p=0.01). The distribution at 60hpf is shifted to the right (i.e. has a greater mean) but is not narrowed compared to the distribution at 48hpf. Thus, there is no increase in regularity from 48hpf to 60hpf.

analysed, the average intercell distances (mean ± SEM) at 60hpf (71.41 ± 1.796; n=300) was significantly greater than at 48hpf (65.89 ± 1.368; n=465), (p=0.01). However, the later distribution of distances did not show any narrowing (Fig. 4.3), and the coefficients of variance were similar for both distributions (44.78% at 48hpf, 43.56% at 60hpf). This may reflect generalised growth and expansion of the retina. It is possible that the time interval analysed was too short to notice a significant difference in mosaic regularity or that mosaic regularity is established later on in development. In addition, it is known that regularity is only maintained within mosaics of the same subtypes of cells, and that cells of different subtypes are randomly situated relative to each other (Cameron and Carney, 2000; Galli-Resta, 2000), so if more than one subtype is indeed labelled by GFP in these transgenics, spatial regularity would be difficult to determine. Importantly, the number of elements considered is likely to be too small to reliably determine whether they form a regular cell mosaic.

III. Amacrine cell death in the retina

Although the evidence for mosaic regularity was lacking in these experiments, scrutiny of the resulting time-lapse movies showed a number of amacrine cells disappearing suddenly from the field of view. Often cells disappeared completely from one timepoint to the next (i.e. within 15 to 20 minutes), (Fig. 4.4a-b). Fading or photobleaching of GFP and migration out of the field of view could be excluded as causes for the disappearance as both would normally show signs of gradual change, and the disappearing cells were generally found far from the boundaries of the imaged volumes. Other cells seemed to disintegrate, leaving behind fluorescent fragments that disappeared more gradually (Fig. 4.4c-d). Given their timing and characteristics, these events are likely to represent apoptosis, which is known to take place in the amacrine cell layer of the zebrafish retina (Biehlmaier et al., 2001). The timecourse for apoptosis of retinal cells in rat has been shown to be about 40 minutes (Cellerino et al., 2000) and a clearance time of 3 hours estimated in the zebrafish (Li et al., 2000a), which is consistent with a timecourse between 15 minutes and 1.5 hours as seen in the time-lapse experiments described here. Nuclear fragmentation is characteristic of apoptosis and may be represented by the noticeable fragmentation of the fluorescent cells seen in some cases (Fig. 4.4c-d). Apoptotic events were noticed from the very beginning of the time-lapse series at 49hpf. The latest event was seen at 110hpf in a series that lasted to 114hpf. Apoptotic events

were noted at various times during the time-lapses, thus it is unlikely that amacrine cell apoptosis is limited between 48hpf and 110hpf. Nonetheless, a study of apoptosis in fixed retinal sections showed levels peaking between 3 and 4dpf (72 to 120hpf) in the inner nuclear layer (Biehlmaier et al., 2001). The same study showed that very few cell deaths occurred in the zebrafish retina with a peak of 0.34% apoptotic cells in the entire inner nuclear layer at 3dpf. The average proportion of apoptotic cells found in the time-lapse experiments compared to the total number of labelled cells was 30.4±0.75% (mean±SEM; n=5). These proportions are cumulative over the entire time of the experiments and do not reflect cell death levels at any particular point in time.

IV. Cell death and intercell distance

If the apoptosis of amacrine cells was involved in the formation of regularly-spaced cell mosaics, and cell-cell interactions are responsible for ensuring a minimum distance between cells (Galli-Resta, 2000; Galli-Resta et al., 2002), apoptosis might be expected to occur more often with shorter intercell distances. The distance between neighbouring cells was measured at regular intervals from two time-lapse experiments as described in the Materials and Methods section and the data pooled. The distance between each cell

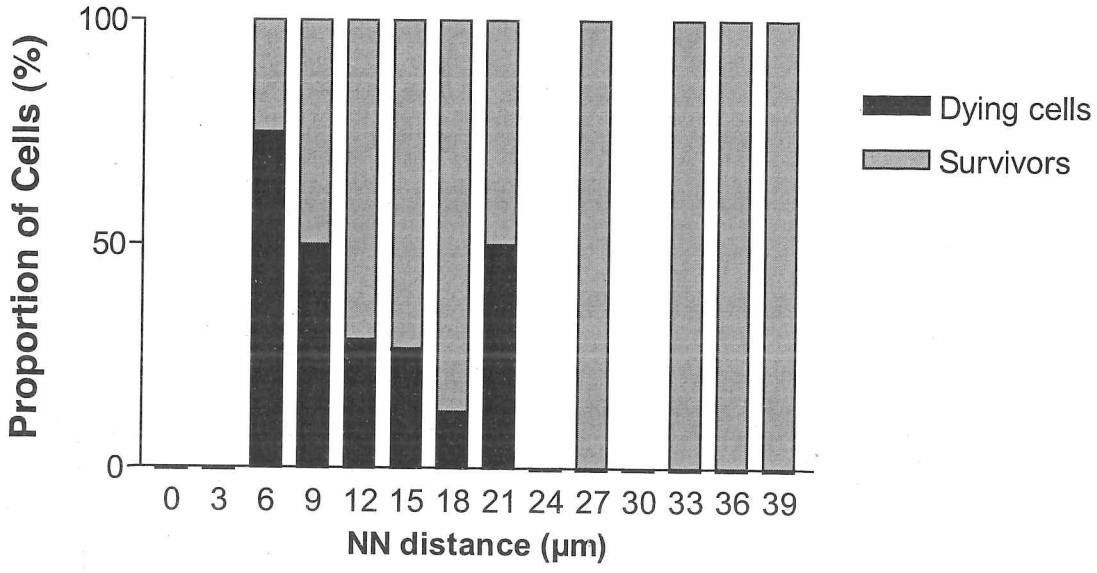

Fig. 4.5 ***Comparison of dying cells and survivors with respect to distance from the nearest neighbour (NN) to each cell.*** The frequency distribution graph shows the relative proportion of dying and surviving cells that have encountered other cells at the specified distance. The shorter the distance between two cells, the higher the chance of one cell undergoing apoptosis.

and its closest neighbour, or the nearest neighbour (NN) distance, was the variable used to compare two subsets of the cell population: the cells that died and the surviving cells. For each cell, the least NN distance experienced by a cell in the entire time-lapse was determined, as the distance between the same cells would vary from one timepoint to the next. If cell-cell interactions are involved in mosaic formation, any effect on a cell would be most likely to be mediated at the time that two cells are closest to each other (the least NN distance). The distribution of least NN distances for dying cells was compared to the distribution of least NN distances for surviving cells in the retinas (Fig. 4.5).

A larger proportion of cells that experience smaller NN distances undergo apoptosis. NN distances between cells in zebrafish retinal mosaics have previously been found to fit normal distributions (Cameron and Carney, 2000), and an unpaired t-test could be used to compare the average NN distance for dying and surviving cells coming from the same assumed normal population of cells. The mean NN distance (± SEM) for dying cells ($11.50\mu m \pm 0.98\mu m$) is significantly smaller ($p < 0.01$) than the mean NN distance for survivors ($16.49\mu m \pm 1.18\mu m$). The difference is similarly significant if the non-parametric Mann-Whitney U test is used to compare the distributions.

The entire distribution of least NN distances for each population was visualised by

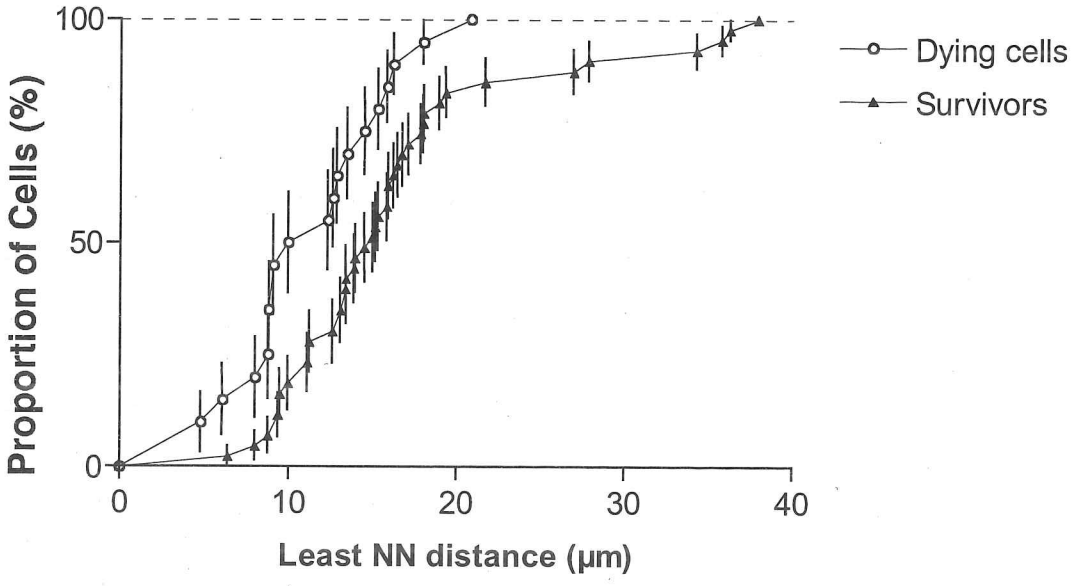

Fig. 4.6 ***Cumulative frequency curves for dying cells and survivors with respect to distance from the nearest neighbour (NN) to each cell.*** A greater proportion of dying cells have had closer encounters with other cells. The distributions are significantly different (p=0.005) by the log-rank test.

plotting cumulative frequency curves, where the total proportion of cells found within a least NN distance value is plotted against the least NN distance (Fig. 4.6). These were compared using the log-rank test. The distribution of dying cells is significantly different and changes at twice the rate of the surviving cell distribution ($p = 0.005$).

Thus, the increased likelihood of finding apoptotic cells with shorter distances between neighbouring cells is consistent with a hypothesis where close cell-cell interactions are associated with the cell death of one partner in the interaction.

This analysis is limited in a number of ways. The number of cells in each time-lapse experiment is relatively low, which makes determining mosaic regularity, and therefore any correlation with cell death, difficult. There may be at least two cell subtypes labelled with GFP in the Pax6GFP embryos used. This can confuse the issue of mosaic regularity as well as that of cell death mediated by cell-cell interactions between homotypic cells. Heterotypic cells lying close to each other may not be associated with apoptosis, thus producing results that are more difficult to interpret. Finally, the start and end limits of the time-lapse experiments mean that the past and future histories of many cells cannot be known, with the result that potential cell-cell interaction and apoptosis associations may be missed.

V. Cellular processes and cell death

The growth of amacrine cell processes can often be seen in intensely expressing cells. There seems to be little correlation between the level of differentiation of a cell, deemed from the presence of visible dendritic processes, and the chance of the cell dying, as cells with and without visible processes have been found to undergo apoptosis. Fig. 4.4a-b show amacrine cells without obviously visible processes undergoing apoptosis. Processes are not visible on the amacrine cell undergoing apoptosis in Fig. 4.4c, although it seems to be established in the amacrine cell layer, along with its neighbour. Fig. 4.7a represents an amacrine cell at 101hpf with very extensive processes that ultimately, and perhaps surprisingly, undergoes apoptosis. Only one of the three neighbours to this cell survives by the end of the experiment. The average distance between the survivor and its neighbours was 19.1μm (± 2.9μm; SD). Immediately after the death of the three cells, processes from cells slightly further afield could be seen growing towards the surviving cell (Fig. 4.7b). The death of the three cells could have been mediated by dendritic interactions with the surviving cell or with the growing dendritic processes from the cells

further afield, as the timing of the events is coincidental. The correlation between the dendritic growth of neighbours and cell death has not been analysed quantitatively due to the lack of examples seen in time-lapse experiments. However, in another opportunity to visualise dendritic processes from amacrine cells between 82hpf and 88hpf, one cell is seen to die as it is approached by bright dendritic terminals from several neighbouring cells, while the death of another closer cell reveals a bright dendritic terminal from one of its neighbours immediately beneath it (Fig. 4.8a). The distance traversed by some of the dendritic processes is relatively long (Fig. 4.8b) and may therefore affect cells that are further away than nearest neighbours. However, this extensive dendritic growth has occurred between 65hpf and 101hpf, suggesting that earlier cell deaths, if mediated by cell-cell interactions, would have to occur at shorter intercell distances.

VI. Cell movement within mosaics

Only one case of a cell transitioning from a neuroepithelial morphology to an amacrine cell morphology was picked up in the time-lapse experiments, in a field of view where few other amacrine cells could be seen (Fig. 4.2d). Thus, the hypothesis of cells within an established mosaic moving tangentially to accommodate new cells entering the amacrine cell layer could not be directly tested. Throughout the time-lapse experiments, new cells were noticed in the population. Some were cells in the periphery of the field of view that became part of the observed population if the entire embryo drifted slowly across the field of view, while others were cells expressing increasing amounts of GFP becoming more visible. A few cells seemed to appear suddenly, which may reflect the addition of new cells. For one retina, the distance between new cells that appeared suddenly and all its nearest neighbours was calculated and compared to the average cell displacement of all observed cells (Fig. 4.9). None of a new cell's nearest neighbours underwent any significant displacement away from the new cell ($p > 0.05$; unpaired t-test).

In fact, amacrine cells seemed to undergo minimal tangential movement overall. The cells that moved the most tended to be the cells that were about to die. Apoptotic cells in the retina have been shown to move erratically towards the end of the apoptotic process (Cellerino et al., 2000), and this may be reflected by sudden, erratic movements occasionally seen here (3.10a). Cellerino et al. noticed the movement after nuclear fragmentation had taken place, however, since Pax6GFP is expressed in the cytoplasm, nuclear fragmentation is not necessarily visualised and erratic movement might be seen

before the cell membrane disintegrates visibly. Disintegration of the cell membrane or zeiosis can be seen occasionally, followed by dispersal of the membrane-bound cell fragments typical of apoptosis. Sudden, rapid movements of these fragments may be a reflection of very mobile macrophages engulfing the fragments (3.10b).

Although cell movements in response to the addition of new elements to the amacrine cell mosaic cannot be excluded, tangential migration by established and surviving amacrine cells was not noticed during the duration of these time-lapse experiments. This may take place earlier (between 38 and 48hpf) during the active addition of new cells to the mosaic while amacrine cells are still being born or it may be that such movements are too subtle or ubiquitous to notice in time-lapse experiments. This is also difficult to assess in terms of changes to mosaic regularity as the time at which amacrine cell mosaics are actually established in the zebrafish retina has not been determined.

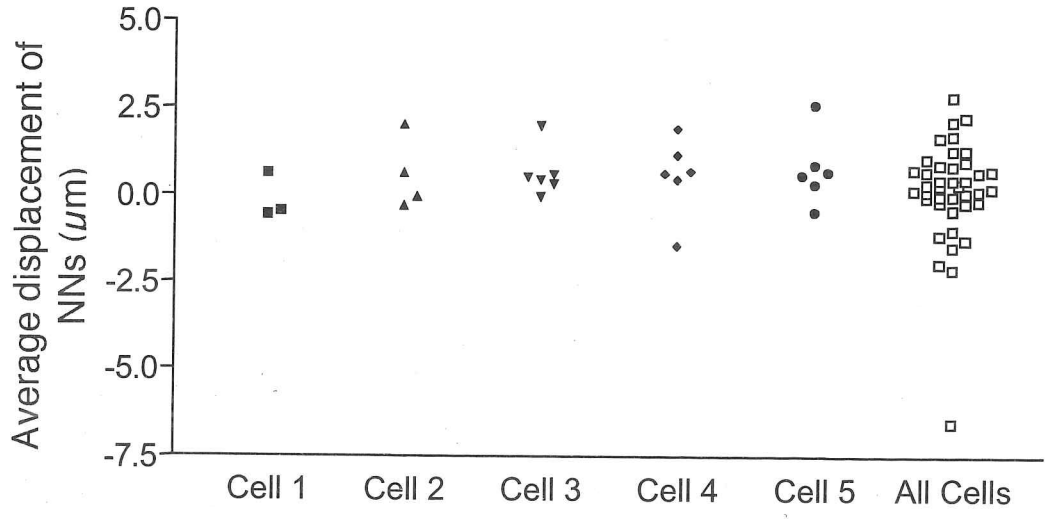

Fig. 4.9 ***The scatter plot shows the time-averaged distance between five 'new' cells in the time-lapse series and their nearest neighbours***, each represented by one point. 'All Cells' represents the distance between all cells and one reference cell that showed little motility throughout the series. The average of each new cell's distribution is not significantly different to the overall average (unpaired t-tests).

Discussion

This study takes advantage of *in vivo* microscopy of transgenic embryos which express GFP specifically in subsets of amacrine cells in the retina to study the behaviour of neurons during development that are known to be part of regularly-spaced arrays in adulthood. In particular, time-lapse analysis in combination with three-dimensional visualisation enabled amacrine cells to be followed through a period of retinal development when many cells are still being born and other layers of the retina are still being modelled. Some amacrine cells were found to undergo apoptosis, the likelihood of which could be correlated with shorter distances between cells of the same type, if not the same subtype, and could be mediated by cell-cell interactions. In addition, by visualising the growth of dendritic processes, some tantalising preliminary evidence is presented that dendritic interactions may be a method by which such apoptosis-inducing interactions are mediated.

I. Amacrine cells undergo apoptosis in the zebrafish retina

Initially, time-lapse *in vivo* microscopy showed that amacrine cells do undergo apoptosis, as determined by cells disappearing suddenly from the field of view within 15 to 20 minutes. All cells considered to have undergone apoptosis were confirmed not to be close to the edges of the field of view, where they might have migrated out of view. Characteristics of apoptosis such as membrane blebbing (zeiosis), cell fragmentation and erratic cell movement were seen in some cells disappearing in this way. None of the cells faded gradually before disappearing, excluding photobleaching as a cause of the disappearance, nor did there seem to be any correlation between GFP expression levels and death. Both intensely expressing and weakly expressing cells could be found amongst the dying and surviving cells, excluding photodamage-induced cell death as a cause of apoptosis. A surprising result was the high proportion (approximately 30%) of observed amacrine cells that underwent apoptosis. This is much higher than previous estimates of apoptosis levels in the zebrafish retina. One study estimated cell death in the inner nuclear layer of the zebrafish retina to be less than 0.5% at its peak at 3dpf or 72hpf (Biehlmaier et al., 2001). However, this study considered the entire inner nuclear layer as opposed to populations of particular cell types, and was conducted using fixed retinal sections, in which only snapshots of the proportion of apoptotic cells in the retina can be counted.

Since apoptosis is a dynamic and relatively short-lived process (Cellerino et al., 2000), single timepoint studies are likely to miss most apoptotic events that are taking place around a particular time period, and will underestimate the frequency of apoptosis. In a different study, apoptosis levels were estimated *in vivo* by looking at changes in cell morphology over time while counting new apoptotic cells as these were added (Li et al., 2000a). It was estimated that less than 1% of cells underwent apoptosis, although this was for the entire retina and for embryos younger than 36hpf. In the time-lapse studies presented here, the estimate of cell death levels was made over the entire time for each experiment, ranging between 14 and 80 hours. As the number of new cells added to the observed population was very low, the number of apoptotic cells accumulated through the length of the experiments. Furthermore, the number of cell deaths is being compared to a small population of labelled, observed amacrine cells. Both of these reasons may explain the large discrepancy between cell death estimates of this study and previous reports.

II. The role of cell-cell interactions in amacrine cell apoptosis

Cell-cell interactions are thought to play an important role in the formation of regularly-spaces arrays or mosaics of cells. Most retinal cell mosaics can be simulated by simply restricting elements to maintain a minimum distance between each other (Galli-Resta, 1998; Galli-Resta et al., 1999; Galli-Resta et al., 1997; Scheibe et al., 1995). The probability of finding cells beyond a particular exclusion zone is independent of the cell at the source of the exclusion zone, suggesting that the distance limiting interaction is of a short-range nature (Galli-Resta, 2000). The results presented in Fig. 4.5 show that cells that undergo apoptosis are more likely to have come within a shorter distance of neighbouring cells compared to cells that survived the length of the time-lapse experiment. The correlation of apoptosis with short intercell distances suggests that short-range interactions between cells may have a role to play in mediating cell death. Apoptosis has been suggested as a possible mechanism to increase regularity in cell mosaics by removing cells that do not fit into the mosaic (Cook and Chalupa, 2000). Thus, it is possible that apoptosis, mediated by short-range interactions between cells, is used in the zebrafish retina to ensure that a minimum distance is maintained between amacrine cells, or prevent the formation of dense clusters of cells. There is contrasting evidence for the role of cell death in improving cell regularity. Cell death of cholinergic amacrine cells in the rat retina did not lead to any improvement in cholinergic cell

regularity that could not be explained by retinal expansion (Galli-Resta and Novelli, 2000). However, cell death of α-ganglion cells in the cat retina does improve cell mosaic regularity, a possibility confirmed by computer simulations of the mosaics (Jeyarasasingam et al., 1998). Unfortunately, the small number of cells observed in the *in vivo* time-lapse experiments do not provide a reliable means of measuring or comparing mosaic regularity, usually determined by comparing the distributions of distances between nearest neighbours at different times or for different arrays. Whether the death of amacrine cells in the developing zebrafish retina contribute to an increase in mosaic regularity has not been determined. Interestingly, apoptosis was dismissed as a mechanism for maintaining or improving cell mosaic regularity in anamniotes due to the rarity of neuronal cell death observed in their retinas (Cook and Chalupa, 2000). The work here suggests that dismissing the role of apoptosis in the zebrafish retina may be premature.

Short-range interactions in the context of mosaic maintenance have been shown to be mediated by interactions between dendrites of neuronal cells of the same type. Lohmann et al use two-photon microscopy to show direct contacts between ferret retinal neuronal cells of the same subtype, such as ON-type α-ganglion cells but none with cells of different subtypes, including OFF-type α-ganglion cells (Lohmann and Wong, 2001). Disruption of microtubules within the dendrites of cholinergic amacrine cells in the rat retina reversibly affected the three-dimensional structure of the arrays that they formed. Dendritic connections between cells were disrupted, and cells were scattered in a more random distribution (Galli-Resta et al., 2002). Removal of the disruptive agents returned the arrays to their regular structure, compared to a tight net forming a hemispherical dome with stiff dendritic processes forming the links between the nodes in the net. Dendritic processes could only be visualised *in vivo* in the zebrafish retina if the cell itself expressed high levels of GFP, however there were two cases in which the growth of dendritic processes could be followed from the cells of origin towards neighbouring cells. A number of interesting observations can be made from the *in vivo* experiments. First, well-differentiated amacrine cells with visible dendrites underwent apoptosis, as did less visibly differentiated cells. Secondly, the interesting aspect of having followed dendritic process growth is that in both cases, groups of apoptotic cell bodies were seen just beyond the reach or at the ends of the growing processes. This suggests that the area covered by the dendritic processes from one cell may form an exclusion area for other

cells, such that any other cell encountered by those processes undergoes apoptosis. Fig. 4.10c shows two frames of an amacrine cell with an easily visualised dendritic tree from a time-lapse series between 56hpf and 70hpf. No other labelled amacrine cell bodies within the area are in direct contact with the dendrites. This cannot explain the results entirely as some examples of cells lying close to each other while growing dendritic trees can be also be seen (Fig. 4.8b). One possibility may be that these cells are of different subtypes and therefore do not interact with each other in terms of mosaic formation. Finally, apoptosis was noticed in all experiments well before the time that visible dendritic growth could be followed (68hpf onwards). In most cases, dendritic trees could not be visualised so that any correlation of apoptosis to dendritic interaction between cells could not be determined. It is likely that cells that respond to cell death cues also require some dendritic processes. This would explain the influence of cells with small dendritic trees over neighbouring cells that lie beyond the reach of the offending dendrites.

A different clue to the importance of apoptosis in the zebrafish retina during early development comes from a study of early macrophages in the zebrafish (Herbomel et al., 2001). Early macrophages originate in the rostral lateral mesoderm of the embryo, close to the cardiac fields, and differentiate in the yolk sac. These macrophages actively invade the head tissues before these are actually vascularised. Interestingly, a wave of macrophage activity is seen within the retina from 36hpf, with the macrophages remaining within the ganglion cell layers and inner nuclear layers – both layers in which retinal cell mosaics are found. Rapidly and erratically moving fluorescent fragments from cells that underwent apoptosis can occasionally be seen in the *in vivo* time-lapse series of Pax6GFP retinas (Fig. 4.10). The photoreceptor cell layer, from which macrophages seem to be excluded, does not contain the typical cell mosaics with elements spread apart, but rather regular arrays in which cells are found closely apposed to each other. Perhaps such arrays do not require apoptosis for their refinement.

The existence of cell death amongst amacrine cells, its correlation with short intercell distances and a possible association with cellular dendritic trees that may mediate intercell interactions, suggest that a role for cell death in refining cell mosaics is a plausible possibility and warrants further investigation. In addition, the presence of early macrophages that specifically invade the retina around the same time period as the beginning of ganglion cell and inner nuclear layer cell differentiation and apoptosis provides further weight to the importance of the role of programmed cell death.

III. Tangential cell movement

Amacrine cells are dynamic objects, at the level of the soma as well as the dendrites. Time-lapse movies show the cell bodies changing shape slightly, as if jostling for space, but essentially remaining in the same place once established within the amacrine cell layer. Analysis of cell movement from one retina shows that cells move very little overall, and that even the appearance of new cells does not provide enough stimulus to force neighbouring amacrine cells to move away. The noticeable movement seen in some cells was always due to the cell undergoing apoptosis. Of the five new cells analysed, three underwent apoptosis within four hours of appearing. Tangential movements occur in the mouse retina as shown by the presence of neurons outside of their radial clone of origin using X-inactivated transgenic mice (Reese et al., 1995; Reese et al., 1999). In the zebrafish retina, small displacements of amacrine cells can certainly be seen, but none specifically in response to neighbouring cells. It is possible that tangential cell movement is involved in mosaic formation as cells migrate to the amacrine cell layer from the ventricular zone and occurred earlier than the time that the time-lapse movies were started. However, very few labelled amacrine cells could be seen earlier than 48hpf. Since amacrine cells are thought to be born between 38 and 48hpf, one would expect at least some amacrine cells to be migrating into the inner nuclear layer after 48hpf. Tangential migration may play a role in maintaining mosaic regularity later in development or through adulthood, when the retinas were not observed. Intuitively, it is unlikely that cells would be born exactly at the right place in the ventricular zone and migrate radially to the correct spot in a mosaic. In the mouse retina, migrating cholinergic amacrine cells can be labelled with antibodies against Islet-1, which also labels the resulting mosaics of cholinergic cells (Galli-Resta et al., 1997). Migrating cells did not form regular arrays until they had reached the amacrine (or ganglion) cell layer. It is also possible that tangential migration is a subtle process that cannot be differentiated from random cell movement by only analysing cell movement in movies. A combination of movement analysis *in vivo* with mosaic regularity estimates would help to determine whether any movement observed correlates with improvements in the regularity of the mosaic. This could not be determined using the low cell count in the time-lapse experiments presented here. *In vivo* microscopy of specific cell populations in the zebrafish retina, and the ability to follow cells through space and time, has enabled the behaviour of cells that form regularly spaced mosaics to be studied. The regularity of cell mosaics has implied

that cells must interact with each other to some extent to maintain this regularity. Proposed mechanisms for this include tangential movement of cells to accommodate other cells in the mosaic and apoptosis of unwanted elements in the mosaic (Cook and Chalupa, 2000). Apoptosis had been dismissed in anamniotes such as the zebrafish due to the low levels of apoptosis seen in the retina, however the *in vivo* experiments here show that apoptosis occurs to a significant level in amacrine cell populations and that it may be the result of short-range interactions between cells, leading to the possibility of apoptosis playing an important role in the formation of retinal cell mosaics. Surprisingly, tangential movement of cells, for which strong evidence exists in the mouse and, which one would expect to be able to visualise by *in vivo* microscopy, was not noticed to a significant degree.

The *in vivo* experiments were possible due to the availability of transgenic zebrafish that express GFP in populations of a specific cell type (although they may consist of multiple subtypes). Similar work in transgenic embryos expressing GFP in other cell types will be of value. Embryos expressing GFP in retinal ganglion cells (such as Shh-GFP) exist, although they seem to express GFP in all ganglion cell types. Transgenic embryos that express a membrane-bound GFP in amacrine cells exist (Fig. 4.2c) and may prove useful to visualise cell dendrites and the interaction between amacrine cells *in vivo*. They may also be useful to study the morphological changes that occur during the differentiation of amacrine cells. The difficulty with these embryos is that cell bodies are more difficult to see, especially in three-dimensional reconstructions. Finally, whether cell mosaics are established as regular entities in the early, developing zebrafish retina still needs to be determined, and will be an important step forward in correlating the evidence for apoptosis to cell mosaic formation.

Retinal cell mosaics represent cooperation amongst cell populations to form structures that efficiently cover a large area of the retina, producing minimal overlap or redundancy for processing visual information. Much of the work on cell mosaics has so far been conducted in the mammalian retina. But the potential for *in vivo* studies in the zebrafish retina mean that the zebrafish could become an important tool in the search for the nature of the mechanisms that govern the formation of ordered arrays of cells.

Fig. 4.2 ***Pax6-GFP transgenic embryos express GFP in amacrine cells.*** **a)** 3D reconstruction of a 35hpf Pax6-GFP retina. GFP is expressed in a subset of neuroepithelial cells. Some cells have little or no expression, which has allowed neighbouring expressing cells to be visualised in 3D. **b)** Cryosection of a 7dpf Pax6-GFP retina. GFP is expressed only by amacrine cells (arrows) and their dendritic projections in the inner plexiform layer (arrowheads). Other layers of the retina (retinal pigment epithelium; rpe, outer nuclear layer; onl, inner nuclear layer; inl, and ganglion cell layer; gcl) can be seen in the transmitted light image of the section. **c)** Optical sections from a 2dpf Pax6-GAP-GFP transgenic embryo are projected to show the different layers occupied by the amacrine cell bodies (arrows and arrowheads), although their dendritic projections still seem to occupy a single stratum in the inner plexiform layer. **d)** 3D reconstruction of a Pax6-GFP retina seen sideways on. The arrows point to a neuroepithelial cell that is found to differentiate into an amacrine cell without losing GFP expression when followed through time.

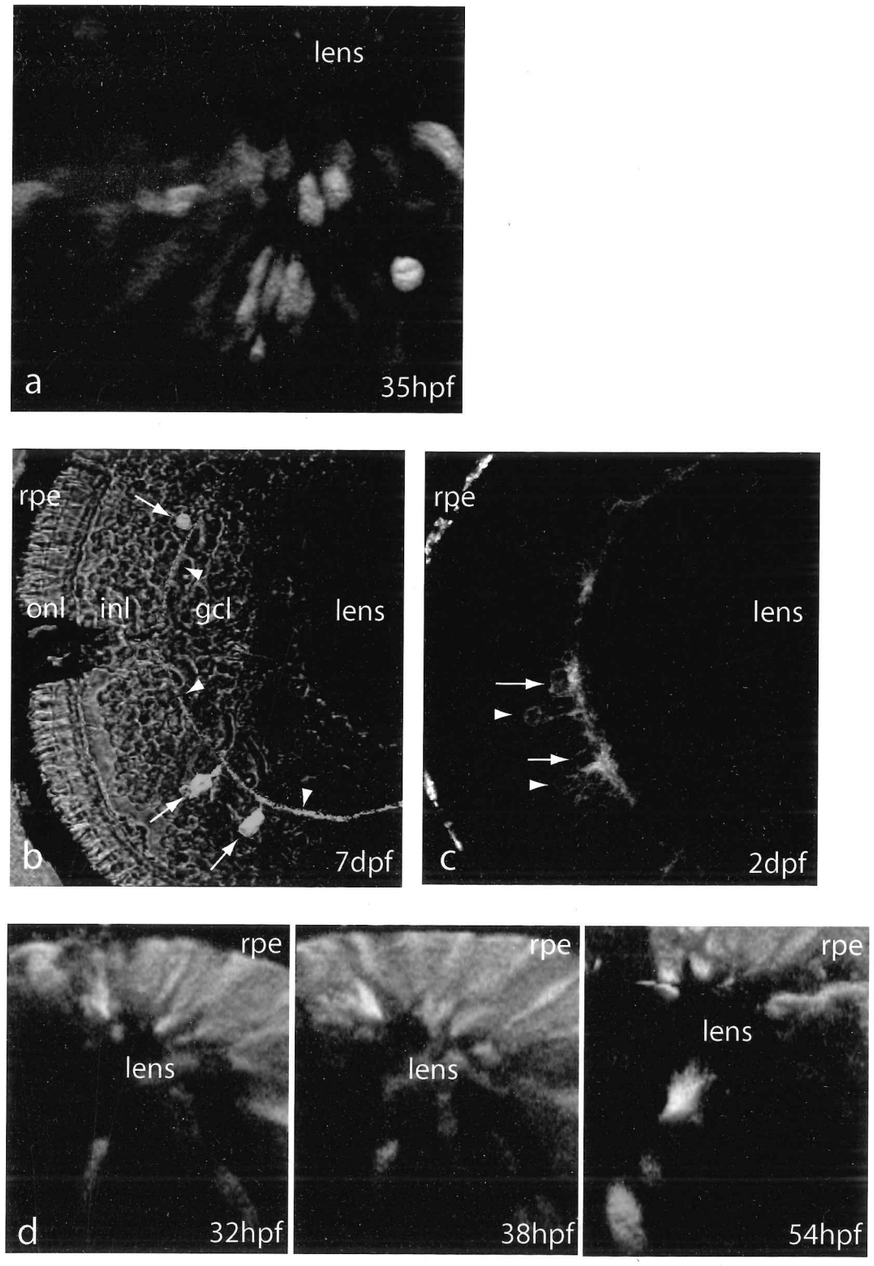

Fig. 4.4 ***Apoptosis of amacrine cells in the developing zebrafish retina.*** **a-d**) GFP-expressing amacrine cells are seen in 3D reconstructions of 2dpf Pax6-GFP retinas. Some amacrine cells (arrowheads) disappear from one timepoint to the next (arrowheads in **a**, **b**) while others disintegrate over a short period of time (arrowheads in **c**, **d**). All frames are 15 minutes apart.

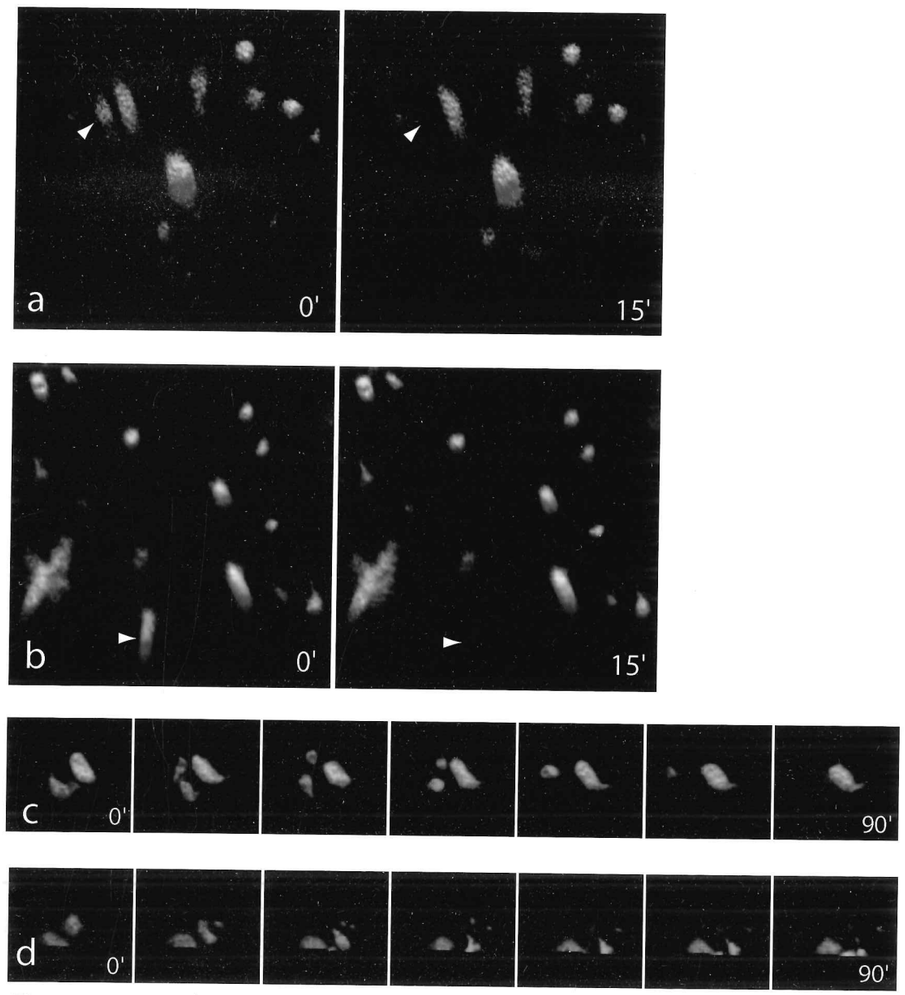

Fig. 4.4

Fig. 4.7 ***Established amacrine cells can undergo apoptosis.*** **a)** A well differentiated amacrine cell with multiple, prominent dendritic projections also undergoes apoptosis (arrow), although the time over which the cell degenerates is longer than expected for typical apoptotic cells. Of the three nearest neighbours (arrowheads), only the left most will survive. **b)** Dendrites from neighbouring cells, but not nearest neighbours, reach the cluster of cells seen in (a), around the same time that these are dying. At 95hpf, the dendritic projections are difficult to see. These are marked by bright tips (arrowheads) that arrive closer to the cell cluster over approximately 10 hours, covering approximately 35μm. The direction of movement of the dendrites suggests one of the cells marked with arrows as their origin.

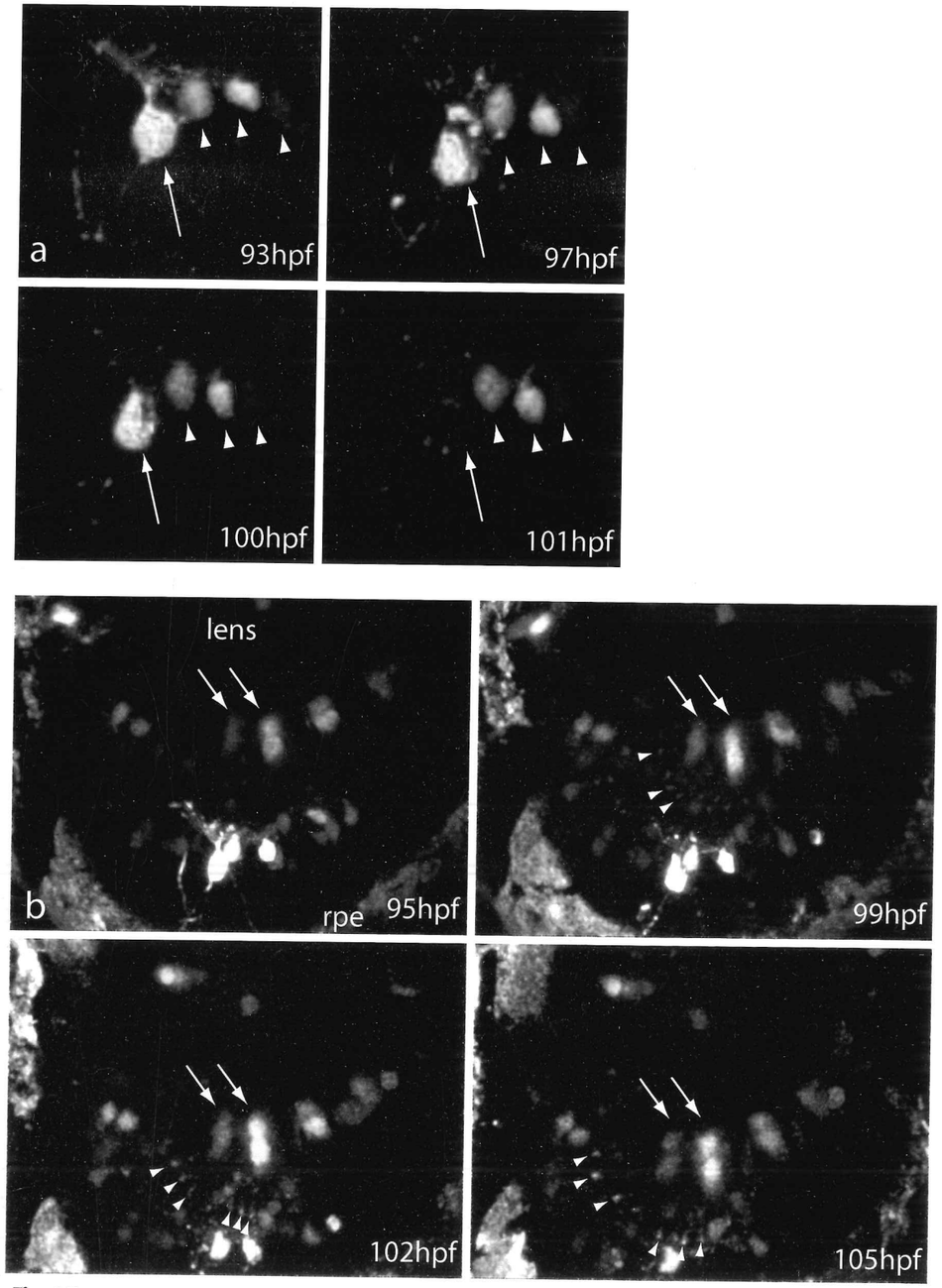

Fig. 4.7

Fig. 4.8 ***Amacrine cell death coincides spatially and temporally with the approach of dendrites from neighbouring cells.*** **a)** An amacrine cell (open arrow) undergoes apoptosis with the approach of dendritic tips (arrowhead). The death of another amacrine cell (arrow) reveals the presence of a dendritic tip immediately beneath it. **b)** 3D reconstruction of the same retina as in (a), rotated to visualise amacrine cell dendrites. Those marked by arrowheads originated from the more central amacrine cell (arrow) and have travelled through a single stratum in the inner plexiform layer towards more peripheral targets, covering a distance of approximately 53μm. The amacrine cell marked with a double arrowhead lies close to the cell with the extensive dendritic tree, and may be extending its own, yet it is not affected by the dendritic tree of its neighbour.

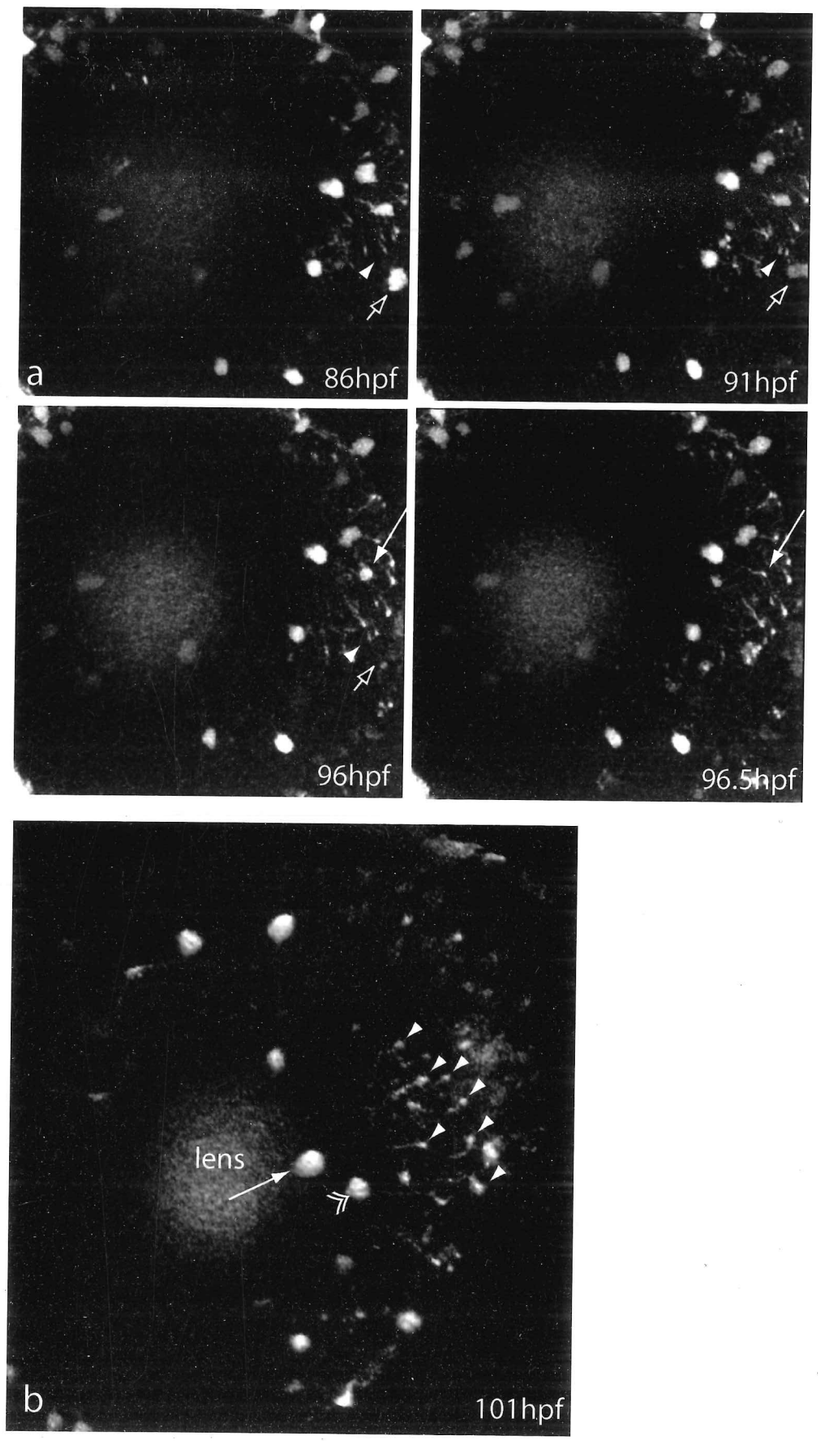

Fig. 4.8

Fig. 4.10 ***Relatively rapid moving cells (highlighted in green) tend to undergo apoptosis or may be macrophages.*** **a)** A moving amacrine cell is highlighted. The white circle serves as a reference for the displacement of the cell per frame. The most sudden movement with the greatest displacement occurs in the last 30 minutes for the cell. **b)** Small islands of GFP signal may be cellular debris from apoptotic amacrine cells. Rapid displacement of these islands in a relatively coherent manner may represent macrophages ingesting the debris while migrating within the retina

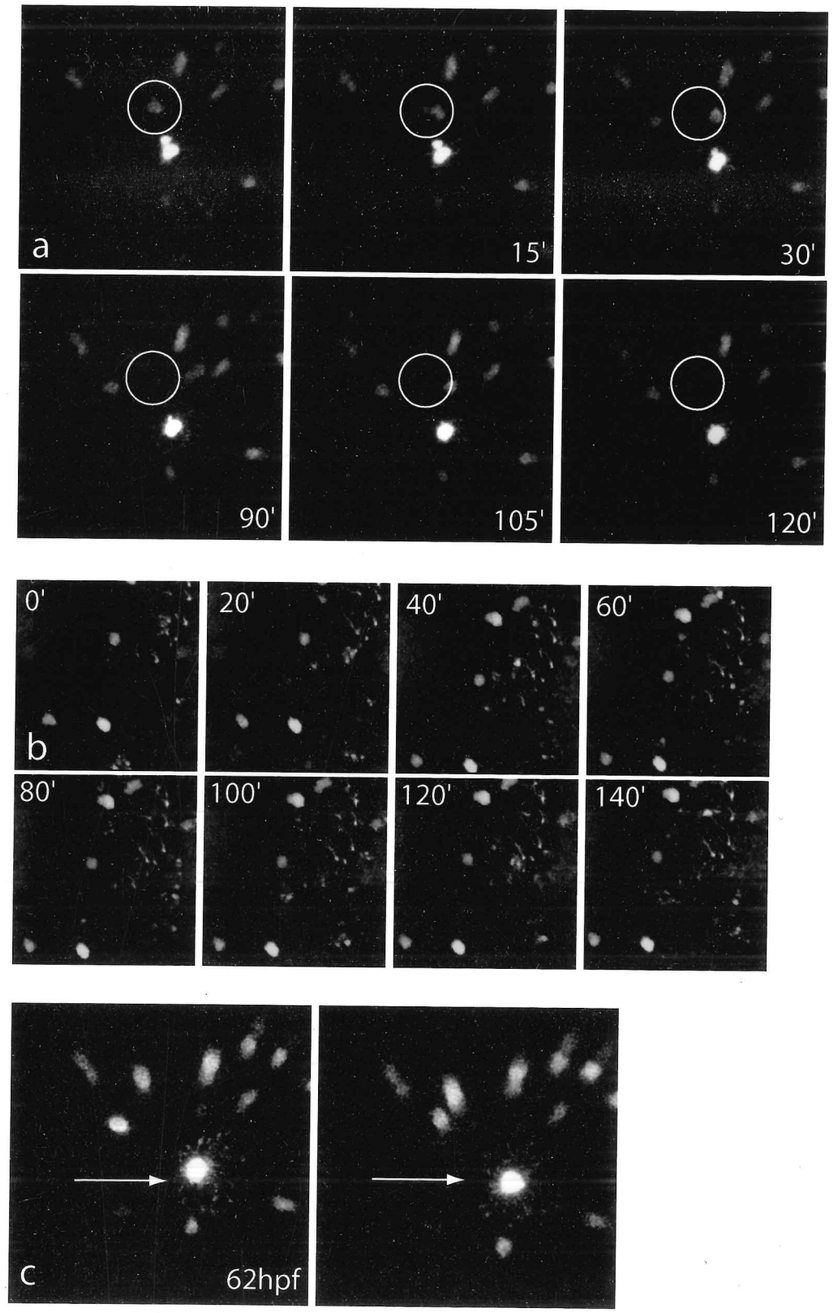

Fig. 4.10

Chapter 5: General Summary

The work presented in this thesis consists of two main sections. The first section presented in Chapter 2, is both an introduction to *in vivo* imaging using two-photon excitation laser scanning microscopy and an account of the knowledge gained during the use of this tool, that can hopefully be of benefit to others. The second section, dealt with primarily in Chapters 3 and 4, presents questions on zebrafish retinal development that were addressed by means of *in vivo* imaging. Two-photon excitation microscopy has the potential to open many new vistas for researchers by allowing *in vivo* phenomena to be studied over a longer time than is normally possible using confocal microscopy. Four-dimensional imaging, or the acquisition of three-dimensional data over time, is more feasible using TPELSM because of its fundamental advantage over confocal microscopy in terms of reduced photodamage to the specimen or fluorescent probe given an equivalent amount of laser exposure. For many, analysing four-dimensional data may seem like a daunting task due to the vast amounts of data needing to be collected and the intensive technical needs required for analysis. However, the availability of specialised and user-friendly software has been very important in the management and analysis of these large data sets. Importantly, the zebrafish retina was determined to be well suited to imaging by TPELSM so that the advantages that this method offers could be exploited. Chapter 3 is a study of cell division in the zebrafish retina, particularly neurogenesis and cell division symmetry. In contrast to current models of cell division during neurogenesis, this research did not observe any apico-basal divisions, thought to represent asymmetric divisions, in the zebrafish retina. This research was the first time a changing bias in the orientation of cell division within the plane of the ventricular surface was observed in vertebrates. In our results, a high proportion of cells tended to initially divide closer to a central-peripheral orientation but was later biased towards circumferential divisions. We believe that this change in bias approximately coincided with the onset of neurogenesis. In *sonic you* mutant zebrafish, neurogenesis is delayed as evidenced by a lack of retinal ganglion cells. In support of a correlation between neurogenesis and a change in orientation of cell division, a delay in the shift in bias from central-peripheral to circumferential divisions was observed in the *syu* mutant. The time-dependent bias in orientation of cell division was also observed in rat retina, indicating that it may be a general feature of retinal development in vertebrates. In these experiments, we could not

establish whether the planar orientation of division is directly related to the symmetry of cell division. Experiments that attempted to follow cells *in vivo* from their division to their fate were technically challenging, mainly due to their retrospective nature (i.e. tracking cells back through datasets) and the time required (more than 24 hours) to keep cells within the field of view of the microscope. However, this research did succeed in retrospective tracking in a few cases, demonstrating that this type of experiment is feasible. As such, we recommend that future studies attempt to further explore the dynamics and sequence of cell fate determination.

Data presented in Chapter 3 also showed that retinal progenitor cells spanning the entire thickness of the retina do not lose their attachment to the basal surface of the retina when dividing. We demonstrated that a cell's basal process maintains its attachment to the basal surface through the cell's division. Often, the process is inherited by one daughter cell, which may be a sign of asymmetry of division but does not correlate to the orientation of cell division. The maintenance of the basal process may play a functional role in maintaining clones of cells within radial columns as they migrate to different retinal layers.

After differentiating and migrating to their appropriate layers, many retinal cells form regular arrays with other cells of the same type that can span the entire retina. These arrays are thought to be established early in retinal development, soon after the differentiation of the cells in question. In Chapter 4, *in vivo* imaging was used to study the behaviour of amacrine cells in the developing retina, soon after they had differentiated and migrated to the inner nuclear layer. At this stage, these were likely to be forming rudimentary arrays. Apoptosis, which was previously thought to occur minimally in zebrafish retina, was seen relatively frequently among amacrine cells. Furthermore, the hypothesis that apoptosis plays a role in the formation of regular arrays of cells was supported by the finding that cells that were closer to other cells were more likely to undergo cell death. This phenomenon may help maintain a minimum distance between cells, a requirement for the formation of regular cell mosaics. *In vivo* imaging also showed preliminary evidence that interactions between cells at the dendritic level might be responsible for causing some cells to die, as the tip of dendrites growing from neighbouring cells could be seen close to regions where dying cells lay a short time previously. Currently, there are few studies of the role of apoptosis in the formation of

cell mosaics in the vertebrate retina. The *in vivo* data presented here, however, suggests that apoptosis may have an important part to play in cell mosaic formation.

Ideally, by imaging zebrafish retina *in vivo*, cells can be followed from birth, through differentiation and migration, to their establishment in mosaics. Although the technological barriers to achieving this have not been fully overcome, it is no longer as remote a possibility as once thought. Tracing cell lineages *in vivo* or charting the history of individual cells during the development of the retina can shed much light on critical issues in retinal or neural development, including the degree to which progenitor cells are multipotent, and what the nature of extrinsic or intrinsic cues might be, that cells experience at different times destining them to a particular fate.

It is hoped that the contributions made by this work are two-fold. First, that it demonstrates the feasibility and power of *in vivo* imaging, and provides some guidance to its technique and the most appropriate circumstances for its use. Secondly, it is hoped that the findings in Chapters 3 and 4, some of which had not been considered previously, provide some stimuli for future work in the development of neural tissues.

References

Adams, R. J. (1996). Metaphase spindles rotate in the neuroepithelium of rat cerebral cortex. *J Neurosci* **16**, 7610-8.

Artinger, K. B., Fedtsova, N., Rhee, J. M., Bronner-Fraser, M. and Turner, E. (1998). Placodal origin of Brn-3-expressing cranial sensory neurons. *J Neurobiol* **36**, 572-85.

Austin, C. P., Feldman, D. E., Ida, J. A., Jr. and Cepko, C. L. (1995). Vertebrate retinal ganglion cells are selected from competent progenitors by the action of Notch. *Development* **121**, 3637-50.

Bellaiche, Y., Gho, M., Kaltschmidt, J. A., Brand, A. H. and Schweisguth, F. (2001). Frizzled regulates localization of cell-fate determinants and mitotic spindle rotation during asymmetric cell division. *Nat Cell Biol* **3**, 50-7.

Bevis, B. J. and Glick, B. S. (2002). Rapidly maturing variants of the Discosoma red fluorescent protein (DsRed). *Nat Biotechnol* **20**, 83-7.

Biehlmaier, O., Neuhauss, S. C. and Kohler, K. (2001). Onset and time course of apoptosis in the developing zebrafish retina. *Cell Tissue Res* **306**, 199-207.

Bornfleth, H., Edelmann, P., Zink, D., Cremer, T. and Cremer, C. (1999). Quantitative motion analysis of subchromosomal foci in living cells using four-dimensional microscopy. *Biophys J* **77**, 2871-86.

Buehler, C., Kim, K. H., Dong, C. Y., Masters, B. R. and So, P. T. (1999). Innovations in two-photon deep tissue microscopy. *IEEE Eng Med Biol Mag* **18**, 23-30.

Burglin, T. R. (2000). A two-channel four-dimensional image recording and viewing system with automatic drift correction. *J Microsc* **200**, 75-80.

Byers, J. A. (1992). Dirichlet tesselation of bark beetle spatial attack points. *Journal of Animal Ecology* **61**, 759-68.

Cameron, D. A. and Carney, L. H. (2000). Cell mosaic patterns in the native and regenerated inner retina of zebrafish: implications for retinal assembly. *J Comp Neurol* **416**, 356-67.

Cayouette, M., Alan Whitmore, Glen Jeffery and Raff, a. M. (2001). Asymmetric Segregation of Numb in Retinal Development and the Influence of the Pigmented Epithelium. *J Neurosci* **21**, 5643-51.

Cellerino, A., Galli-Resta, L. and Colombaioni, L. (2000). The dynamics of neuronal death: a time-lapse study in the retina. *J Neurosci* **20**, RC92.

Cepko, C. L., Austin, C. P., Yang, X., Alexiades, M. and Ezzeddine, D. (1996). Cell fate determination in the vertebrate retina. *Proc Natl Acad Sci U S A* **93**, 589-95.

Charpak, S., Mertz, J., Beaurepaire, E., Moreaux, L. and Delaney, K. (2001). Odor-evoked calcium signals in dendrites of rat mitral cells. *Proc Natl Acad Sci U S A* **98**, 1230-4.

Chen, J., Tucker, C. L., Woodford, B., Szel, A., Lem, J., Gianella-Borradori, A., Simon, M. I. and Bogenmann, E. (1994). The human blue opsin promoter directs transgene expression in short- wave cones and bipolar cells in the mouse retina. *Proc Natl Acad Sci U S A* **91**, 2611-5.

Chenn, A. and McConnell, S. K. (1995). Cleavage orientation and the asymmetric inheritance of Notch1 immunoreactivity in mammalian neurogenesis. *Cell* **82**, 631-41.

Chiu, M. I. and Nathans, J. (1994). Blue cones and cone bipolar cells share transcriptional specificity as determined by expression of human blue visual pigment-derived transgenes. *J Neurosci* **14**, 3426-36.

Cole, L. K. and Ross, L. S. (2001). Apoptosis in the developing zebrafish embryo. *Dev Biol* **240**, 123-42.

Concha, M. L. and Adams, R. J. (1998). Oriented cell divisions and cellular morphogenesis in the zebrafish gastrula and neurula: a time-lapse analysis. *Development* **125**, 983-94.

Cook, J. E. and Chalupa, L. M. (2000). Retinal mosaics: new insights into an old concept. *Trends Neurosci* **23**, 26-34.

Cooper, M. S., D'Amico, L. A. and Henry, C. A. (1999). Analyzing morphogenetic cell behaviors in vitally stained zebrafish embryos. *Methods Mol Biol* **122**, 185-204.

Cormack, B. P., Valdivia, R. H. and Falkow, S. (1996). FACS-optimized mutants of the green fluorescent protein (GFP). *Gene* **173**, 33-8.

Curcio, C. A., Allen, K. A., Sloan, K. R., Lerea, C. L., Hurley, J. B., Klock, I. B. and Milam, A. H. (1991). Distribution and morphology of human cone photoreceptors stained with anti-blue opsin. *J Comp Neurol* **312**, 610-24.

Daly, F. J. and Sandell, J. H. (2000). Inherited retinal degeneration and apoptosis in mutant zebrafish. *Anat Rec* **258**, 145-55.

Denk, W., Strickler, J. H. and Webb, W. W. (1990). Two-photon laser scanning fluorescence microscopy. *Science* **248**, 73-6.

Diaspro, A. (1999). Two-photon microscopy. *IEEE Eng Med Biol Mag* **18**, 16-7.

Doe, C. Q. and Bowerman, B. (2001). Asymmetric cell division: fly neuroblast meets worm zygote. *Current Opinion in Cell Biology* **13**, 68-75.

Dowling, J. E. (1987). The retina : an approachable part of the brain. Cambridge, Mass.: Belknap Press of Harvard University Press.

Easter, S. S., Jr. and Nicola, G. N. (1996). The development of vision in the zebrafish (Danio rerio). *Dev Biol* **180**, 646-63.

Eglen, S. J., van Ooyen, A. and Willshaw, D. J. (2000). Lateral cell movement driven by dendritic interactions is sufficient to form retinal mosaics. *Network* **11**, 103-18.

Fini, M. E., Strissel, K. J. and West-Mays, J. A. (1997). Perspectives on eye development. *Dev Genet* **20**, 175-85.

Frankfort, B. J. and Mardon, G. (2002). R8 development in the Drosophila eye: a paradigm for neural selection and differentiation. *Development* **129**, 1295-306.

Galli-Resta, L. (1998). Patterning the vertebrate retina: the early appearance of retinal mosaics. *Semin Cell Dev Biol* **9**, 279-84.

Galli-Resta, L. (2000). Local, possibly contact-mediated signalling restricted to homotypic neurons controls the regular spacing of cells within the cholinergic arrays in the developing rodent retina. *Development* **127**, 1509-16.

Galli-Resta, L. and Novelli, E. (2000). The effects of natural cell loss on the regularity of the retinal cholinergic arrays. *J Neurosci* **20**, RC60.

Galli-Resta, L., Novelli, E., Kryger, Z., Jacobs, G. H. and Reese, B. E. (1999). Modelling the mosaic organization of rod and cone photoreceptors with a minimal-spacing rule. *Eur J Neurosci* **11**, 1461-9.

Galli-Resta, L., Novelli, E. and Viegi, A. (2002). Dynamic microtubule-dependent interactions position homotypic neurones in regular monolayered arrays during retinal development. *Development* **129**, 3803-14.

Galli-Resta, L., Resta, G., Tan, S. S. and Reese, B. E. (1997). Mosaics of islet-1-expressing amacrine cells assembled by short-range cellular interactions. *J Neurosci* **17**, 7831-8.

Gho, M. and Schweisguth, F. (1998). Frizzled signalling controls orientation of asymmetric sense organ precursor cell divisions in Drosophila. *Nature* **393**, 178-81.

Haffter, P., Granato, M., Brand, M., Mullins, M. C., Hammerschmidt, M., Kane, D. A., Odenthal, J., van Eeden, F. J., Jiang, Y. J., Heisenberg, C. P. et al. (1996). The

identification of genes with unique and essential functions in the development of the zebrafish, Danio rerio. *Development* **123**, 1-36.

Hatten, M. E. and Mason, C. A. (1990). Mechanisms of glial-guided neuronal migration in vitro and in vivo. *Experientia* **46**, 907-16.

Hegyi, L., Hardwick, S. J., Siow, R. C. and Skepper, J. N. (2001). Macrophage death and the role of apoptosis in human atherosclerosis. *J Hematother Stem Cell Res* **10**, 27-42.

Heim, R. and Tsien, R. Y. (1996). Engineering green fluorescent protein for improved brightness, longer wavelengths and fluorescence resonance energy transfer. *Curr Biol* **6**, 178-82.

Herbomel, P., Thisse, B. and Thisse, C. (1999). Ontogeny and behaviour of early macrophages in the zebrafish embryo. *Development* **126**, 3735-45.

Herbomel, P., Thisse, B. and Thisse, C. (2001). Zebrafish early macrophages colonize cephalic mesenchyme and developing brain, retina, and epidermis through a M-CSF receptor-dependent invasive process. *Dev Biol* **238**, 274-88.

Higashijima, S., Okamoto, H., Ueno, N., Hotta, Y. and Eguchi, G. (1997). High-frequency generation of transgenic zebrafish which reliably express GFP in whole muscles or the whole body by using promoters of zebrafish origin. *Dev Biol* **192**, 289-99.

Hinds, J. W. and Hinds, P. L. (1974). Early ganglion cell differentiation in the mouse retina: an electron microscopic analysis utilizing serial sections. *Developmental Biology* **37**, 381-416.

Hinds, J. W. and Hinds, P. L. (1978). Early development of amacrine cells in the mouse retina: an electron microscopic, serial section analysis. *J Comp Neurol* **179**, 277-300.

Hinds, J. W. and Hinds, P. L. (1979). Differentiation of photoreceptors and horizontal cells in the embryonic mouse retina: an electron microscopic, serial section analysis. *Journal Of Comparative Neurology* **187**, 495-511.

Hirsch, N. and Harris, W. A. (1997). Xenopus Pax-6 and retinal development. *J Neurobiol* **32**, 45-61.

Hoffmann, K., Stucker, M., Altmeyer, P., Teuchner, K. and Leupold, D. (2001). Selective femtosecond pulse-excitation of melanin fluorescence in tissue. *J Invest Dermatol* **116**, 629-30.

Holt, C. E. (1989). A single-cell analysis of early retinal ganglion cell differentiation in Xenopus: from soma to axon tip. *J Neurosci* **9**, 3123-45.

Holt, C. E., Bertsch, T. W., Ellis, H. M. and Harris, W. A. (1988). Cellular determination in the Xenopus retina is independent of lineage and birth date. *Neuron* **1**, 15-26.

Hopt, A. and Neher, E. (2001). Highly nonlinear photodamage in two-photon fluorescence microscopy. *Biophys J* **80**, 2029-36.

Hu, M. and Easter, S. S. (1999). Retinal neurogenesis: the formation of the initial central patch of postmitotic cells. *Dev Biol* **207**, 309-21.

Hume, D. A., Perry, V. H. and Gordon, S. (1983). Immunohistochemical localization of a macrophage-specific antigen in developing mouse retina: phagocytosis of dying neurons and differentiation of microglial cells to form a regular array in the plexiform layers. *J Cell Biol* **97**, 253-7.

Huttner, W. B. and Brand, M. (1997). Asymmetric division and polarity of neuroepithelial cells. *Current Opinion In Neurobiology* **7**, 29-39.

Jarman, A. P. (2000). Developmental genetics: vertebrates and insects see eye to eye. *Curr Biol* **10**, R857-9.

Jeyarasasingam, G., Snider, C. J., Ratto, G. M. and Chalupa, L. M. (1998). Activity-regulated cell death contributes to the formation of ON and OFF alpha ganglion cell mosaics. *J Comp Neurol* **394**, 335-43.

Johansson, C. B., Momma, S., Clarke, D. L., Risling, M., Lendahl, U. and Frisen, J. (1999). Identification of a neural stem cell in the adult mammalian central nervous system. *Cell* **96**, 25-34.

Kanda, T., Sullivan, K. F. and Wahl, G. M. (1998a). Histone-GFP fusion protein enables sensitive analysis of chromosome dynamics in living mammalian cells. *Curr Biol* **8**, 377-85.

Kanda, T., Sullivan, K. F. and Wahl, G. M. (1998b). Histone-GFP fusion protein enables sensitive analysis of chromosome dynamics in living mammalian cells. *Current Biology* **8**, 377-85.

Kay, J. N., Finger-Baier, K. C., Roeser, T., Staub, W. and Baier, H. (2001). Retinal Ganglion Cell Genesis Requires lakritz, a Zebrafish atonal Homolog. *Neuron* **30**, 725-36.

Kimmel, C. B., Warga, R. M. and Kane, D. A. (1994). Cell cycles and clonal strings during formation of the zebrafish central nervous system. *Development* **120**, 265-76.

Knoblich, J. A. (2001). Cell division asymmetric cell division during animal development. *Nat Rev Mol Cell Biol* **2**, 11-20.

Knoblich, J. A., Jan, L. Y. and Jan, Y. N. (1995). Asymmetric segregation of Numb and Prospero during cell division. *Nature* **377**, 624-7.

Koester, H. J., Baur, D., Uhl, R. and Hell, S. W. (1999). Ca2+ fluorescence imaging with pico- and femtosecond two-photon excitation: signal and photodamage. *Biophys J* **77**, 2226-36.

Konig, K. (2000). Multiphoton microscopy in life sciences. *J Microsc* **200**, 83-104.

Kouyama, N. and Marshak, D. W. (1997). The topographical relationship between two neuronal mosaics in the short wavelength-sensitive system of the primate retina. *Visual Neuroscience* **14**, 159-67.

Laessing, U. and Stuermer, C. A. (1996). Spatiotemporal pattern of retinal ganglion cell differentiation revealed by the expression of neurolin in embryonic zebrafish. *J Neurobiol* **29**, 65-74.

Larison, K. D. and Bremiller, R. (1990). Early onset of phenotype and cell patterning in the embryonic zebrafish retina. *Development* **109**, 567-76.

Li, Z., Hu, M., Ochocinska, M. J., Joseph, N. M. and Easter, S. S., Jr. (2000a). Modulation of cell proliferation in the embryonic retina of zebrafish (Danio rerio). *Dev Dyn* **219**, 391-401.

Li, Z., Joseph, N. M. and Easter, S. S., Jr. (2000b). The morphogenesis of the zebrafish eye, including a fate map of the optic vesicle. *Dev Dyn* **218**, 175-88.

Linser, P. J., Schlosshauer, B., Galileo, D. S., Buzzi, W. R. and Lewis, R. C. (1997). Late proliferation of retinal Muller cell progenitors facilitates preferential targeting with retroviral vectors in vitro. *Dev Genet* **20**, 186-96.

Livesey, F. J. and Cepko, C. L. (2001). Vertebrate neural cell-fate determination: lessons from the retina. *Nat Rev Neurosci* **2**, 109-18.

Llopis, J., McCaffery, J. M., Miyawaki, A., Farquhar, M. G. and Tsien, R. Y. (1998). Measurement of cytosolic, mitochondrial, and Golgi pH in single living cells with green fluorescent proteins. *Proc Natl Acad Sci U S A* **95**, 6803-8.

Lohmann, C. and Wong, R. O. (2001). Cell-type specific dendritic contacts between retinal ganglion cells during development. *J Neurobiol* **48**, 150-62.

Lu, B., Jan, L. and Jan, Y. N. (2000). Control of cell divisions in the nervous system: symmetry and asymmetry. *Annual Review of Neuroscience* **23**, 531-56.

Lu, B., Rothenberg, M., Jan, L. Y. and Jan, Y. N. (1998). Partner of Numb colocalizes with Numb during mitosis and directs Numb asymmetric localization in Drosophila neural and muscle progenitors. *Cell* **95**, 225-35.

Lu, B., Usui, T., Uemura, T., Jan, L. and Jan, Y. N. (1999). Flamingo controls the planar polarity of sensory bristles and asymmetric division of sensory organ precursors in Drosophila. *Current Biology* **9**, 1247-50.

Maiti, S., Shear, J. B., Williams, R. M., Zipfel, W. R. and Webb, W. W. (1997). Measuring serotonin distribution in live cells with three-photon excitation. *Science* **275**, 530-2.

Malatesta, P., Hartfuss, E. and Gotz, M. (2000). Isolation of radial glial cells by fluorescent-activated cell sorting reveals a neuronal lineage. *Development* **127**, 5253-63.

Malicki, J. (2000). Harnessing the power of forward genetics--analysis of neuronal diversity and patterning in the zebrafish retina. *Trends Neurosci* **23**, 531-41.

Marquardt, T., Ashery-Padan, R., Andrejewski, N., Scardigli, R., Guillemot, F. and Gruss, P. (2001). Pax6 is required for the multipotent state of retinal progenitor cells. *Cell* **105**, 43-55.

Marquardt, T. and Gruss, P. (2002). Generating neuronal diversity in the retina: one for nearly all. *Trends Neurosci* **25**, 32-8.

Masai, I., Stemple, D. L., Okamoto, H. and Wilson, S. W. (2000). Midline signals regulate retinal neurogenesis in zebrafish. *Neuron* **27**, 251-63.

Mathis, L. and Nicolas, J. F. (2000). Different clonal dispersion in the rostral and caudal mouse central nervous system. *Development* **127**, 1277-90.

McCabe, K. L., Gunther, E. C. and Reh, T. A. (1999). The development of the pattern of retinal ganglion cells in the chick retina: mechanisms that control differentiation. *Development* **126**, 5713-24.

McFarlane, S., Zuber, M. E. and Holt, C. E. (1998). A role for the fibroblast growth factor receptor in cell fate decisions in the developing vertebrate retina. *Development* **125**, 3967-75.

Miyata, T., Kawaguchi, A., Okano, H. and Ogawa, M. (2001). Asymmetric inheritance of radial glial fibers by cortical neurons. *Neuron* **31**, 727-41.

Miyawaki, A., Griesbeck, O., Heim, R. and Tsien, R. Y. (1999). Dynamic and quantitative Ca2+ measurements using improved cameleons. *Proc Natl Acad Sci U S A* **96**, 2135-40.

Miyawaki, A., Llopis, J., Heim, R., McCaffery, J. M., Adams, J. A., Ikura, M. and Tsien, R. Y. (1997). Fluorescent indicators for Ca2+ based on green fluorescent proteins and calmodulin. *Nature* **388**, 882-7.

Mochizuki, A. (2002). Pattern Formation of the Cone Mosaic in the Zebrafish Retina: A Cell Rearrangement Model. *J Theor Biol* **215**, 345-361.

Mohler, W. A. (1999). Visual reality: using computer reconstruction and animation to magnify the microscopist's perception. *Mol Biol Cell* **10**, 3061-5.

Mullins, M. C., Hammerschmidt, M., Haffter, P. and Nusslein-Volhard, C. (1994). Large-scale mutagenesis in the zebrafish: in search of genes controlling development in a vertebrate. *Current Biology* **4**, 189-202.

Nawrocki, L. W. (1985). DEVELOPMENT OF THE NEURAL RETINA IN THE ZEBRAFISH, BRACHYDANIO RERIO (NEUROGENESIS). In *Neuroscience*, (ed., pp. 162: University of Oregon.

Neil, M. A., Juskaitis, R., Booth, M. J., Wilson, T., Tanaka, T. and Kawata, S. (2000). Adaptive aberration correction in a two-photon microscope. *J Microsc* **200 (Pt 2)**, 105-8.

Neumann, C. J. and Nuesslein-Volhard, C. (2000). Patterning of the zebrafish retina by a wave of sonic hedgehog activity. *Science* **289**, 2137-9.

Nimchinsky, E. A., Oberlander, A. M. and Svoboda, K. (2001). Abnormal development of dendritic spines in FMR1 knock-out mice. *J Neurosci* **21**, 5139-46.

Noctor, S. C., Flint, A. C., Weissman, T. A., Dammerman, R. S. and Kriegstein, A. R. (2001). Neurons derived from radial glial cells establish radial units in neocortex. *Nature* **409**, 714-20.

Oheim, M., Beaurepaire, E., Chaigneau, E., Mertz, J. and Charpak, S. (2001). Two-photon microscopy in brain tissue: parameters influencing the imaging depth. *J Neurosci Methods* **111**, 29-37.

Ohnuma, S., Philpott, A., Wang, K., Holt, C. E. and Harris, W. A. (1999). p27Xic1, a Cdk inhibitor, promotes the determination of glial cells in Xenopus retina. *Cell* **99**, 499-510.

Oppenheim, R. W. (1991). Cell death during development of the nervous system. *Annu Rev Neurosci* **14**, 453-501.

Parnavelas, J. G. (2000). The origin and migration of cortical neurones: new vistas. *Trends Neurosci* **23**, 126-31.

Peterson, R. E., Fadool, J. M., McClintock, J. and Linser, P. J. (2001). Muller cell differentiation in the zebrafish neural retina: evidence of distinct early and late stages in cell maturation. *J Comp Neurol* **429**, 530-40.

Piston, D. W. (1999). Imaging living cells and tissues by two-photon excitation microscopy. *Trends Cell Biol* **9**, 66-9.

Piston, D. W., Masters, B. R. and Webb, W. W. (1995). Three-dimensionally resolved NAD(P)H cellular metabolic redox imaging of the in situ cornea with two-photon excitation laser scanning microscopy. *J Microsc* **178**, 20-7.

Potter, S. M. (1996). Vital imaging: two photons are better than one. *Curr Biol* **6**, 1595-8.

Potter, S. M., Wang, C. M., Garrity, P. A. and Fraser, S. E. (1996). Intravital imaging of green fluorescent protein using two-photon laser- scanning microscopy. *Gene* **173**, 25-31.

Rakic, P. (1995). A small step for the cell, a giant leap for mankind: a hypothesis of neocortical expansion during evolution. *Trends in Neurosciences* **18**, 383-8.

Ramâon y Cajal, S. (1995). Histology of the nervous system of man and vertebrates. New York: Oxford University Press.

Rapaport, D. H. and Dorsky, R. I. (1998). Inductive competence, its significance in retinal cell fate determination and a role for Delta-Notch signaling. *Semin Cell Dev Biol* **9**, 241-7.

Raymond, P. A., Barthel, L. K. and Curran, G. A. (1995). Developmental patterning of rod and cone photoreceptors in embryonic zebrafish. *J Comp Neurol* **359**, 537-50.

Reese, B. E. and Galli-Resta, L. (2002). The role of tangential dispersion in retinal mosaic formation. *Prog Retin Eye Res* **21**, 153-68.

Reese, B. E., Harvey, A. R. and Tan, S. S. (1995). Radial and tangential dispersion patterns in the mouse retina are cell- class specific. *Proc Natl Acad Sci U S A* **92**, 2494-8.

Reese, B. E., Necessary, B. D., Tam, P. P., Faulkner-Jones, B. and Tan, S. S. (1999). Clonal expansion and cell dispersion in the developing mouse retina. *Eur J Neurosci* **11**, 2965-78.

Reid, C. B., Tavazoie, S. F. and Walsh, C. A. (1997). Clonal dispersion and evidence for asymmetric cell division in ferret cortex. *Development* **124**, 2441-50.

Reilander, H., Haase, W. and Maul, G. (1996a). Functional expression of the Aequorea victoria green fluorescent protein in insect cells using the baculovirus expression system. *Biochem Biophys Res Commun* **219**, 14-20.

Reilander, H., Haase, W. and Maul, G. (1996b). Functional expression of the Aequorea victoria green fluorescent protein in insect cells using the baculovirus expression system. *Biochem Biophys Res Commun* **219**, 14-20.

Robinson, J., Schmitt, E. A. and Dowling, J. E. (1995). Temporal and spatial patterns of opsin gene expression in zebrafish (Danio rerio). *Visual Neuroscience* **12**, 895-906.

Rockhill, R. L., Euler, T. and Masland, R. H. (2000). Spatial order within but not between types of retinal neurons. *Proc Natl Acad Sci U S A* **97**, 2303-7.

Roegiers, F., Younger-Shepherd, S., Jan, L. Y. and Jan, Y. N. (2001). Two types of asymmetric divisions in the Drosophila sensory organ precursor cell lineage. *Nat Cell Biol* **3**, 58-67.

Sausedo, R. A., Smith, J. L. and Schoenwolf, G. C. (1997). Role of nonrandomly oriented cell division in shaping and bending of the neural plate. *J Comp Neurol* **381**, 473-88.

Scheibe, R., Schnitzer, J., Rohrenbeck, J., Wohlrab, F. and Reichenbach, A. (1995). Development of A-type (axonless) horizontal cells in the rabbit retina. *J Comp Neurol* **354**, 438-58.

Schmitt, E. A. and Dowling, J. E. (1994). Early eye morphogenesis in the zebrafish, Brachydanio rerio. *J Comp Neurol* **344**, 532-42.

Shamim, K. M., Scalia, F., Tóth, P. and Cook, J. E. (1997). Large retinal ganglion cells that form independent, regular mosaics in the ranid frogs Rana esculenta and Rana pipiens. *Visual Neuroscience* **14**, 1109-27.

Shamim, K. M., Toth, P., Becker, D. L. and Cook, J. E. (1999). Large retinal ganglion cells that form independent, regular mosaics in the bufonoid frogs Bufo marinus and Litoria moorei. *Visual Neuroscience* **16**, 861-79.

Silva, A. O., Ercole, C. E. and McLoon, S. C. (2002). Plane of cell cleavage and numb distribution during cell division relative to cell differentiation in the developing retina. *J Neurosci* **22**, 7518-25.

Spana, E. P. and Doe, C. Q. (1996). Numb antagonizes Notch signaling to specify sibling neuron cell fates. *Neuron* **17**, 21-6.

Stiemke, M. M. and Hollyfield, J. G. (1995). Cell birthdays in Xenopus laevis retina. *Differentiation* **58**, 189-93.

Takahashi, H., Murayama, M., Takashima, A., Mercken, M., Nakazato, Y., Noguchi, K. and Imahori, K. (1996). Molecular cloning and expression of the rat homologue of presenilin-1. *Neurosci Lett* **206**, 113-6.

Takesue, A., Mochizuki, A. and Iwasa, Y. (1998). Cell-differentiation rules that generate regular mosaic patterns: modelling motivated by cone mosaic formation in fish retina. *J Theor Biol* **194**, 575-86.

Thomas, C. F. and White, J. G. (1998). Four-dimensional imaging: the exploration of space and time. *Trends Biotechnol* **16**, 175-82.

Tirlapur, U. K. and Konig, K. (1999). Technical advance: near-infrared femtosecond laser pulses as a novel non-invasive means for dye-permeation and 3D imaging of localised dye- coupling in the Arabidopsis root meristem. *Plant J* **20**, 363-70.

Tohya, S., Mochizuki, A. and Iwasa, Y. (1999). Formation of cone mosaic of zebrafish retina. *J Theor Biol* **200**, 231-44.

Tsien, R. Y. (1998). The green fluorescent protein. *Annu Rev Biochem* **67**, 509-44.

Tuckett, F. and Morriss-Kay, G. M. (1985). The kinetic behaviour of the cranial neural epithelium during neurulation in the rat. *J Embryol Exp Morphol* **85**, 111-9.

Turner, D. L. and Cepko, C. L. (1987). A common progenitor for neurons and glia persists in rat retina late in development. *Nature* **328**, 131-6.

Turner, D. L., Snyder, E. Y. and Cepko, C. L. (1990). Lineage-independent determination of cell type in the embryonic mouse retina. *Neuron* **4**, 833-45.

Wakamatsu, Y., Maynard, T. M., Jones, S. U. and Weston, J. A. (1999). NUMB localizes in the basal cortex of mitotic avian neuroepithelial cells and modulates neuronal differentiation by binding to NOTCH-1. *Neuron* **23**, 71-81.

Wassle, H., Boycott, B. B. and Illing, R. B. (1981). Morphology and mosaic of on- and off-beta cells in the cat retina and some functional considerations. *Proc R Soc Lond B Biol Sci* **212**, 177-95.

Westerfield, M. (1993). The zebrafish book : a guide for the laboratory use of zebrafish (Brachydanio rerio). [Eugene, OR]: M. Westerfield.

Wetts, R. and Fraser, S. E. (1988). Multipotent precursors can give rise to all major cell types of the frog retina. *Science* **239**, 1142-5.

Wikler, K. C., Rakic, P., Bhattacharyya, N. and Macleish, P. R. (1997). Early emergence of photoreceptor mosaicism in the primate retina revealed by a novel cone-specific monoclonal antibody. *J Comp Neurol* **377**, 500-8.

Wilson, T. (1989). Three-dimensional imaging in confocal systems. *J Microsc* **153**, 161-9.

Wolf, E., Black, I. B. and DiCicco-Bloom, E. (1996). Mitotic neuroblasts determine neuritic patterning of progeny. *J Comp Neurol* **367**, 623-35.

Xu, C., Zipfel, W., Shear, J. B., Williams, R. M. and Webb, W. W. (1996). Multiphoton fluorescence excitation: new spectral windows for biological nonlinear microscopy. *Proc Natl Acad Sci U S A* **93**, 10763-8.

Young, R. W. (1985a). Cell differentiation in the retina of the mouse. *Anat Rec* **212**, 199-205.

Young, R. W. (1985b). Cell proliferation during postnatal development of the retina in the mouse. *Brain Res* **353**, 229-39.

Yuste, R., Lanni, F. and Konnerth, A. (1999). Imaging neurons, pp. 11.4. Cold Spring Harbor, N.Y.: Cold Spring Harbor Laboratory Press.

Zhang, X. M. and Yang, X. J. (2001). Regulation of retinal ganglion cell production by Sonic hedgehog. *Development* **128**, 943-57.

Zhong, W., Feder, J. N., Jiang, M. M., Jan, L. Y. and Jan, Y. N. (1996). Asymmetric localization of a mammalian numb homolog during mouse cortical neurogenesis. *Neuron* **17**, 43-53.

Zhong, W., Jiang, M. M., Weinmaster, G., Jan, L. Y. and Jan, Y. N. (1997). Differential expression of mammalian Numb, Numblike and Notch1 suggests distinct roles during mouse cortical neurogenesis. *Development* **124**, 1887-97.